GRAPHENE OXIDE-BASED MATERIALS: SYNTHESIS, CHARACTERIZATION AND APPLICATIONS

NANYANG TECHNOLOGICAL UNIVERSITY

GRAPHENE OXIDE-BASED MATERIALS: SYNTHESIS, CHARACTERIZATION AND APPLICATIONS

ZHOU XIAOZHU

SCHOOL OF MATERIALS SCIENCE AND ENGINEERING

2010

ZHOU XIAOZHU

2010

GRAPHENE OXIDE-BASED MATERIALS: SYNTHESIS, CHARACTERIZATION AND APPLICATIONS

ZHOU XIAOZHU

School of Materials Science and Engineering

A thesis submitted to the Nanyang Technological University
in partial fulfillment of the requirement for the degree of
Doctor of Philosophy

2010

Acknowledgements

I wish to thank my advisors Prof. Freddy Boey and Asst/Prof. Hua ZHANG for their consistent support and instruction, without which this dissertation would not have been possible.

I would like to express my sincere thanks to my committee members, Prof. Subbu S Venkatraman, Prof. Subodh Mhaisalkar and Asst/Prof. Alex Yan Qingyu. Very special thanks go to our collaborators, Asst/Prof. Peng Chen, Dr. Agarwal Shuchi and Mr. Guo Chunxian.

This dissertation was completed with help from many of Zhang group members. I would like to thank them Dr. Chen Yanhong, Li Bing, Qi Xiaoying, Lu Gang, Huang Xiao, Dr. Yin Zongyou, Dr. Li Hai and Dr. Wang Zhijuan. Other group members are also acknowledged. Your inspiration and enlightenment will be remembered and will keep me moving forward in future.

I am indebted to my wife, Zhou Xuexia, for her love, support and encouragement for the past three years of my Ph. D. study.

Table of Contents

Abstract

In this study, the properties and applications of graphene oxide-based materials have been explored. Specifically, graphene oxide, i.e. a single layer of graphite oxide, reduced graphene oxide and their thin films were investigated. The interest in graphene oxide stems from the ability of its surface to be easily chemically modified. Thin film of reduced graphene oxide also shows exceptional properties as scaffolds for cell culture and matrix for mass spectroscopy.

The composites of graphene and nanoparticles show promises in various fields. The author proposes a straightforward one-step chemical method for in-situ synthesis of silver nanoparticles on both graphene oxide and reduced graphene oxide surfaces. Silver nanoparticles with different morphology were grown on graphene oxide and reduced graphene oxide surfaces after heating 3-aminopropyltriethoxysilane-modified silicon oxide substrates adsorbed with graphene oxide and reduced graphene oxide in a sodium nitrate solution. Atomic force microscopy and scanning electron microscopy revealed that well-distributed and small size silver nanoparticles were grown on graphene oxide, while large silver particles were grown on the reduced graphene oxide. The silver nanoparticles were proved active in surface enhanced Raman spectroscopy for the detection of p-aminothiolphenol.

The thesis also studied the fabrication of graphene oxide nanoribbons. Wrinkles of three layers of graphene oxide, with a typical width of less than 100 nm and length of a few microns, were formed when graphene oxide were deposited on 3-

aminopropyltriethoxysilane-modified silicon oxide substrates. Graphene oxide nanoribbons of single- or double-layer were obtained by plasma etching of graphene oxide wrinkles, in which top-layers of wrinkles were used as sacrificial layers. The thesis also demonstrated that the graphene oxide ribbons could be readily seeded with silver nanoparticles.

The thesis systematically studied the ability of reduced graphene oxide film and single-walled carbon nanotubes (SWCNT) network in interfacing several types of cells, such as neuroendocrine PC12 cells, oligodendroglia cells, and osteoblasts. It was found that reduced graphene oxide was biocompatible to all these cell types, whereas SWCNT networks were inhibitory to the proliferation, viability and neuritegenesis of PC12 cells, and the proliferation of oligodendroglia cells. These observations could be attributed to the distinct nanotopographic features of these two kinds of nanocarbon susbtrates.

The unique structure of reduced graphene oxide led to its use as matrix for matrix-assisted laser desorption/ionization time-of-flight mass spectrometry. Thin film of reduced graphene oxide outrivals graphite powders, carbon nanotubes and activated carbon as matrix to detect octa-chlorinated dioxin, an environment pollutant. The graphene oxide film cannot be used as matrix. This study helps us understand the structure of reduced graphene oxide, compared with that of graphene oxide, graphite, and other carbon allotropes.

The realization of the use of graphene in nanoelectronics requires the integration and alignment of millions of graphene on a single chip, which has been pursed

vigorously in CNT nanoelectronics. Two approaches have been employed to pattern graphene oxide. In the first method, by using microcontact printing, graphene oxide was directly printed on solids substrates. In the second one, the patterned molecular templates were used to adsorb graphene oxide on solid substrates.

List of Figures

List of Tables

Chapter 1

Introduction

1.1 Background

Graphene, an allotrope of carbon, is a single layer of bonded-sp^2 carbons compacted into a two-dimensional honeycomb lattice. Owing to its rich physics and fascinating properties[1], graphene has received increasing interests from the research community. Its properties have the potential to be comparable to and even exceed carbon nanotubes (CNTs). For example, the bandgap engineering of graphene[2, 3] makes graphene an excellent semi-conductor useful in nanoelectronics. Like CNTs, graphene has been used for sensor applications, e.g. gas sensing[4] and DNA sensing[5]. The large surface area of graphene offers its promise in supercapacitance applications[6].

Graphene was initially obtained by micromechanical cleavage method (nicknamed "Scotch Tape Method")[7, 8], in which a scotch tape was applied to peel highly ordered pyrolytic graphite (HOPG) and rubbed onto target substrates (e.g. 300 nm SiO_2 silicon wafer) to get tiny pieces of single-layer graphene with a size of several microns. This method is impractical to provide enough quantity of graphene if its use in nanoelectronics (e.g. field effect transistors), sensors, or filler materials is expected. Therefore, an alternative and reproducible approach to make a large quantity of graphene is required.

To achieve large quantities of graphene, we have employed a chemical method to oxidize graphite to graphite oxide. Upon mechanic shaking or mild sonication in water, graphite oxide will exfoliate into graphene oxide (GO, referred to as a single layer of graphite oxide). The chemical process will alter the properties of graphite and render GO (or graphite oxide) insulating. However, with hydrazine reduction or heat treatment under gases or in vacuum, the electrical properties of GO will be restored to certain extend. The reduced GO (rGO), with residual functional groups, will behave differently from that of graphene. Moreover, owing to the ease with which its surface can be functionalized, GO is ready to be modified for various applications.

1.2 Current challenges and objectives

Much effort has so far been devoted to the modifications of graphene to accomplish its promises. However, in order to realize the full potential of graphene, it is necessary to understand how GO can be modified. This thesis seeks to study the potential of GO in various applications and understand more of its structure. Its ability as templates for growth of nanomaterials and to fabricate GO nanoribbons for future nanoelectronics will be investigated. In addition, rGO, as an alternative to graphene, is also studied in its thin form for cell culture and as matrix for mass spectroscopic analysis.

Specifically, the following questions need to be answered:

(i). How and why does the growth of metal nanoparticles occur on GO and rGO? What properties will these nanoparticles deliver?

(ii). Is there a simple method to make GO nanoribbons?

(iii). Is there any convenient method to pattern GO for future integrated nanoelectronics devices?

(iv). Is the rGO thin film biocompatible or even bioactive with respect to specific cells? Can it be used as a matrix (just like other forms of carbon) for mass spectroscopic analysis?

Towards these ends, the objectives for this thesis have therefore been formulated as:

(i). To develop a simple method to in situ grow silver nanoparticles with different morphology on GO and rGO. The underlying growth mechanism will be proposed.

(ii). GO nanoribbons, single- or double-layered, will be fabricated.

(iii). GO will be patterned on silicon oxide substrates. These patterns will find use in future nanoelectronics.

(iv). The rGO thin film will be used as scaffolds to culture cells. Comparative studies will be carried out on single-walled carbon nanotubes. The different cell behaviors on these two substrates will be studied. The rGO thin film will be also used as matrix for mass spectroscopic analysis. Its unique advantages over other materials as matrix will be investigated.

1.3 Scope

In this thesis, GO and rGO will be used because of their close relationship with graphene as well as the advantage of being easier to scale up compared to graphene, as mentioned above. The hydrazine reduction method has been chosen

as it has been previously shown to work well in reducing graphene oxide to give rGO.

The silver nanoparticles with different morphology will be characterized by AFM, SEM, TEM and XRD. The obtained silver nanoparticles will be tested by surface enhanced Raman spectroscopy to detect p-aminothiolphenol.

GO nanoribbons with different layers and varied length and width are important in nanoelectronics. Therefore, the fabrication of these kinds of ribbons is tried. Moreover, the modification of GO nanoribbons is also important. The growth of silver nanoparticle on GO nanoribbons will also be carried out.

Understanding the behavior of cells on rGO films would be critical to fully evaluate the biocompatibility of rGO films. Hence, cell adhesion, viability, proliferation, and differentiation will be studied. In addition, comparative studies on other carbon materials, such as single-walled carbon nanotubes are also required and carried out.

The ability of rGO thin film as matrix would also be tested for the detection of octa-chlorinated dioxin (OCDD), an environment hazard, in matrix-assisted laser desorption/ionization time-of-flight mass spectrometry (MALDI-TOF-MS).

1.4 Overview

A critical literature review is reported in Chapter 2, which will cover the introduction to graphene, GO and rGO with emphases on their definition, structure, properties, applications and characterization techniques. Chapter 3 will describe the materials and experimental details. Chapter 4 reports on the properties and related applications to single- to few-layer GO and rGO. The properties and applications of reduced graphene oxide thin films will be reported in Chapter 5. Chapter 6 focuses on conclusions and recommendations.

Chapter 2

Literature Review

2.1 What is graphene?

Graphene is a two dimensional (2D) single layer sheet made of sp^2-carbon compactly packed to a honeycomb lattice[1, 9]. It could be viewed as the basic building-up block of other graphitic materials of various dimensionalities. For example, it can be wrapped up into 0D fullerenes, rolled into metallic and semiconducting 1D carbon nanotubes (CNTs), or stacked to form semi-metallic 3D graphite, Figure 2-1a. It should be mentioned here that graphite is considered of stacking of graphenes, when the layer number is >10. The crystal structure of graphite is shown in Figure 2-1b[10]. The unique hexagonal lattice structure and 2D delocalized π-conjugated network lend graphene (one layer shown as in Figure 2-1c) many unusual properties. For instance, its charge carriers behave as relativistic particles, which are satisfactorily described by Dirac equation rather than commonly used Schrödinger equation in condensed-matter physics[1]. This relativistic feature makes graphene a useful material for physicists to test quantum electrodynamics in table-top experiments, e.g. Klein tunneling has been verified[11]. Although many other 2D crystals have been found, most experimental and theoretical efforts have so far focused on graphene, because of its huge potential as a highly efficient electronic material. It is the exceptional electrical properties that drive graphene rush forward. Many field-effect transistors have been demonstrated, with the discovery that graphene exhibits ambipolar characteristics of its charge carriers[1, 9], Figure 2-2a. Graphene has been

measured as the strongest mechanical material by AFM indentation test[12], revealing that Young's modulus E is 1.0 terapascals, Figure 2-2b.

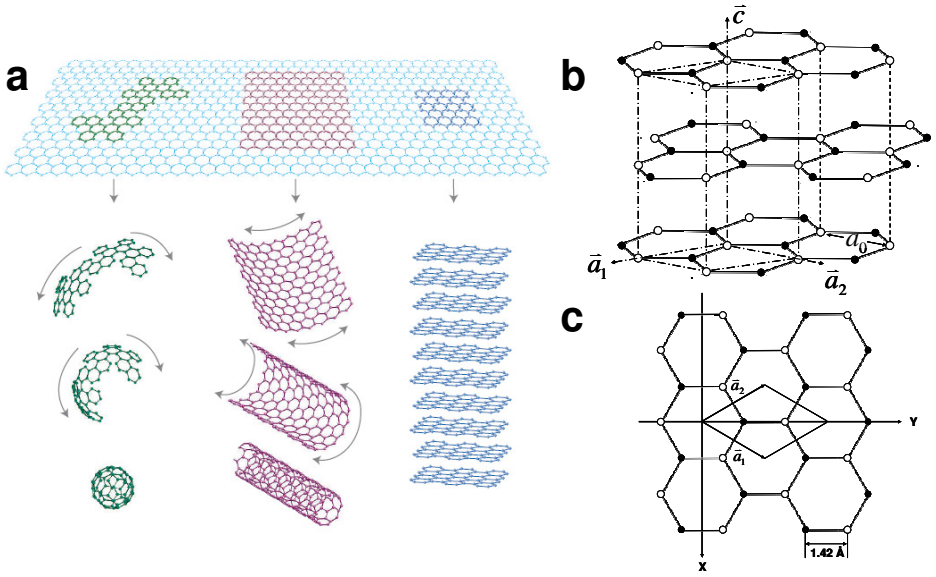

Figure 2-1 (a) Graphene can be wrapped up into 0D buckyball, rolled into 1D nanotubes or stacked into 3D graphite[1]. (b) Crystal structure of hexagonal single crystal graphite (P63/mmc). Graphene layers are stacked as an ..ABAB.. sequence. The nearest-neighbor carbon distance in graphite and plane-plane distance are 0.14 and 0.34 nm, respectively [10]. (c) Lattice of graphene.

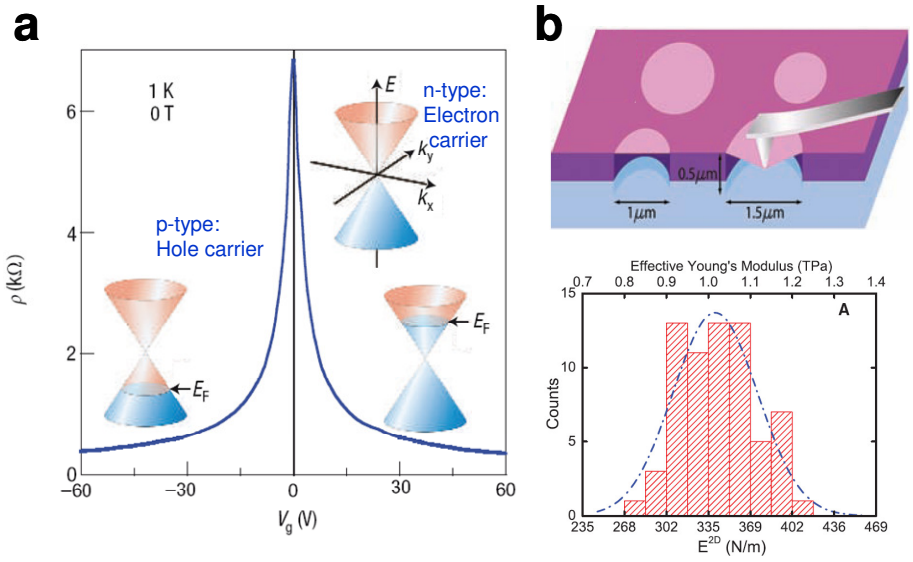

Figure 2-2 (a) Ambipolar electric field effect in single-layer graphene[1, 9]. (b) (Upper) Schematic illustration of nanoindentation on suspended graphene membrane by AFM. (Bottom) Histogram of Young's modulus E centered at 1 terapascals[12].

Nevertheless, all of these applications will be feasible only if the reliable methods for large-scale production of graphene exist.

2.2 Various methods for obtaining graphene

Considerable efforts have been taken to make graphite samples that approach single-layer graphene. Kim's group[13] developed a method by attaching a graphite microcrystal to a tipless cantilever of atomic force microscope (AFM) and then scratched the crystal on silicon substrates. Islands of graphite as thin as 10 nm, or ~30 layers were stamped on SiO_2, Figure 2-3a.

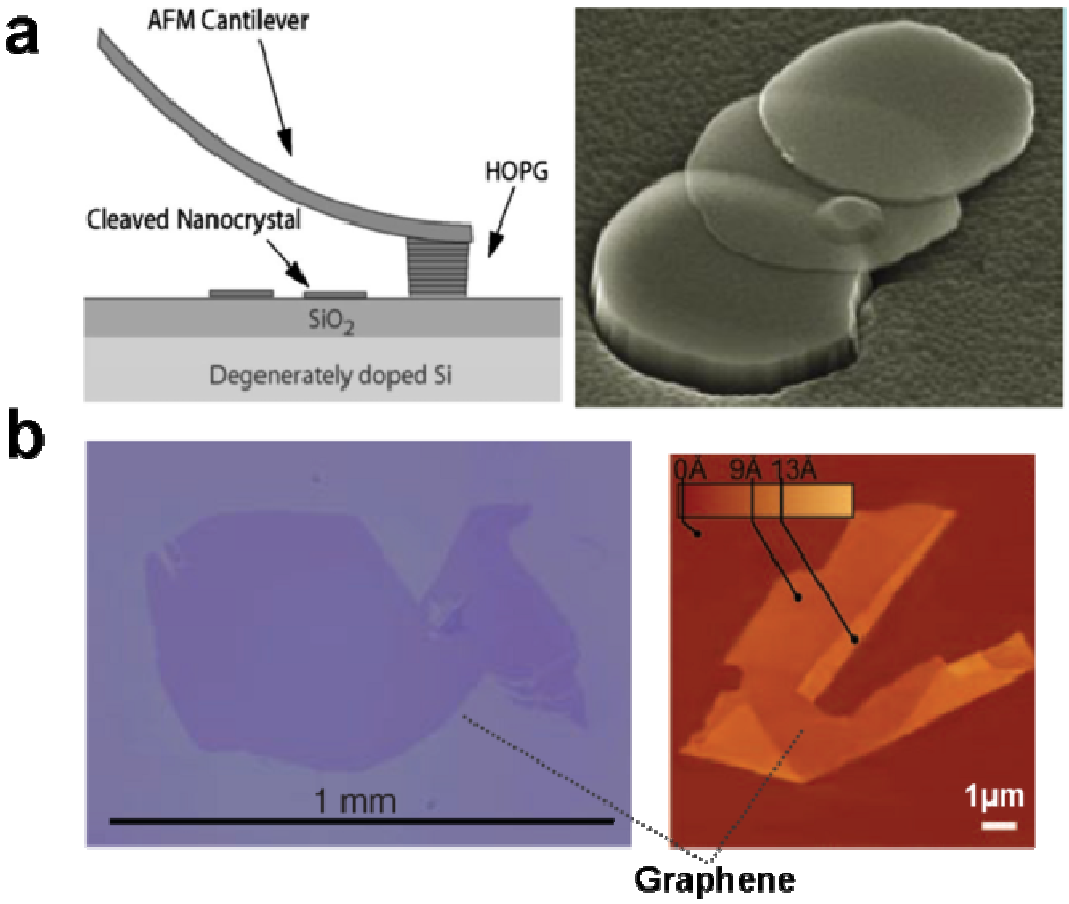

Figure 2-3 (a) (Left) Schematic illustration of rubbing graphitic pancakes to substrates by AFM cantilever. (Right) Typical SEM image of graphitic pancakes received[13]. (b) (Left) Optical image of graphene sheets as large as 1 mm[14]. (Right) AFM image of graphene sheets with single- and double-layer[7].

Even with this elegant method, the resulting material is still graphite, rather than graphene which is a single layer of graphite. The imaginary graphene was first made by Geim's group in University of Manchester in 2004 by mechanical cleavage of graphite[7, 9], Figure 2-3b. Although this method is competent in giving high quality graphene with good electrical and optical properties satisfactory for most fundamental studies, it is tedious and unreliable because of its low yield. This method, therefore, hinders graphene from the realization of real applications. To avoid these shortcomings, a few methods have been developed.

i. Chemical vapor deposition of carbon on Ni and Cu with hydrocarbon flow has realized wafer-scale production of few-layer and single-layer graphene[15, 16]. However, the graphene obtained by this method has many defects and is non-uniform compared to that produced by micromechanical cleavage method. In addition, the need to transfer the as-grown graphene to other substrates is also problematic. Last, the quantity produced by this method is far less than needed in other applications, such as scaffolds for tissue engineering[17].

ii. To fully investigate the electrical properties, efforts are made on the epitaxial growth of graphene film to generate high-quality graphene and considerable progress has been achieved[18]. However, it should be noted that this method relies heavily on expensive silicon carbide substrates and strict conditions, e.g. UHV vacuum. Therefore, this method is of limited value for practical applications.

iii. More recently, liquid phase exfoliation[19] of graphite appears to be a simpler and cheaper method to make graphene. However its low yield (~1 wt %) and small pieces of graphene obtained prove disadvantageous.

Table 2-1 lists several common techniques to obtain graphene-based materials. The chemical exfoliation method[20] is the most flexible, low cost and simplest.. While the electrical properties of graphene oxide (GO, referred to as the single layer of graphite oxide, similar to graphene that is single layer of graphite.) is not preserved, other characteristics and properties are worth investigation and may make graphene oxide useful for a range of applications, e.g. as a component of composite materials. Reduced graphene oxide (rGO) could be obtained by

reduction of graphene oxide, enabling it to be used like graphene, as reported by several papers[21, 22]. The process for obtaining rGO potentially opens up many applications. For example, rGO has been used as substrates for field emitters[23], charge carriers[24], or transparent electrodes[25] for solar cells.

Table 2-1 Comparison of various methods to produce graphene

Method	**Advantages**	**Problems**
MMC[a]	– Pristine and perfect graphene with few defects – Useful for fundamental research	– Low throughput and unreliable
CVD[b]	– Inexpensive (Ni, Cu) – Wafer-scale	– Non-uniform – High temperature – Low yield of single-layer
EG[c]	– Relatively large pieces for device fabrication	– Too expensive of the growth substrates (SiC) – - Strict conditions required, e.g. UHV
LPE[d]	– Facile way to make nearly-perfect graphene	– Low yield – Piece too small to integrate with fabrication
CE[e]	– Large yield – Cheap and affordable – High solubility in solvents and transferrable to various substrates	– Deteriorated electrical properties (graphene oxide, not graphene)

[a]Micromechanical cleavage method ("scotch tape method")
[b]Chemical vapor deposition method
[c]Epitaxial growth method
[d]Liquid phase exfoliation method
[e]Chemical exfoliation method

2.3 Graphene oxide: synthesis method and structure

We should clarify here that graphene oxide (GO) is an individual layer of graphite oxide, similar to graphene that is an individual layer of graphite, Figure 2-1b, c. GO can be obtained by exfoliation of graphite oxide. Therefore the synthesis method and structure of GO is corresponding to that of graphite oxide.

Although graphite oxide is gaining attention recently, it is not a new material. Graphite oxide was first prepared by oxidizing graphite with $KClO_3/HNO_3$ by the Oxford chemist Brodie dating back to the 1850's[26]. Staudenmaier modified this method by adding one more acid H_2SO_4 as the oxidizing agent[27, 28]. However, these two methods are time consuming and hazardous. In 1957, Hummers and Offeman[29] developed a more rapid and safer method to prepare graphite oxide from graphite in which an essentially anhydrous mixture of $NaNO_3$, H_2SO_4 and $KMnO_4$ was used as the oxidizing agent. The Hummers method turns out to be effectively judged by the ratio of carbon to oxygen in the final product. Well reacted samples will have a ratio between 2.1 and 2.9. With the surge of graphene research, the preparation of graphite oxide has revived and the Hummers method had been recently modified to be more effective by adding pre-oxidation steps[30].

Even with its long history of preparation, the detailed structure of GO remains unclear. The most up to date structural model is given by Lerf and Klinowski[31], Figure 2-4a. From this structure, the surface of GO is abundant with C-OH and C-O-C (epoxide, 1,2- ether rather than 1,3-ether proposed by Mermoux[32]) groups with a few numbers of ketone, carbonyl and carboxyl groups presumably scattered

at the edges. A few points should be noted in the Lerf-Klnowski model. First, the surface of GO involves two kinds of regions: aromatic regions with unoxidized benzene rings and regions containing six-membered rings. The distribution of these two regions is random. This hypothetical structure is recently verified by scanning tunneling microscopy of GO[21, 33] where two kinds of regions are clearly distinguishable, Figure 2-4b. The relative size of the two regions depends on the level of oxidation. Second, the epoxide and the C-OH groups are very close to one another. Third, the functional groups are not necessary to distribute evenly on the surface but with varying density at different regions. Fourth, both sides of the GO surface are decorated with these functional groups.

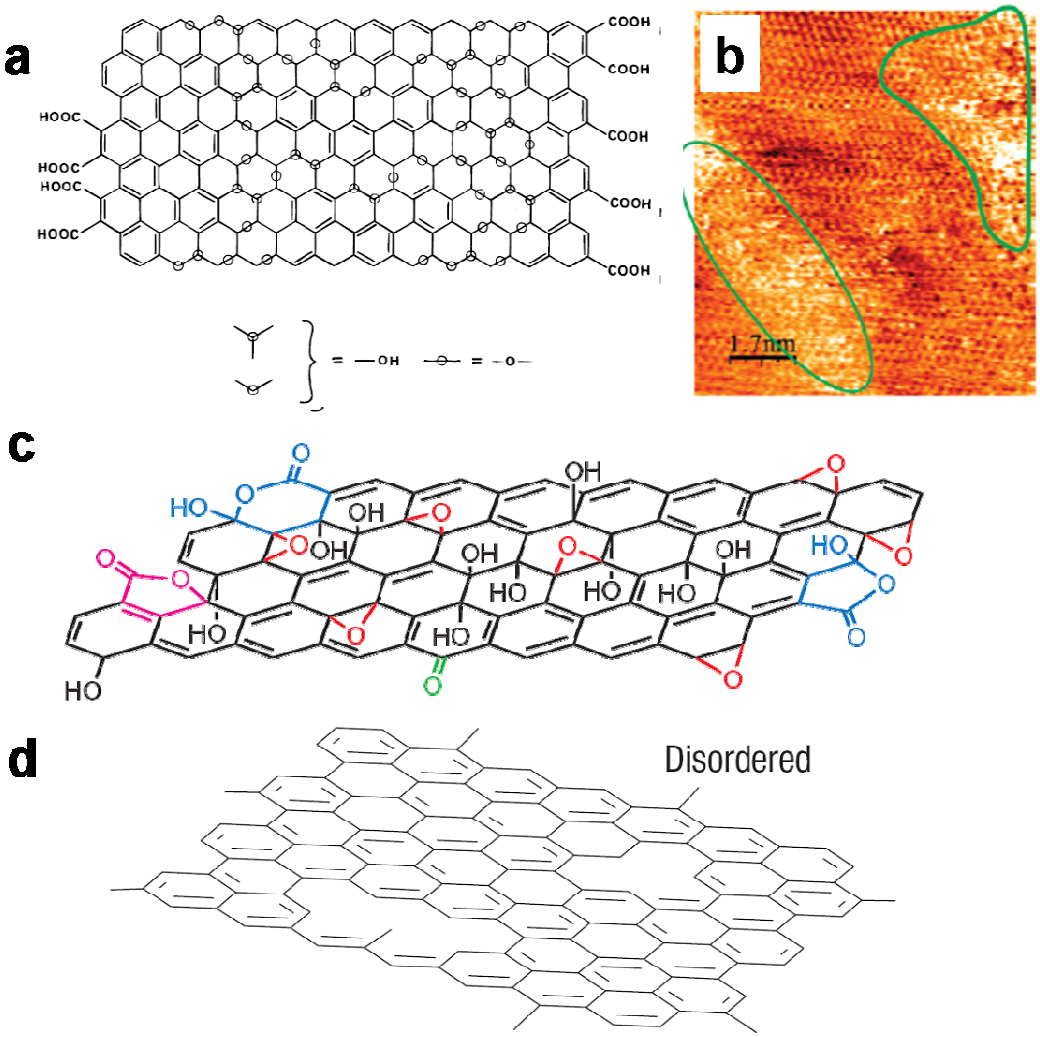

Figure 2-4 (a, c) Chemical structure of GO[31, 34]. (b) STM image of GO showing the regions of oxidation and non-oxidation[21]. (d) Approximate structure of rGO[35]. The remaining functional groups depend on the reduction method.

The Lerf-Klinowski model outlines the most satisfactory structure of GO, which is consistent with the experimental observations, and predicts its new properties. However, the model is still not perfect. Gao et al.[34] added some new insights to the structure of GO, Figure 2-4c, in which the periphery of GO was decorated with five- and six-membered lactol rings. This suggested ring functionalities are in good agreement with the NMR spectra. Besides this flat 2D structure model, more recently Dékány et al.[36] proposed a 3D corrugated structure.

Nonetheless, the structure of GO is not reaching a consensus yet and more work is required.

2.4 Properties and applications of graphene oxide

The clarified structure of GO sheds light on its properties and instructs its use in various fields. The following two properties are of special interest.

i. *Rich chemical groups.* As discussed in section 2.3, many chemical groups are introduced to the surface of GO during oxidation of graphite. These chemical groups on GO are chemically active and ready to be functionalized. The easy functionalization could lead to various GO-based composites or make GO a suitable material for sensing applications. For example, surface functionalization of GO with DNA and bacteria has been recently achieved[5]. A graphene-based bacterium biodevice and DNA sensor have been demonstrated. The abundant surface functional groups are also used as nucleation site in our study to grow nanoparticles.

ii. *Hydrophilicity.* The oxygen-containing groups on GO render it hydrophilic. The hydrophilicity makes GO soluble in various polar solvents (e.g. H_2O) and affords it flexibility to process. Solubility allows GO to be deposited on a wide range of solid substrates as a single layer or thin film. For example, GO dissolved in a mixed solvent MeOH: H_2O (v:v=5:1) is readily spread on the surface of water to form a Langmuir film (Figure 2-5), which finds its crucial role in device fabrication and optical studies[37]. The resulting single-layer GO is also easily functionalized by nanoparticles or other biomolecules. The flexibility offered by GO is advantageous compared to the graphene obtained by other methods (Section 2.2). For example, the application of graphene in solar cells requires thin films of graphene. It could be easily achieved by drop-casting or spin-coating GO in organic solvents onto solid substrates to form GO thin films. This spin-coating method is also used in our study to obtain rGO thin film for biological studies and used as matrix in mass spectroscopy.

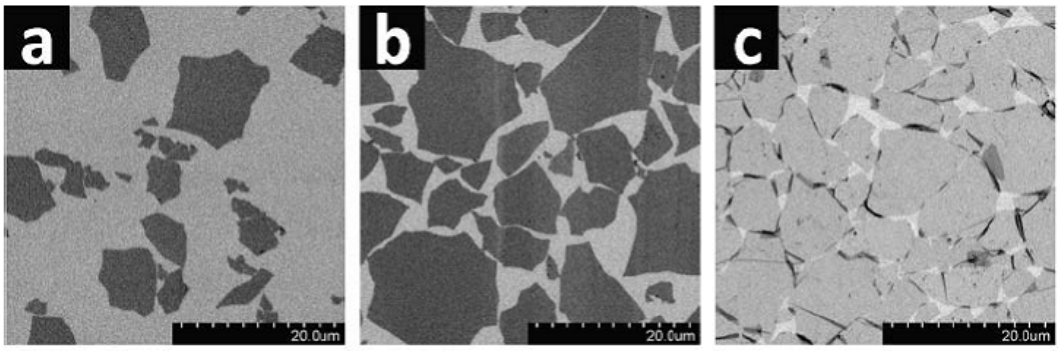

Figure 2-5 (a-c) SEM images of obtained GO Langmuir-Blodgett film with increasing surface pressure.

GO shows promise in the graphene research also because it can be reduced to rGO which show electrical properties similar to graphene. A few reduction methods have been developed:

i. *Thermal annealing.* Various groups[22, 25, 38] have demonstrated that thermal annealing of GO at high temperatures with or without a gas flow can effectively restore the electrical properties from GO to graphene. The functional groups are removed and many disorders are introduced, Figure 2-4d. However, the high temperature involved in this method hinders its use in plastic devices, in which the low-temperature melting polymer substrates are required[39].

ii. *Electrochemical reduction.* Recently our group and others independently reported the electrochemical reduction of GO[40, 41]. This method, compared with hydrazine reduction, is much more environmentally friendly. No high temperature is needed. At the same time, our group also showed that the rGO could be functionalized with glucose oxidase for biosensing applications[41]. However, the electrochemical reduction can only be performed on conductive electrodes, such as glassy carbon electrodes or ITO, which is of little value for nanoelectronics because insulating substrates are needed.

iii. *Chemical reduction.* Many reducing agents are used for the chemical reduction of GO, such as $NaBH_4$ and hydrazine. Till now, the reduction of GO in hydrazine vapor or solution is the most commonly adopted method. It

has been found that the electrical properties of single-layer GO or GO thin film can be largely restored if reduced in hydrazine vapor at elevated temperatures[21, 22] (e.g. 80 °C). The restored π-conjugated networks and functional groups make rGO similar but not exactly the same with graphene. This uniqueness will result in rGO with different chemical structure and electrical properties. In our study, we also adopt the hydrazine vapor reduction method to reduce single-layer or thin film of GO, used for cell culture studies and as matrix for mass spectroscopy. Besides this vapor reduction, many efforts are devoted to reduce GO in solution. The final aim is to obtain soluble rGO in solvents so that more flexibility to process will be gained. Surfactants[42] or mixture of solvents[43] are chosen to stabilize rGO after reduction. In our study, the rGO obtained by reducing GO in a mixture solvent [43] (e.g. 9:1 DMF: H_2O) was used a matrix for mass spectroscopy study.

It should be noted that extreme care should be taken when handling hydrazine as it is highly toxic.

In summary, owing to aforementioned unique structure and properties, GO and rGO are promising for various applications and studied in our work.

2.5 Techniques to characterize graphene-based materials

This section will briefly review the techniques to characterize graphene and its derivatives (e.g. GO and rGO).

2.5.1 Optical microscopy

A brief history of discovery of graphene will tell that the critical ingredient is needed for the observation of graphene. With the hindsight, scanning tunneling microscopy is useful to find graphene, but its low throughput never leads to the discovery of graphene. Graphene is discovered and only made visible in an optical microscopy if it is placed on a Si wafer covered by ~300 nm SiO_2[7, 9]. The interference color is responsible for the visibility of graphene which is dependent on both thickness of SiO_2 and wavelength of light. The relationship between the visibility of graphene and thickness of substrate and wavelength of light was recently revealed[44]. The mechanism of the visibility of graphene was also recently studied[45]. Although the optical microscopy is effective to identify graphene, it could not provide the useful information of the deposited graphene, such as layer numbers, the structure, etc. Therefore, other techniques are required.

2.5.2 Raman spectroscopy

With the inspected location of single- or multi-layer graphene by optical microscopy, Raman spectroscopy comes to play an important role in rapidly and accurately identifying the layer number of graphene which can be judged by the changes in the positions and relative peak heights of G and 2D bands[46]. G band arises from the doubly degenerate zone center (E_2g mode) while 2D band is the second order of zone-boundary phonons arising from double-resonance process. Raman "fingerprints" of graphene and graphene layers are shown in Figure 2-6. Raman spectroscopy has also been employed to distinguish GO and rGO[47].

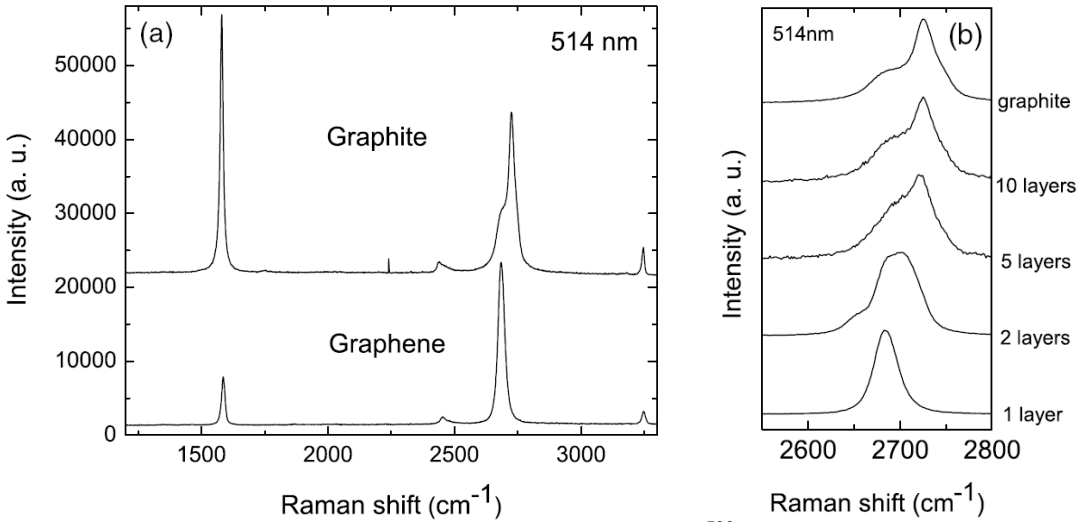

Figure 2-6 Raman spectra show the signals of G (~1584 cm^{-1}) and 2D (~2700 cm^{-1}) bands which change significantly with increasing layer number.

2.5.3 Scanning probe microscopy

A more accurate and direct technique to measure the thickness of graphene is scanning probe microscopy, including atomic force microscopy (AFM) and scanning tunneling microscopy (STM). The theoretical thickness of single-layer graphene is 0.34 nm[10]. However, due to the attraction/repulsion between AFM tips and substrates, the reported thickness ranges from 0.6 to 1 nm for single layer of graphene[9]. The thickness of GO measured by AFM ranges from 1.1 to 1.5 nm[21], in which the functional groups on both sides of GO accounts for the thickness increase.

STM has been an established tool to examine the electronic topography of graphite and other materials for a long time. The AB stacking nature of graphite makes its electronic topographic feature dramatically different from that of graphene, revealed by high resolution STM[48], Figure 2-7, in which the hexagonally symmetric honeycomb structure was observed on graphene while a three-fold symmetry pattern was observed on graphite. A recently developed "true individual atom resolution" AFM[49] would possibly be used to resolve the structure of graphene, with specific potential to resolving the structure of oxidative and non-oxidative regions of GO by identifying specific functional groups, leading to more conclusive evidence of the various structural models of GO[31, 36].

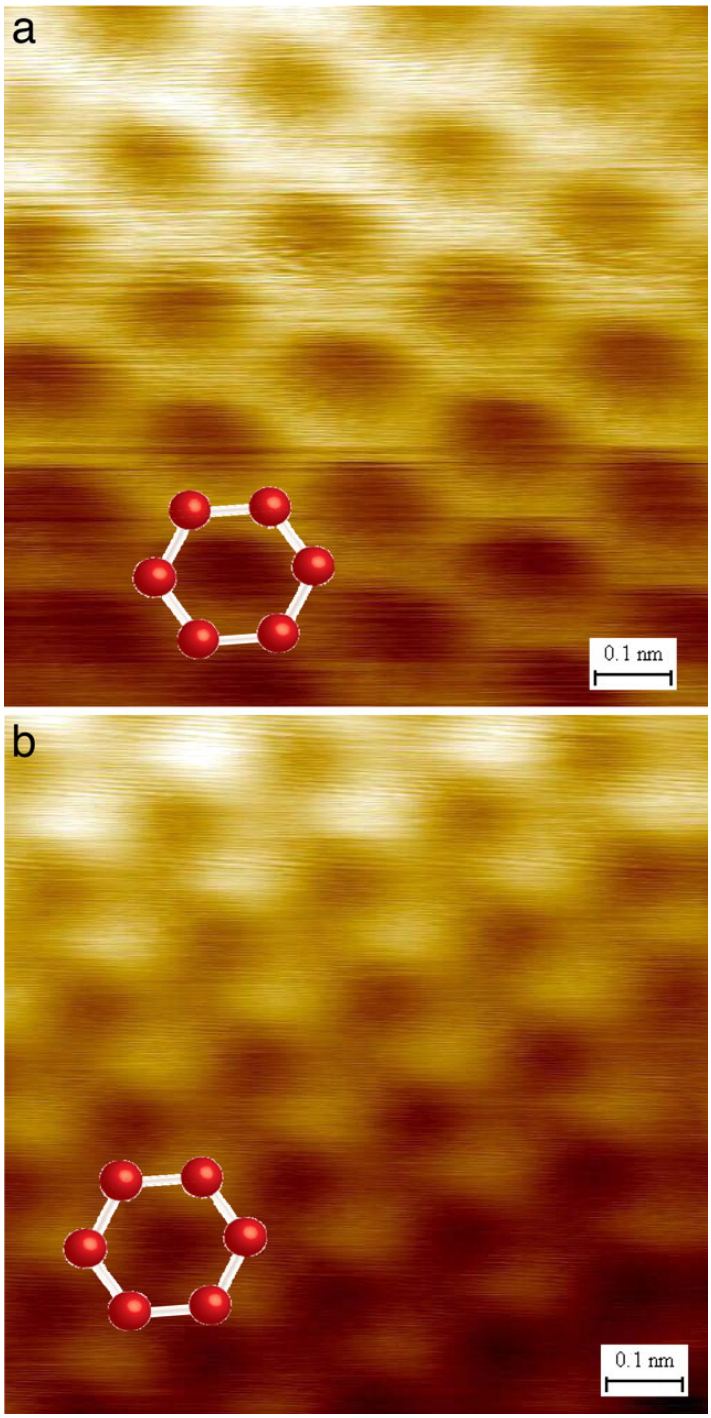

Figure 2-7 STM images of (a) single-layer and (b) multi-layer graphene flakes.

2.5.4 Transmission electron microscopy

Although transmission electron microscopy (TEM) proves difficult to examine the section of single-layer graphene (used for quasi-1D tubes), it has been used to examine the deformation of suspended graphene, the diffraction patterns of graphene and also the layer number of graphene[19, 50]. TEM studies of suspended graphene[50] have demonstrated that graphene is corrugated at a mesoscopic scale, with out-of-plane deformations up to 1 nm. By defining the lattice constants from diffraction pattern, TEM was used to distinguish graphane from graphene[51]. Most recently, TEM has been used to investigate the mechanism of edge reconstruction, and the stability of the "zigzag" edge configuration has been demonstrated by using graphene samples with holes at their center[52]. TEM was also used to analyze the structure of GO and rGO[53, 54].

Many other techniques, including scanning electron microscopy (SEM), X-ray diffraction pattern (XRD), ultraviolet-visible spectroscopy (UV) and X-ray photoelectron spectroscopy (XPS), were used to characterize GO or graphene.

Chapter 3

Materials and Experimental Details

3.1 Materials and reagents

Natural graphite (SP-1) was purchased from Bay Carbon (Bay City, Michigan, USA) and used for synthesizing graphene oxide (GO). Carboxylated single-walled carbon anotubes (SWCNT) P3 was purchased from Carbon Solutions (Riverside, California, USA). 3-aminopropyltriethoxysilane (APTES), 65% Hydrazine monohydrate, 98% H_2SO_4, 30% H_2O_2, potassium permanganate ($KMnO_4$), silver nitrate ($AgNO_3$, 99.9%), 16-Mercaptohexadecanoic acid (MHA), p-aminothiolphenol (p-ATP), and trifluoroacetic acid (TFA) were purchased from Sigma–Aldrich (St. Louis, Missouri, USA) and used in their as-received form. Sylgard@ 184 Silicone Elastomer Kit was purchased from Best Chemical Co (S) Pte Ltd (Singapore) and used for making the soft polydimethylsiloxane (PDMS) stamps. 1,3,5,7-tetravinyl-1,3,5,7-tetramethylcyclotetrasiloxane, (7-8 % vinylmethylsiloxane)-(dimethylsiloxane) copolymer, (25-30% methylhydrosiloxane)-(dimethylsiloxane) copolymer, and platinum-divinyltetramethyldisiloxane complex in xylene were purchased from Gulf Chemical (Freeport, Texas, USA) and used for the fabrication of hard-PDMS stamps. Silicon oxide wafers were purchased from Bonda Technology (Singapore). The standard solution of octachlorodibenzo-p-dioxin (OCDD) (D-801S) in toluene with a concentration at 50 µg/ml (50 ppm) was purchased from AccuStandard

company (New Haven, Connecticut, USA). Ultrapure Milli-Q water (Milli-Q System, Millipore, Billerica, MA, USA) was used in all experiments.

3.2 Sample preparation

3.2.1 Synthesis of graphene oxide (GO)

Graphite oxide was synthesized from natural graphite (SP-1) by a modified Hummers method[20, 29, 55]. 0.3 g graphite was added into a mixture of 2.4 mL 98% H_2SO_4, 0.5 g $K_2S_2O_8$, and 0.5 g P_2O_5, the solution was kept at 80 °C for 4.5 h. The resulting pre-oxidized product was washed by water and dried. After the pre-oxidized product was added into a 12 mL 98% H_2SO_4, followed by slowly adding 1.5 g $KMnO_4$ with the temperature maintained at < 20 °C in order to avoid overheating and explosion, the solution temperature was increased to 35 °C and maintained for 2 h. Then 25 mL H_2O was added. After 2 h, additional 70 mL H_2O was added to dilute the solution, and 2 mL 30% H_2O_2 was injected into the solution to react with the excess $KMnO_4$ completely. A bright yellow solution was obtained. The resulting mixture was washed by HCl and H_2O and the graphite oxide was obtained. The obtained graphite oxide was dispersed in water with a certain concentration and subsequently sonicated to give GO, Figure 3-1a.

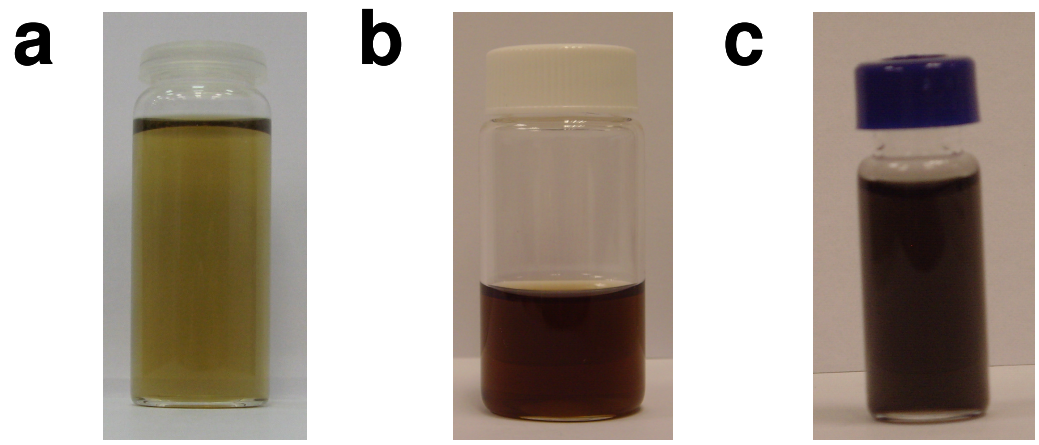

Figure 3-1 (a) GO dissolved in H_2O with low concentration. (b) GO dissolved in a mixed solvent DFM: H_2O (v:v=9:1). (c) rGO dissolved in a mixed solvent DFM: H_2O (v:v=9:1).

3.2.2 Reduction of GO in a mixed solvent of H_2O and DMF

Following the reported method[43], a suspension of GO in a mixture solvent of H_2O and DMF was obtained by sonicating GO in water (3 mg/ml, 2 ml) and then adding DMF (18 ml) to make GO concentration as 0.3 mg/ml, Figure 3-1b. The obtained brown GO suspension was reduced by adding 100 μL hydrazine and heating at 80 °C for 10 h with stirring using the magnetic stir bar. As such, rGO suspension was obtained, Figure 3-1c. Thus resulting black rGO suspension is stable and no precipitation was observed within days. If the precipitation occurred, mild sonication of the suspension would exfoliate rGO.

3.2.3 Adsorption of single-layer GO on substrates and reduction to single-layer reduced graphene oxide (rGO)

Silicon oxide substrates (1 × 1 cm^2) were cleaned in a piranha solution (H_2SO_4 (98%) / H_2O_2 (30%) = 7 : 3) at ca. 100 °C for 30 min (**CAUTION**: very strongly corrosive). The cleaned substrates were thoroughly rinsed with H_2O and dried under a N_2 flow, then treated with APTES (0.5% wt in ethanol)[56]. The obtained APTES-modified substrates were used to adsorb the single-layer GO by immersing them in a GO aqueous solution (Note: few two-layer GO may appear on APTES-modified SiO_2 due to the overlap of 2 pieces of GO sheets). The rGO was obtained by reducing the GO substrates in a hydrazine vapor environment at 65 °C overnight. The resulting GO and rGO substrates were used for growth of metal particles and the fabrication of GO nanoribbons.

3.2.4 Growth of Ag nanoparticles on GO and rGO surfaces

Figure 3-2 shows the experimental process for the synthesis of Ag nanoparticles (Ag NPs) on GO and rGO. SiO_2 substrates adsorbed with GO or rGO were immersed in a bottle containing a 5 mL aqueous solution of 0.1 M $AgNO_3$ which was purged with N_2 for 15 min and under N_2 protection during the heating process. The system was heated to 75 °C and kept for 30 min. The reaction conditions are same throughout the whole experiment unless otherwise stated. After the reaction is complete, the synthesized Ag NPs were protected from oxidation by injecting 50 μL of 2 mM 16-mercaptohexadecanoic acid (MHA) ethanol solution into the

reaction solution and incubation for 1 ~ 2 min. The GO substrates adsorbed with MHA-passivated Ag NPs were rinsed with H_2O and dried with N_2.

The Ag NPs on GO surface were immersed in a 10 mM p-aminothiolphenol (p-ATP) ethanolic solution for ca. 12 h prior to the Raman measurement.

Au NPs on GO substrate were obtained by immersing the freshly prepared Ag NPs on GO in a 2 mM $HAuCl_4$ aqueous solution overnight.

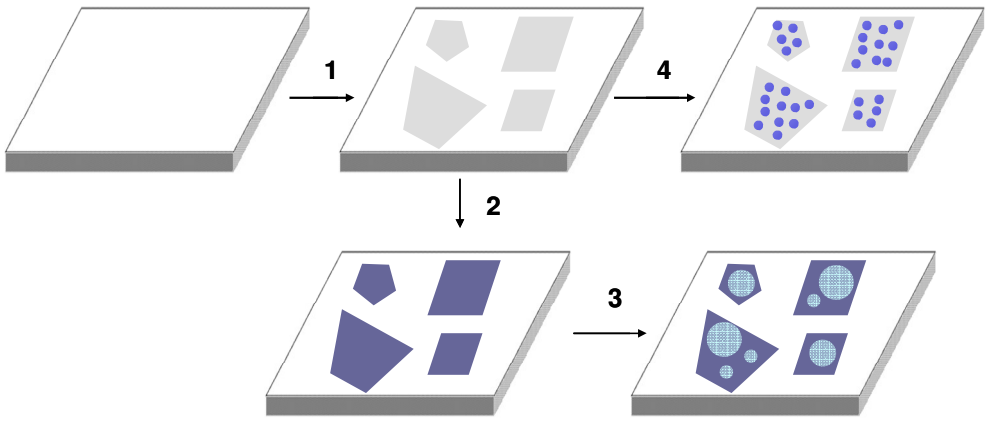

Figure 3-2 (1) GO adsorbed on the APTES-modified SiO_2. (2) rGO is obtained by reducing GO. (3) Growth of Ag particles by heating the rGO substrate in 0.1 M $AgNO_3$ at 75 °C for 30 min. (4) Growth of Ag NPs by heating the GO substrate in 0.1 M $AgNO_3$ at 75 °C for 30 min.

3.2.5 Fabrication of graphene oxide nanoribbons (GONRs)

The plasma etching was carried out in a Harrick Plasma PDC-32G-2 which has O_2 and Ar gas inlets. The SiO_2 substrate adsorbed with GO was put on a quartz tray and then placed in the plasma chamber. Plasma etching conditions, i.e. plasma gas, gas pressure, plasma power and etching time, are optimized and used for fabrication of GONRs. O_2 with a pressure of 140 mTorr was used unless otherwise indicated. The plasma etching was operated at a power of 6.8 W.

The process for fabrication of GONRs is schematically shown in Figure 3-3. Plasma etching with O_2 or Ar will result in the formation of GONRs with double layers (Figure 3-3b) or single layer (Figure 3-3c) from the graphene oxide wirnkles (GOWs) (Figure 3-3a) after the GOWs are exposed to plasma for various times. In our experiment, an etching time of 20 s will give double-layer GONRs, while an etching time of 30 s will generate single-layer GONRs, when the pressure of O_2 is 140 mTorr and the used power is 6.8 W.

The experimental conditions for growth of Ag NPs on GONRs are same as that for the growth of Ag NPs on GO and rGO (Section 3.2.4).

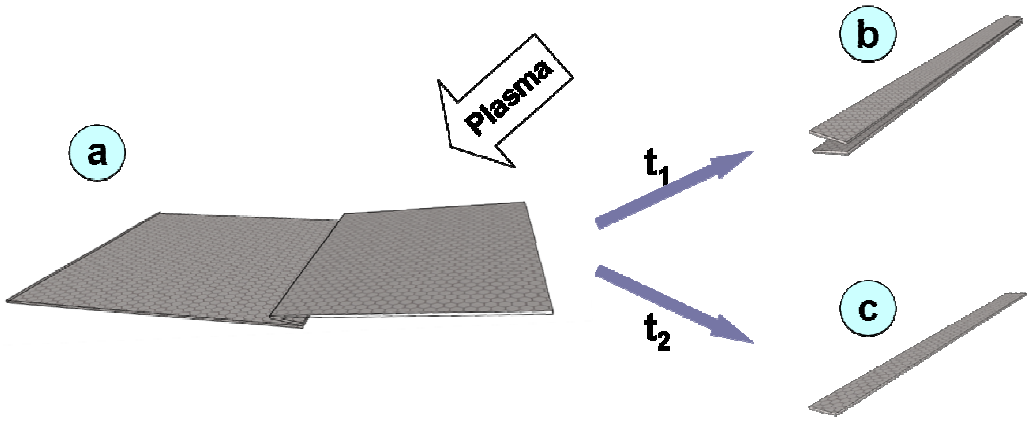

Figure 3-3 GONR generated from GOWs by plasma etching. Double- or single-layer GONRs are obtained by varying the etching time (t_2>t_1). Drawing is not to scale. The underlying SiO_2 substrate is not shown in the scheme.

3.2.6 Preparation of GO thin film and rGO thin film

The preparation of rGO thin film has been described earlier[57]. In brief, GO dispersed in water was firstly centrifuged at 5000~6000 rpm for 30 min. By decanting the supernatant, the GO was redispersed in methanol with a concentration of ~ 1 mg/ml. The redispersed GO in methanol was spin-coated at 4000 rpm onto a cleaned hydrophilic SiO_2 wafer (same cleaning process as described in Section 3.2.3). GO thin film with a reflection of brown color was obtained, Figure 3-4a. The obtained GO film was then chemically reduced with a hydrazine vapor at 65 °C overnight to give rGO film with a thickness of ~ 20 nm, Figure 3-4b.

For cell interaction studies, the resulting rGO film was detached from the SiO_2 wafer in a 0.03 M NaOH solution, then transferred onto coverslips and dried in air

at 80 °C for 1 h. For mass spectroscopic analysis, the rGO film on SiO_2 substrates was used as matrix.

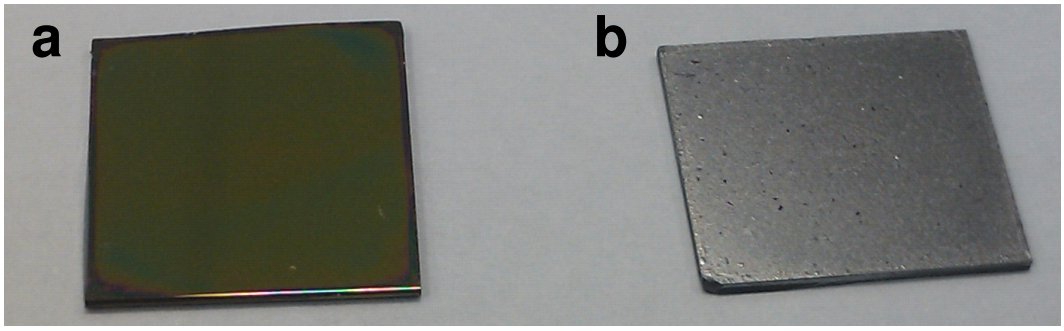

Figure 3-4 (a) GO thin film on SiO_2 obtained by spin-coating. (b) rGO thin film on SiO_2 after reduction of GO film with hydrazine vapor.

3.2.7 Cell culture

(i) Preparation of single-walled carbon anotubes (SWCNT)-networks and rGO thin film

Carboxylated-SWCNTs (SWCNT-COOH, Carbon Solution) were well-dispersed in DI-H_2O (0.2 mg/ml) with assistance of sonication for 30 min (VCX130, Sonics & Materials, Inc., Connecticut, USA). As reported previously, the thin-film of SWCNT network (SWCNT-net) was obtained via phase-separation facilitated self-assembly of dispersed SWCNTs, Figure 3-5 (This figure is adapted from Reference [58]). The resulting thin-film of SWCNT-net (~ 8 mm^2) was then transferred onto a glass cover slip, followed by rinsing with DI-H_2O and drying with N_2. The samples were then heated at 350 °C in a vacuum oven under N_2 protection for 3 h in order to remove the –COOH groups from SWCNTs[59].

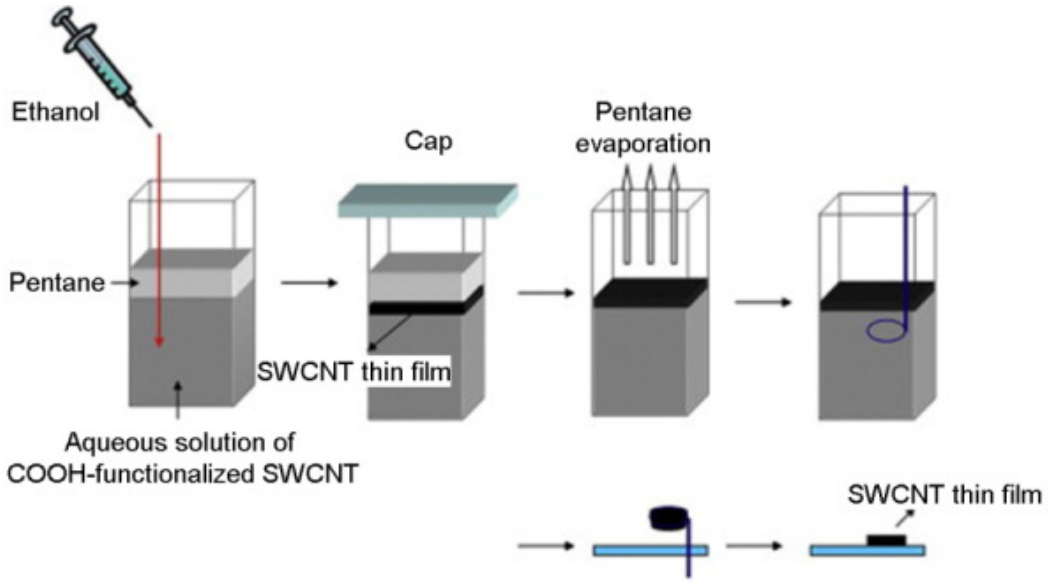

Figure 3-5 Schematic processes to make the SWCNT thin film[58].

(ii) Cell culture: Cells, culture medium and cell culture

The cells used in this study are rat pheochromocytoma (PC12) cell lines, human fetal osteoblasts (hFOB) cells, and human oligodendroglia (HOG) cells. PC12 cell line is derived from the rat adrenal medulla (kidney, according to ATCC description). hFOB osteoblast cells are obtained from human bone marrow. HOG cell line originates from the oligodendrocytes of the brain. PC12 cells were cultured in a RPMI 1640 medium containing 10% fetal bovine serum (FBS), 5% Horse serum and 1% antibiotics (Penicillin and Streptomycin), and incubated at 37 °C in a humidified atmosphere with 95% air and 5% CO_2. HOG cells were grown in Dulbecco's modified Eagle's medium (DMEM) supplemented with 10% FBS,

1% Penicillin and 4 mM L-glutamine. hFOB cells were grown in DMEM supplemented with 10% FBS and geneticin (0.3 mg/ml).

Cells were seeded (5×10^4 cells/cm^2) on SWCNT-net or rGO film substrates which were pre-sterilized by 70% ethanol for 5 min followed by rinsing with sterilized DI water. For proliferation and differentiation assays, the two nanocarbon substrates, SWCNT-net film and rGO film, were put in a small petri dish (diameter of 35 mm). For MTT assays, 24-well plates were used to accommodate the nanocarbon substrates. Cell culture medium was changed the next day after seeding and then changed every 2 days subsequently.

3.2.8 Sample preparation for MALDI-TOF-MS

(i) Preparation of analyte solution

The structure of octachlorodibenzo-p-dioxin (OCDD) is shown in Figure 3-6. The OCDD stock solution was dissolved in toluene at a concentration of 50 ppm, which was used to prepare other solutions with different concentrations (5 ppm, 500 ppb, and 50 ppb) after dilution. The volume of each diluted solution for MALDI analysis is 1 µl. As such, the quantity of the analyte is 50 ng, 5 ng, 500 pg, and 50 pg, respectively.

Unless otherwise stated, cationizing agent trifluoroacetic acid (TFA) was not added. TFA was diluted in water (1%). Before dropping the analyte, TFA solution was deposited on the surface of matrix.

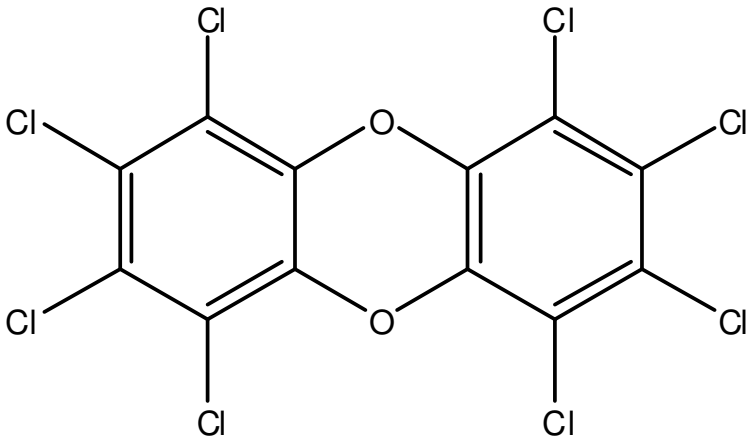

Figure 3-6 Molecular structure of octachlorodibenzo-p-dioxin (OCDD)

(ii) Preparation of samples for mass spectroscopy

The matrix, rGO thin film or carbon nanotubes thin film on SiO_2, were adhered on the ground-steel sample target plate by carbon tapes. Graphite or activated carbon was sonicated and dispersed in saturated sucrose aqueous solution. The resulting sucrose and graphite (or activated carbon) mixture was dropped on the ground-steel sample target plate, used as matrix. Then different quantities of the analyte, OCDD, were dropped on the matrices and dried. For example, if 500 ppg of OCDD was tested, 1 µL OCDD with concentration of 500 ppb was deposited on the matrices. In this experiment, OCDD with different quantity of 50 ng, 5 ng, 500 pg, and 50 pg were tested.

The rGO suspension (in DMF, 0.3 mg/ml) was used as adsorbent of solid-phase extraction and matrix. Four samples (a-d) were prepared. 100 µL (a), 10 µL (b), 5 µL (c), and 1 µL (d) of OCDD stock solution were firstly added to 40 µL rGO suspension. Then DMF was added to get 500 µL solution for all samples. After

that the samples were mixed by vortexer for 1 min to homogeneously mix rGO and OCDD. OCDD was extracted from solution and adsorbed on the surface of rGO after 2 h. Centrifugation of the above solution at 10, 000 rpm and then removal of supernatant leave rGO adsorbed with OCDD at the bottom of centrifuge tube. Finally, DMF was added to the deposit to get a 500 µL solution.

1 µL from the 500 µL final solution (a-d) was dropped on steel plate, which was used for the mass analysis. After calculation, the quantity of rGO used in samples a-d is 24 ng. The quantity of OCDD used in samples a-d is 10 ng, 1 ng, 500 pg, and 100 pg, respectively.

(iii) Mass spectroscopic analysis

All the spectrometric measurements were performed on an Axima TOF^2 mass spectrometry (Shimazu/Kratos, Singapore). Each mass spectrometer uses a nitrogen laser at 337 nm (Pulse 10 ns, 10 Hz) for desorption of analytes. Each spectrum was recorded by adding 100 laser shots using a laser energy of 56.80 µJ. The accelerating voltage is 20 kV, and the operating pressure is 10^{-6} mbar. All the mass spectra shown were obtained in a negative ion mode.

3.2.9 Printing graphene oxide

(i) Preparation of hard-PDMS stamps

The process to fabricate hard-PDMS (h-PDMS) stamps is shown in Figure 3-7 and summarized as follows:

(1) The precursor used for h-PDMS was prepared by firstly mixing (7-8 % vinylmethylsiloxane)-(dimethylsiloxane) copolymer (3.4g), 1,3,5,7-tetravinyl-1,3,5,7-tetramethylcyclotetrasiloxane (0.1g), and platinum-divinyltetramethyl-disiloxane complex in xylene (20µl) with stirring for 10 min. The obtained mixture was degassed for 3 min. 1g (25-30% methylhydrosiloxane)-(dimethylsiloxane) copolymer was then added to the above mixture and stirred for 10 min before degassing for 6 min. The obtained h-PDMS precursor was spin-coated on Si masters, which was degassed for 20 min and then heated at 70 °C for 30 min.

(2) The precursor of soft-PDMS (s-PDMS) was prepared by mixing 10 g elastomer and 1g curing agent (Sylgard® 184 Silicone Elastomer Kit) for 30 min with vigorous stirring. The precursor was then degassed for 30 min and poured on the h-PDMS coated Si masters *(step 1)* and cured at 70 °C overnight.

(3) The obtained stamp on Si master *(Step 1 and 2)* was peeled off to give h-PDMS stamp.

The h-PDMS stamp will be used to print APTES and GO on SiO_2.

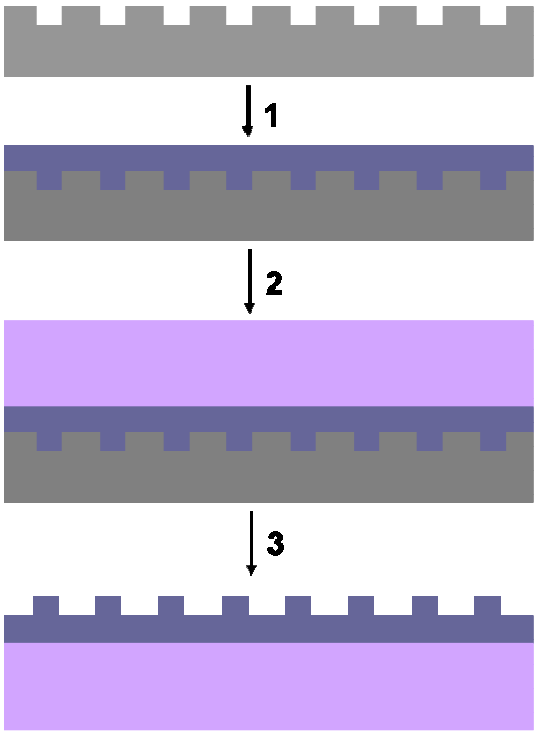

Figure 3-7 (1) The h-PDMS precursors coated and cured on a Si master. (2) The s-PDMS precursor coated and cured on an h-PDMS-coated Si master. (3) h-PDMS stamp was peeled off Si master.

(ii) Preparation of Langmuir-Blodgett film of single-layer GO

The Langmuir film of single-layer GO was formed on water surface by using the reported protocol[37]. The Langmuir-Blodgett (LB) experiment was performed in a KSV 5000 LB-system (KSV Instruments, USA). In brief, after GO was dissolved in a mixture solvent, MeOH: H_2O (v:v=5:1), the solution was dropped on the surface of subphase (water) to spread and form GO film.

(iii) Direct printing of GO

After the h-PDMS stamp was treated to be hydrophilic by O_2 plasma (140 mTorr, 8 W, 1 min), it was vertically dipped into the subphase and GO was transferred on it, as shown in Figure 3-8. The h-PDMS stamp adsorbed with GO was firmly contacted with solid substrates, such as APTES-modified SiO_2 substrates, to transfer GO to form patterns. The APTES functionalization of SiO_2 substrate is performed by incubating SiO_2 substrates in 1% APTES ethanol solution at room temperature for 45 min.

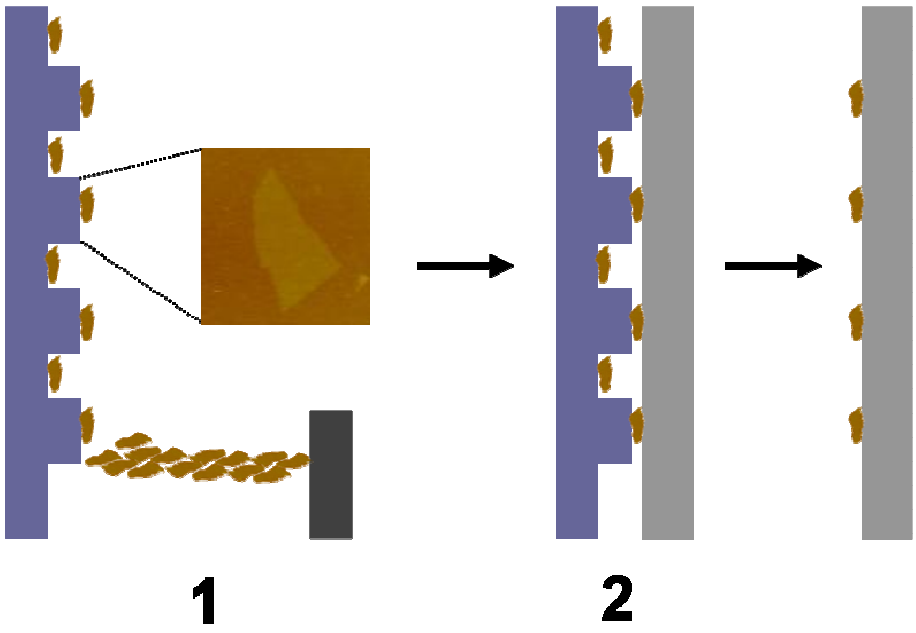

Figure 3-8 (1) Transferring of GO film onto the h-PDMS stamp. (2) Printing of GO onto APTES-modified SiO_2 substrate.

(iv) Indirect printing of GO

Figure 3-9 shows the experimental process of indirect printing of GO. After dropping 100 μL 1%APTES aqueous solution onto the h-PDMS stamp and incubated for 1 min, the solution was decanted and the stamp was dried by N_2 blow. The obtained APTES-coated h-PDMS stamp was brought to contact SiO_2 substrate for 15~20 s and then peeled off. The APTES patterns were formed on SiO_2 substrate, which was immersed in GO solution to adsorb GO on APTES patterns.

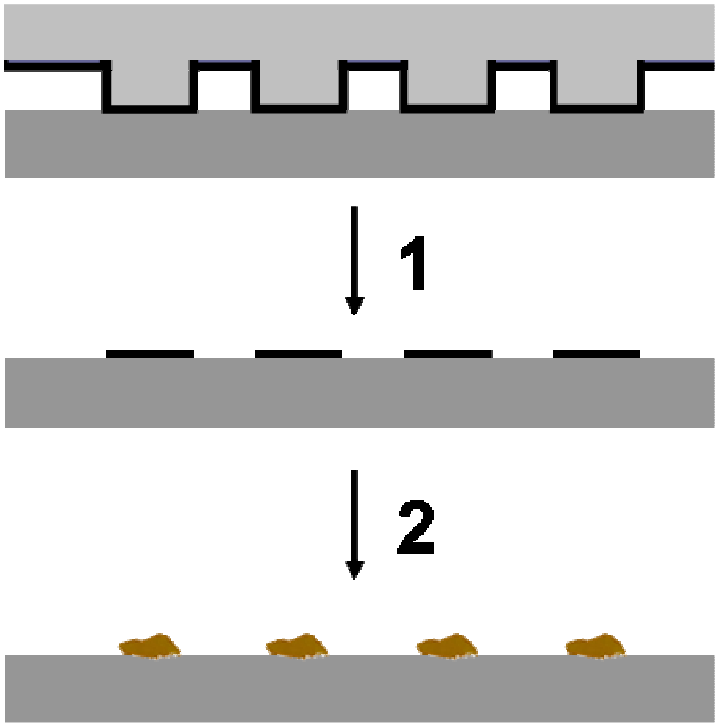

Figure 3-9 (1) APTES patterns were formed on SiO_2 substrates after transferring APTES with h-PDMS stamp. (2) GO sheets were adsorbed on APTES patterns by immersing the APTES-patterned SiO_2 substrate in GO aqueous solution.

3.3 Equipment and characterization techniques

3.3.1 Atomic force microscopy

All Atomic force microscopy (AFM) images were obtained by using Dimension 3100 (Veeco, New York, USA) in tapping mode using a Si tip (Veeco, resonant frequency, 320 kHz; spring constant, 42 N m^{-1}) under ambient conditions with a scanning rate of 1 Hz and scanning line of 512. AFM was used to characterized single layer GO and rGO films and patterns, GO nanoribbons, Ag nanoparticles on GO, SWCNT-net, etc.

3.3.2 Scanning electron microscopy

Scanning electron microscopy (SEM) was performed using a JEOL JSM-6700 field-emission scanning electron microanalyzer. An accelerating voltage of 12 kV was used for Ag nanoparticles analysis. For single-layer GO (or rGO), rGO thin film, and SWCNT-net, an accelerating voltage of 5 kV was used.

3.3.3 Transmission electron microscopy

Transmission electron microscopy (TEM) image were obtained on a JEOL JEM-2010 transmission electron microscope with an accelerating voltage of 200 kV. GO, rGO, rGO nanoribbons and Ag nanoparticles were characterized by TEM. GO in water was deposited onto a TEM copper grid. The rGO suspension in mixture

solvent of H_2O and DMF (section 3.2.2) was sonicated and deposited onto a TEM copper grid. The GO sheets decorated with Ag NPs were scratched off from SiO_2 substrate and dispersed in ethanol, which were used for TEM characterization.

3.3.4 Raman spectroscopy

Raman spectroscopy spectra were recorded with a WITec CRM200 confocal Raman microscopy system with the excitation line of 488 nm and an air cooling charge coupled device (CCD) as the detector (WITec Instruments Corp, Germany). The Raman band of a silicon wafer at 520 cm^{-1} was used as a reference to calibrate the spectrometer. Raman spectra of GO and rGO, and Raman mapping of the GO ribbons and GO patterns were recorded. Surface enhanced Raman spectroscopy (SERS) study was carried out for the Ag nanoparticles grown on GO used to detect p-aminothiolphenol (p-ATP).

3.3.5 X-ray diffraction

The graphite powders, and GO and rGO thin film were analyzed by X-ray diffractometer LabX XRD-6000 (Shimadzu, Kyoto, Japan) with Cu Ka radiation (1.5406 Å). The accelerating voltage and the applied current are 40 kV and 40 mA, respectively. The scanning angle ranges from 8 to 32°.

The MHA-passivated Ag NPs on GO were analyzed by X-ray diffraction (XRD) using X-ray diffractometer (Rigaku Dmax 2200) with Cu Ka radiation (1.5406 Å).

The accelerating voltage and the applied current are 40 kV and 40 mA, respectively. The scanning angle ranges from 35 to 85°.

3.3.6 Energy dispersive X-ray spectroscopy

Energy dispersive X-ray spectroscopy (EDX) measurements were performed on a JOEL 6360A scanning electron microscope. Ag and Au nanoparticles grown on GO and rGO were analyzed.

3.3.7 X-ray photoelectron spectroscopy

X-ray photoelectron spectroscopy (XPS) (AXIS ultra spectrometer, Kratos) with a monochromatized Al Kα X-ray source (1486.71 eV) operated at a reduced power of 150 W (15 kV and 10 mA). The base pressure in the analysis chamber was 2.66×10^{-7} Pa. The core-level spectra were obtained at a photoelectron take-off angle of 90° measured with respect to the sample surface and were recorded in 0.1 eV step with the pass energy of 40 eV. XPS was used to characterize the composition of GO, rGO and SWCNT-net before and after heating.

3.3.8 MALDI-TOF-MS instrument

All the spectrometric measurements were performed on an Axima TOF^2 mass spectrometry (Shimazu/Kratos, Singapore)

3.3.9 Cell culture: optical microscopy observation and MTT assay

(i) Optical microscopy observations

Optical microscopy (OM) was used to observe the cell adhesion and viability of PC12, hFOB, and HOG cells which were seeded and grown on rGO thin film and SWCNT-net. Cell numbers of the proliferation studies of PC12, hFOB and HOG, and of the differentiation of PC12 neuritegneisis were counted by using OM. The neurite length of neuronal differentiated PC12 cells were measured by OM.

(ii) MTT assay

PC12 cells were plated at density of 1×10^4 cells / 90 µl on SWCNT-net or rGO substrates for 4 days before MTT assay was conducted using MTT Assay Kit (Sigma-Aldrich). After cells were treated with a 10 µl MTT solution (final concentration, 0.5 mg/ml) for 4 h, the dark blue formazan crystals were solubilized with the MTT solvent (0.1 N HCl in anhydrous isopropanol) and the absorbance at 570 nm was measured with a microplate reader (Bio-Tek Instruments).

Chapter 4

Properties and Applications of Single- and Few-Layer Graphene Oxide and Reduced Graphene Oxide

4.1 Overview

This chapter focuses on the properties and applications of single- and few-layer graphene oxide (GO) and reduced graphene oxide (rGO). Three parts of work will be discussed. First, single-layer GO and rGO are used as templates to grow Ag and Au nanoparticles (NPs). Ag particles with different morphologies were observed on GO and rGO. Second, graphene oxide nanoribbons (GONRs) were fabricated by oxygen plasma etching graphene oxide wrinkles (GOWs). Single- and double-layered GONRs were obtained. The GONRs were also successfully decorated with Ag NPs. Third, patterning GO on solid substrates was demonstrated. The scroll of rGO was observed and will be discussed.

4.2 Characterization of GO and rGO

The following techniques, commonly used to characterize graphene made by micromechanical cleavage method, are also used to characterize GO and rGO. The basic properties of the synthesized GO and rGO are revealed below.

4.2.1 Atomic force microscopy

Atomic force microscopy (AFM) has been a powerful tool to characterize graphene for its thickness and size. After the synthesized GO was deposited the APTES-modified SiO_2 substrate, the substrate was characterized by AFM, as shown in Figure 4-1a. It was found that GO with a size of several μm has been adsorbed on the APTES-modified SiO_2 substrate. The measured thickness of GO sheet was ~ 1.3 nm, which means that single layer GO sheet was obtained. This is in good agreement with the previous report[20]. Figure 4-1b shows the AFM image of rGO at the same location as that in Figure 4-1a. By comparing Figure 4-1a and Figure 4-1b, the height of rGO is seen to decrease to 1 nm after the GO was reduced with a hydrazine vapor. This height decrease arises from the removal of functional groups on GO surface after reduction. The height of both GO and rGO was different than that of pristine graphene (~ 0.7 nm), mainly due to the different interaction of AFM tip with GO, rGO and graphene.

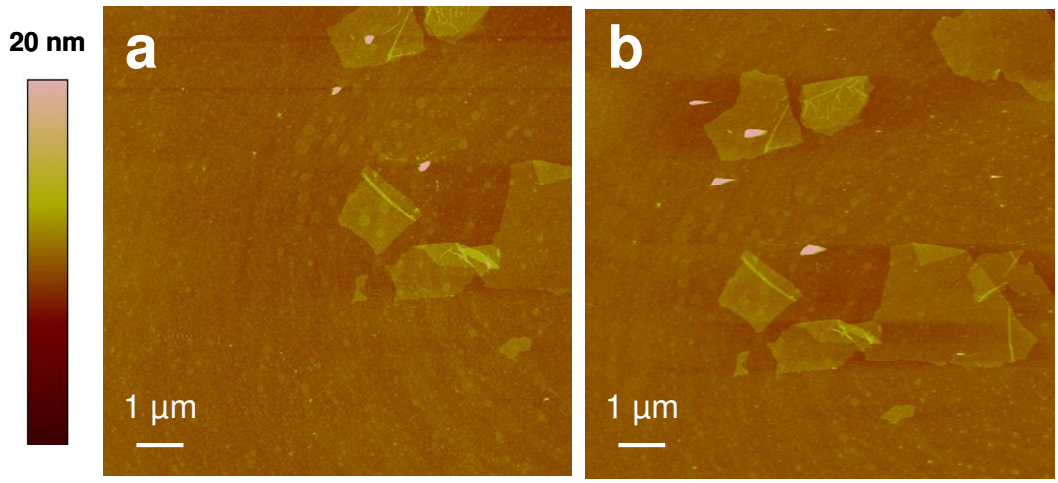

Figure 4-1 AFM topographic images of (a) GO and (b) rGO at the same location.

4.2.2 Transmission electron microscopy

Transmission electron microscopy (TEM) has been applied to characterize the crystallinity of graphene. Analysis of the diffraction patterns can help to distinguish if the graphene has a single, double or multilayer structure. Due to the strong oxidation process, GO becomes amorphous as the order of graphitic plane was destroyed and many functional groups were introduced. Figure 4-2a shows the TEM image of a GO sheet. The diffraction pattern, inset of Figure 4-2a, confirms that GO is amorphous. Whereas, after hydrazine reduction (section 3.2.2), the crystallinity was restored to rGO. Its diffraction pattern is similar to that of graphene, Figure 4-2b. The restored crystallinity means the rGO is also composed of π-conjugated carbon networks, affording it high conductivity.

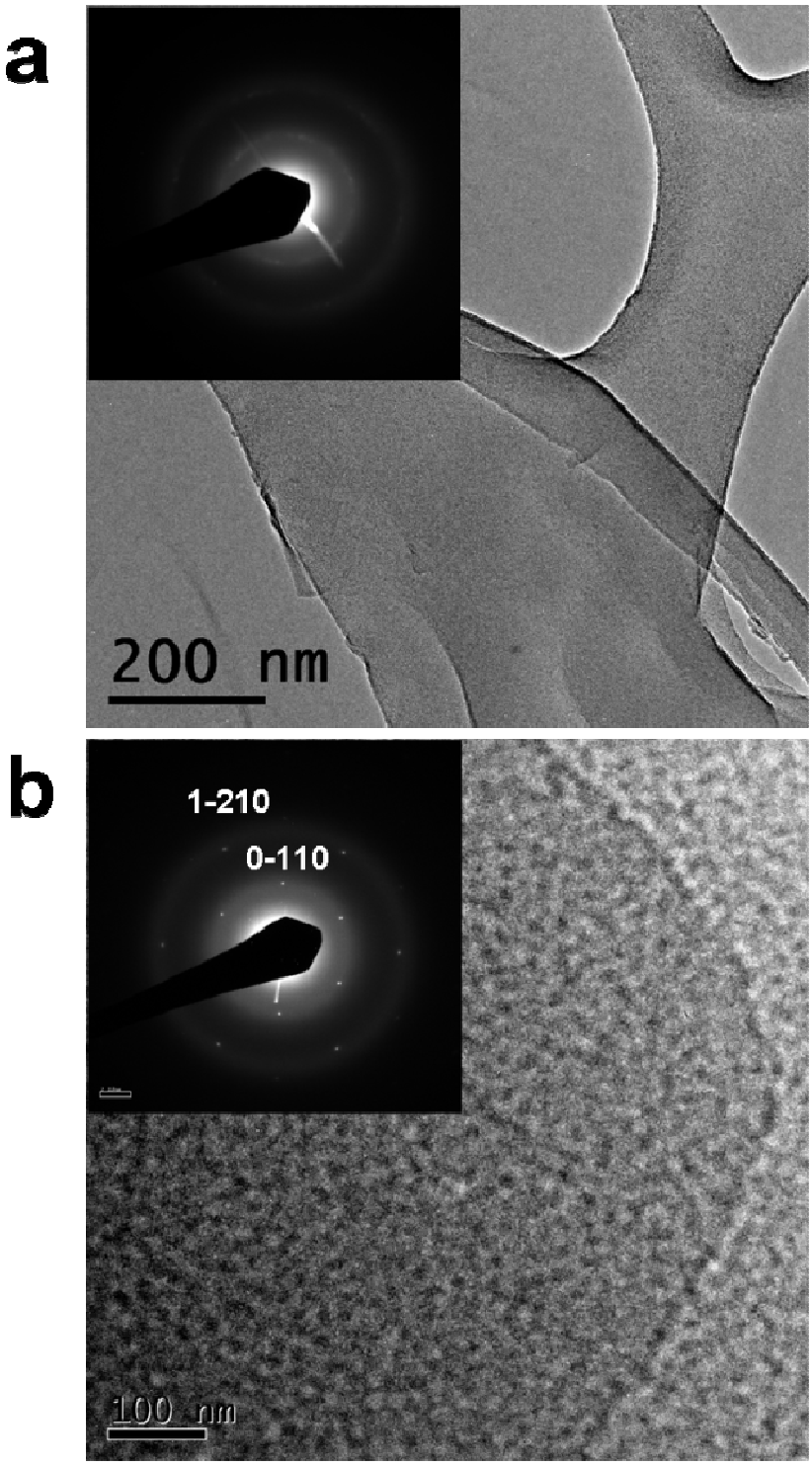

Figure 4-2 TEM image of (a) GO and (b) rGO sheets. Insets: the respective diffraction pattern of GO and rGO.

4.2.3 X-ray diffraction pattern

Graphite is composed of stacking layers of graphene. The plane-to-plane distance of the graphene was measured at 0.34 nm by using the X-ray diffraction pattern (XRD). Due to oxygen functional groups introduced onto GO, the plane-to-plane distance of graphite oxide is increased. We can easily obtain the inter-planer spacing by solving the Bragg's equation $\lambda = 2d \times \sin(\theta)$, where λ is the wavelength of the X-ray, d is the spacing between the planes in the atomic lattice, and θ is the angle between the incident ray and the scattering planes. Figure 4-3 shows the XRD pattern of GO film (a), rGO film (b), and graphite (c). The GO film pattern (a) has a peak at $2\theta = 11.58°$, corresponding to the inter-plane spacing of 7.64 Å. While rGO film and graphite have an intense peak at $2\theta = 26.16°$ and $2\theta = 26.6°$, corresponding to the inter-plane spacing of 3.40 Å and 3.35 Å. The results indicate that the rGO is almost fully reduced, but the residual functional groups render the inter-plane distance of rGO slightly bigger than that of graphite.

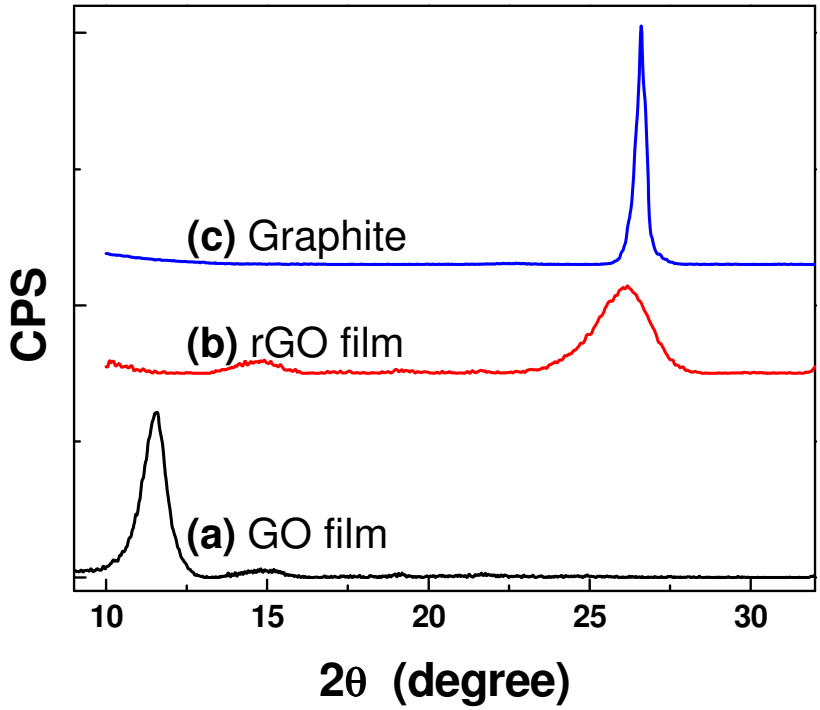

Figure 4-3 XRD patterns of (a) GO film, (b) rGO film and (c) graphite.

4.2.4 X-ray photoelectron spectroscopy

X-ray photoelectron spectroscopy (XPS) is a powerful tool to characterize the elemental composition and chemical states of the elements in materials. We have employed XPS to analyze the GO and rGO, Figure 4-4. The C1s spectrum of GO (Figure 4-4a) clearly indicates that the considerable degree of oxidation occurred with three components that are attributed to different carbon states: (1) the benzene-ring carbon (248.8 eV), (2) C-O bonds (~286.9 eV) and C=O bonds (~288.6 eV). Therefore, GO is rich in oxygenated functional groups on its surface. While the C1s spectrum of rGO (Figure 4-4b) shows that much of the oxygenated functional groups are removed: the intensity of C-O and C=O bonds are greatly

decreased. Note that an additional component at 285.9 eV appeared after reduction. This component is assigned to C-N bond which was introduced by the reaction of hydrazine with GO. Figure 4-4c shows the XPS spectra of GO and rGO with a whole range of binding energy whereby C1s, N1s and O1s spectra were identified. Comparison of the spectrum of GO and rGO, Figure 4-4c, clearly shows that a large amount of oxygenated functionalities have been removed from GO after reduction. Taken together, XPS analysis indicates that both deoxygenation and nitrogen incorporation occurred during the GO reduction process.

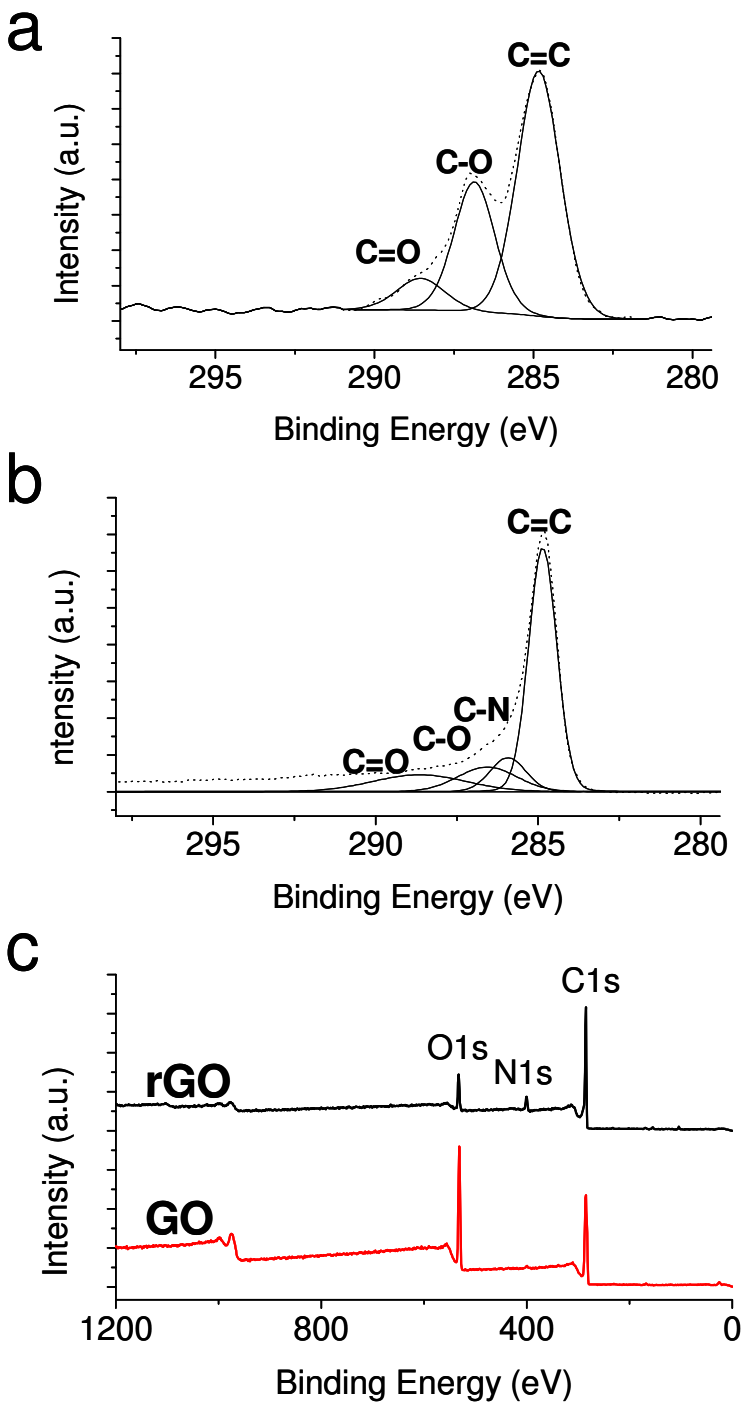

Figure 4-4 XPS spectra of C1s for (a) GO and (b) rGO, and (c) survey scan of GO and rGO at whole binding energy range.

4.3 In-situ synthesis of metal nanoparticles on single-layer graphene oxide and reduced graphene oxide surfaces

4.3.1 Introduction

As introduced in Chapter 2, GO and rGO have many potential applications due to their unique structures and properties. Among them, it is of great interest and importance to make nanoparticle (NP)-GO (or rGO) composites. For example, metal oxide NPs, such as Co_3O_4[60] and TiO_2[61] have been deposited on GO sheets to form composites. Due to the catalytic activities of the aforementioned NPs, the resulted composites showed promises in catalysis applications.

However, few reports used GO or rGO as a template to directly synthesize metal NPs, and fabricate metal NP-GO composites on substrates. Metal NPs are important due to their optical, catalytic and electrical properties[62]. It is also a long-term desire to integrate metal NPs into composite materials to explore their properties and applications. Therefore, it is critically interesting if metal NPs can be integrated with GO or rGO or synthesized by using GO or rGO as a template. Recently, Muszynski et al.[63] have synthesized Au NPs by using the chemical reduction of $HAuCl_4$ with $NaBH_4$ in the graphene-octadecylamine suspension. However, there is no report to directly synthesize metal NPs on single-layer GO surface without adding any reducing agent. We present a simple method to synthesize metal Ag nanoparticles (NPs) on GO and rGO surfaces as follows.

4.3.2 Growth of Ag nanoparticles on GO and rGO

Figure 4-5 shows the SEM image of Ag particles grown on rGO surface. A lot of large plate-like Ag particles are adsorbed on the rGO surface. The plate-like particles were also confirmed by AFM, Figure 4-6. The height of the Ag particles is ~ 80 nm. Figure 4-7 shows the XRD and EDX patterns of the particles on rGO, which confirm that Ag particles other than Ag_2O particles were obtained by this heating process. Importantly, note that in our experiment, no additional reducing agent was added. During the experiment, the UV-Vis spectra did not show any characteristic evidence of Ag particles forming in the solution. Therefore, we believe that the rGO substrate serves as not only a template to adsorb Ag particles but also the donor of electrons for the growth of Ag particles. Very recently, similar to our work, Jung et al. used rGO films to directly reduce $HAuCl_4$ to get Au NPs without adding any reducing agent[64]. They proposed the mechanism for reduction of Au NPs on rGO which likely involves Galvanic displacement and redox reaction due to the relative potential difference. The similar mechanism has been proposed to explain the decoration of carbon nanotubes with metal particles[65]. Based on their description, our observation can be explained in the following reasons. First, since the electrons in the negatively charged substrate can participate in the reduction of metal cations[66], Ag^+ could obtain the electron present in the negatively charged rGO (zeta potential measured as -6.5 mV) surface to form Ag NPs.

Second, since the reduction potential of the rGO is +0.38 V vs. SHE (standard hydrogen electrode)[64], which is lower than that of Ag^+ (+0.73 V vs. SHE)[a]. Therefore, it is possible for Ag^+ in an aqueous solution to be reduced spontaneously on rGO surface since the electrons can be donated from negative-charged rGO surface, which also has lower reduction potential. The size of Ag particles is not uniform, ranging from a few tens of nm to 1 µm (Figure 4-5). The large distribution of formed Ag particles is similar to that of Au NPs formed on rGO sheets with size ranging from several to 200 nm[64].

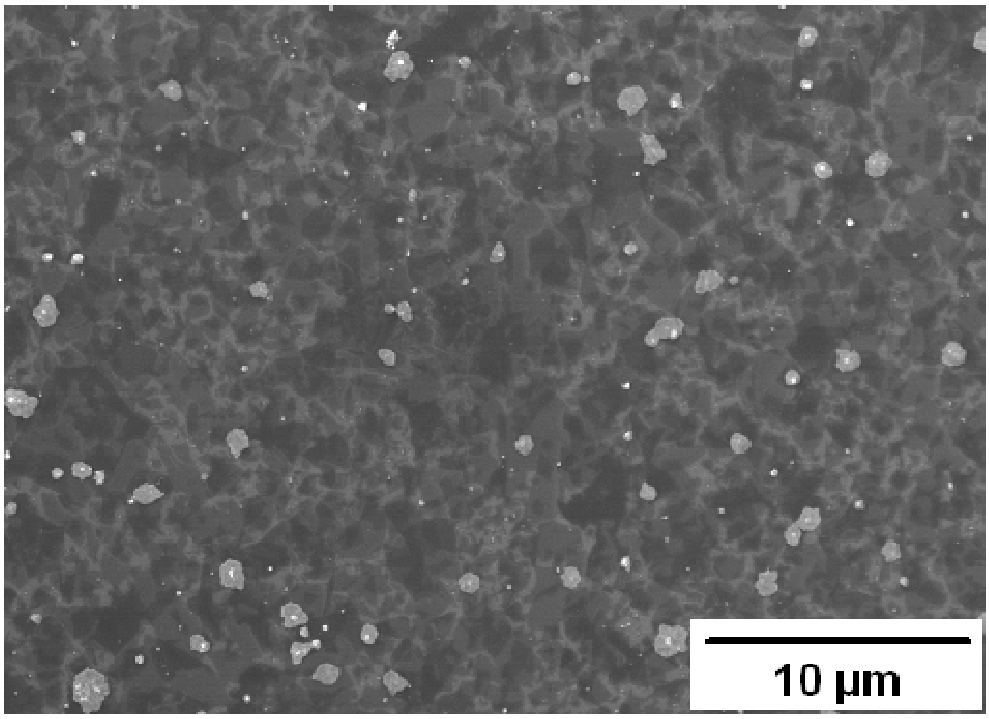

Figure 4-5 SEM image of large Ag particles grown on rGO surface.

[a] Nernst equation, $E = E^0 + \frac{RT}{nF}\ln\frac{[Ag^+]}{[Ag]}$, was used for reaction $Ag^+ + e^- \rightarrow Ag$, where $[Ag^+]$ and [Ag] are the concentrations of Ag^+ and Ag, respectively, R is the universal gas constant (8.314 J K^{-1} mol^{-1}), T is the absolute temperature, F is the Faraday constant (96485 C mol^{-1}), and n is the number of electrons transferred in the half-cell reaction. E^0 (Ag^+/Ag) = 0.80 V *vs.* SHE. When T = 75 °C = 348.15 K and $[Ag^+]$ = 0.1 M, the calculated E (Ag^+/Ag) = 0.73 V *vs.* SHE, which is higher than the reduction potential of rGO.

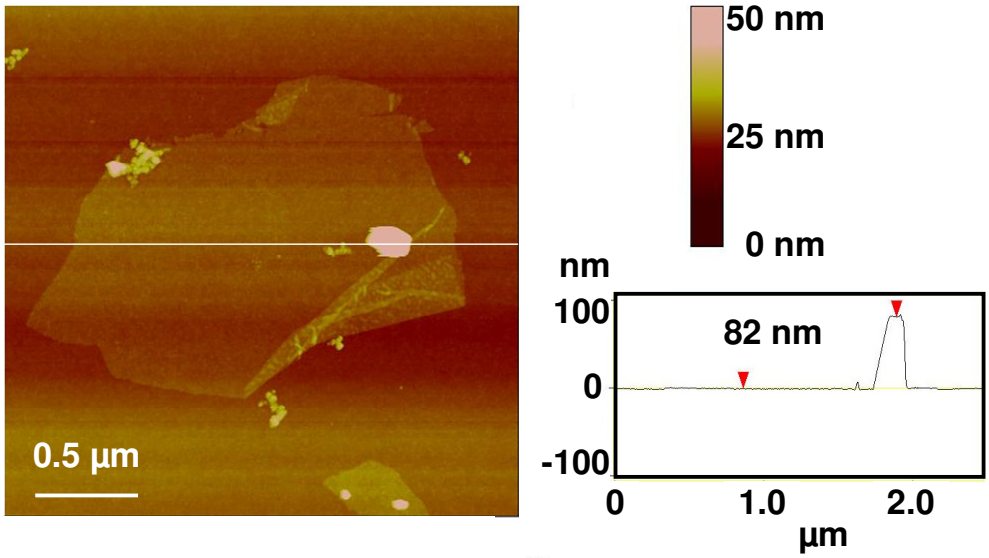

Figure 4-6 AFM topographic image and a height profile of large Ag particles grown on rGO.

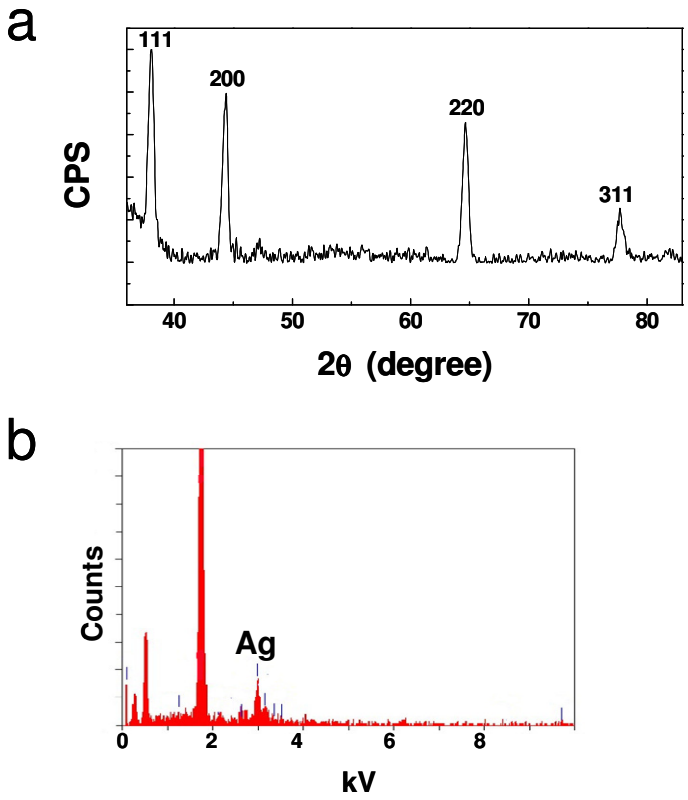

Figure 4-7 Confirmation of Ag particles grown on rGO by (a) XRD pattern and (b) EDX (the most intense signal is Si from underlying SiO_2 substrate).

In contrast, the Ag particles synthesized on GO surface by the same procedure are different. Figure 4-8 shows the SEM image of Ag nanoparticles (NPs) grown on GO surface. Lots of small Ag NPs are observed and sitting exclusively on GO surface. Note that nearly no Ag NPs adsorbed on the bare APTES-modified SiO_2. The measured NP size is 6.0 ± 3.6 nm, based on TEM analysis, Figure 4-9a. Figure 4-9b shows the high resolution TEM (HRTEM) image of individual NPs with perfect crystallinity. The inter-plane distance of (111) is measured as 2.3Å. This value is in agreement with the distance calculated from XRD, Figure 4-10, by solving Bragg's equation, $\lambda = 2d \times \sin(\theta)$, where λ =1.54 Å and 2θ =38.36°. The component of the particles is assigned to be Ag based on EDX results and the XRD pattern which matches that of Ag, Figure 4-10.

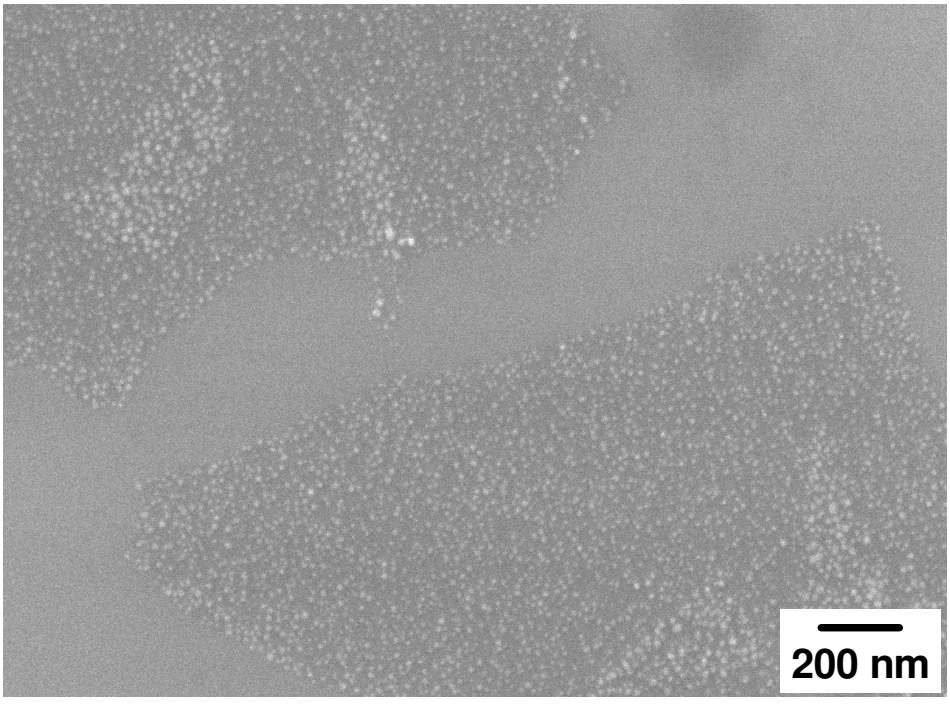

Figure 4-8 SEM image of Ag NPs grown on GO.

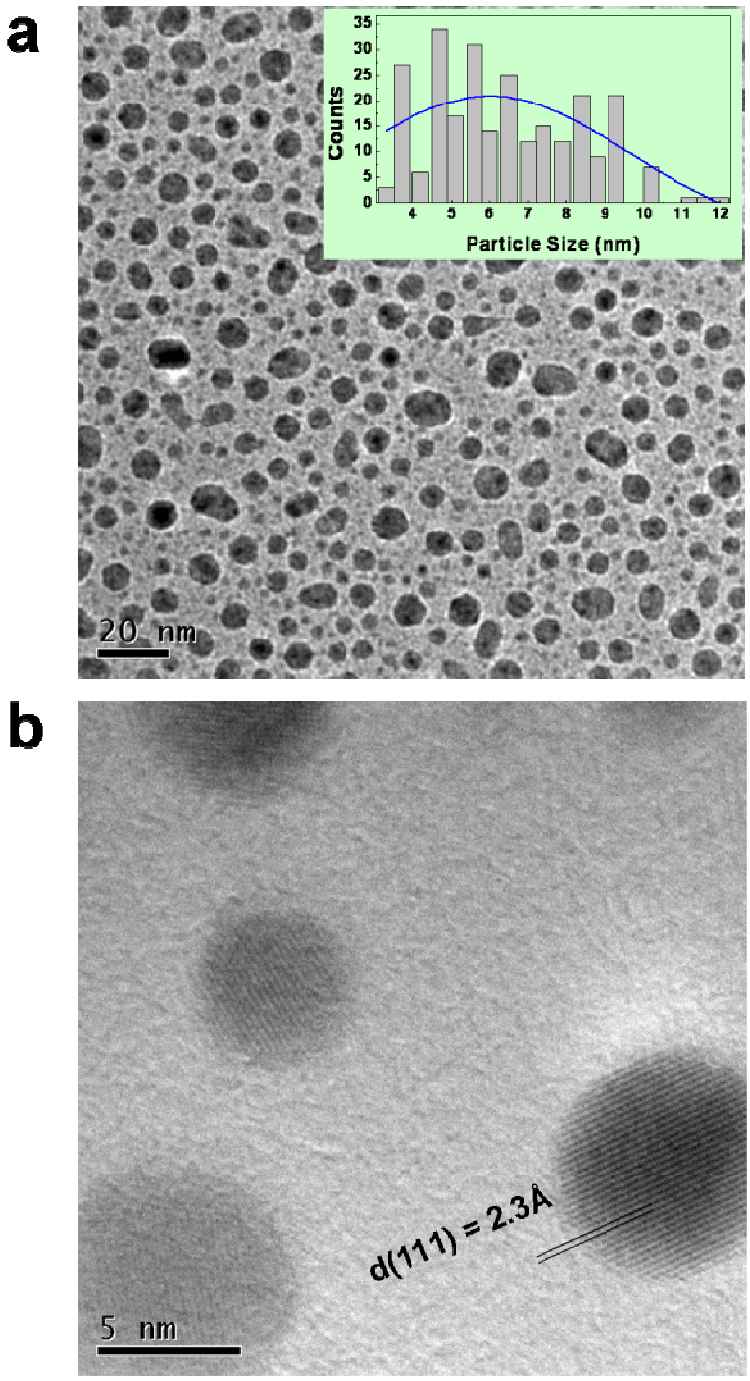

Figure 4-9 (a) TEM image of Ag NPs grown on GO. The diameter of Ag NPs are 6.0±3.6 nm. Inset: histogram of particle size distribution. (b) HRTEM images of the Ag NPs. The inter-plane distance of (111) lattice planes was indicated.

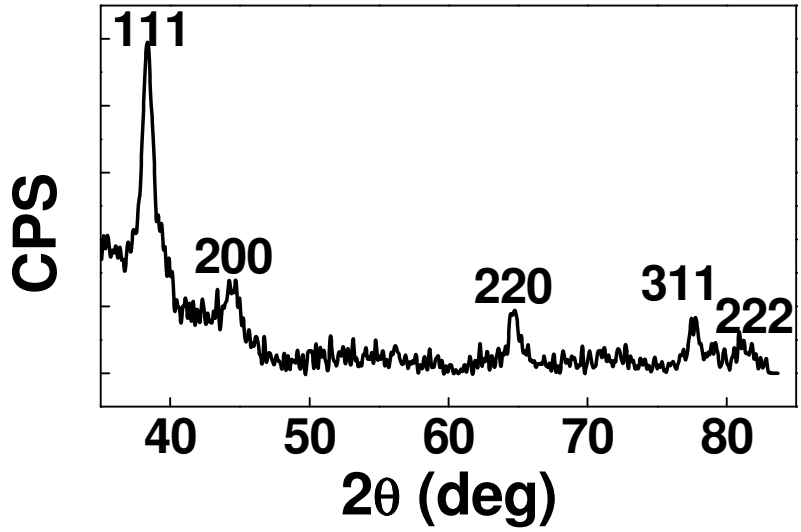

Figure 4-10 XRD pattern of Ag NPs grown on GO surface.

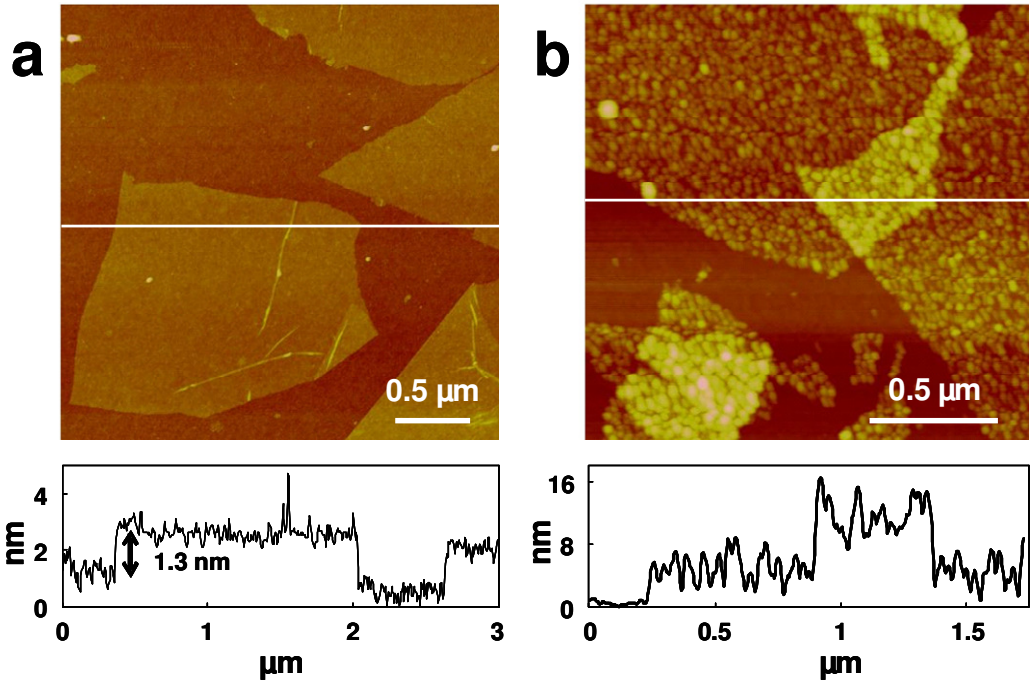

Figure 4-11 AFM topographic image and height profile of (a) single-layer GO adsorbed on APTES-modified SiO_2 substrate, and (b) Ag NPs grown on GO.

The morphology of the Ag NPs was also characterized by AFM, Figure 4-11. The cross-section analysis shows that the obtained Ag NPs has a size of ~ 6 nm, which is in agreement with the measurement of TEM.

Interestingly, in Figure 4-8 and 4-11b, the higher density of Ag NPs with smaller size are formed on GO surface compared to the lower-density and bigger Ag particles formed on rGO (Figure 4-5). This is reasonable if we take a look at the structure of GO. The GO sheet, which contains carboxylic acid, hydroxyl and epoxide groups, can be considered as the oxidation of graphene. In other words, it can be said that the GO sheet is composed of many small aromatic conjugated domains modified with the functional groups mentioned above. The more functional groups present on GO provide more nucleation sites; meanwhile, much quantity of small aromatic conjugated domains on GO will act as electron-donating sources to reduce Ag^+ ions and form smaller Ag NPs[21, 31]. This further supports our proposed Ag NP formation mechanism on rGO as mentioned above. Therefore, it is reasonable to believe that the carboxylic acid, hydroxyl or epoxide groups on GO surface might be used as nucleation sites for growth of the metal particles. This also explains why larger and less density Ag NPs are formed on rGO. After rGO is obtained from the reduction of GO, less functional groups will remain on rGO as nucleation sites, resulting in the formation of fewer particles. Meanwhile, the large-restored π-conjugated networks will provide more electrons to reduce Ag^+ ions and form the larger Ag particles.

Importantly, the size of Ag NPs is affected by the reaction time. At reaction time of 10 min, Ag NPs formed on GO show lower density and smaller diameter (2.7 ± 0.8 nm, characterized by AFM, Figure 4-12), as compared to Ag NPs obtained in 30-min reaction (Figure 4-11b). Therefore, our method offers a convenient approach to control the particle size by changing the reaction time.

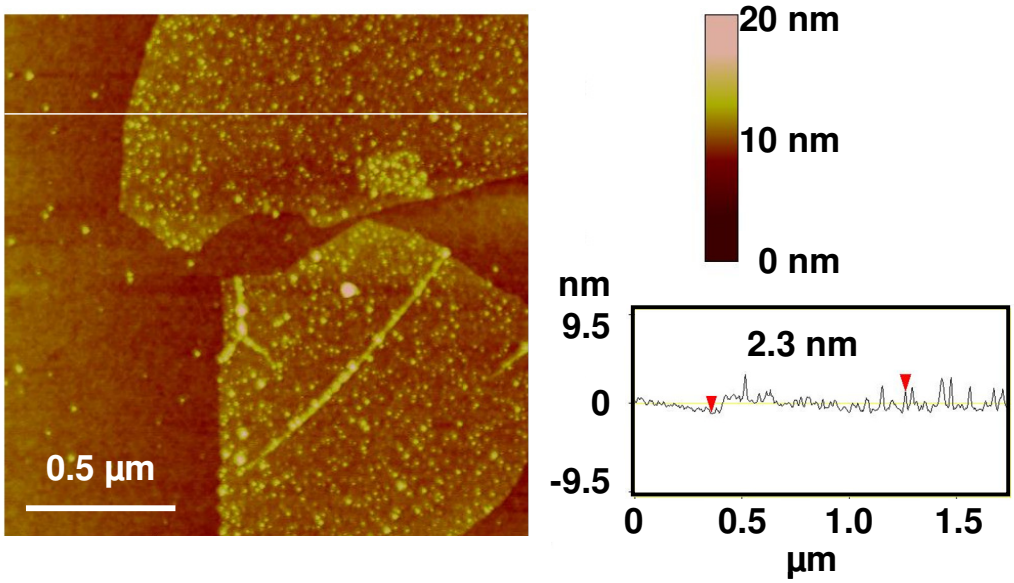

Figure 4-12 AFM topographic image and height profile of Ag NPs grown on GO surface. The particle size on single-layer GO is ~2.7 nm. Reaction conditions: heating GO substrates in 0.1M $AgNO_3$ at 75℃ for 10min.

As is known, without any surface passivation, Ag NPs will be slowly oxidized to Ag_2O once moved out of solution. In our experiment, 16-mercaptohexadecanoic acid (MHA) was added after the reduction reaction was complete. The self-assembled monolayers (SAMs) of MHA can be formed on the Ag NP surface based on the Ag-thiol bonding[67], which protects Ag NPs from oxidation.

Figure 4-13 shows that Ag NPs are grown on GO line patterns (the method to pattern GO is described in Section 3.2.9). Combining the GO patterns and Ag NP growth, the patterns of Ag NPs are easily achieved.

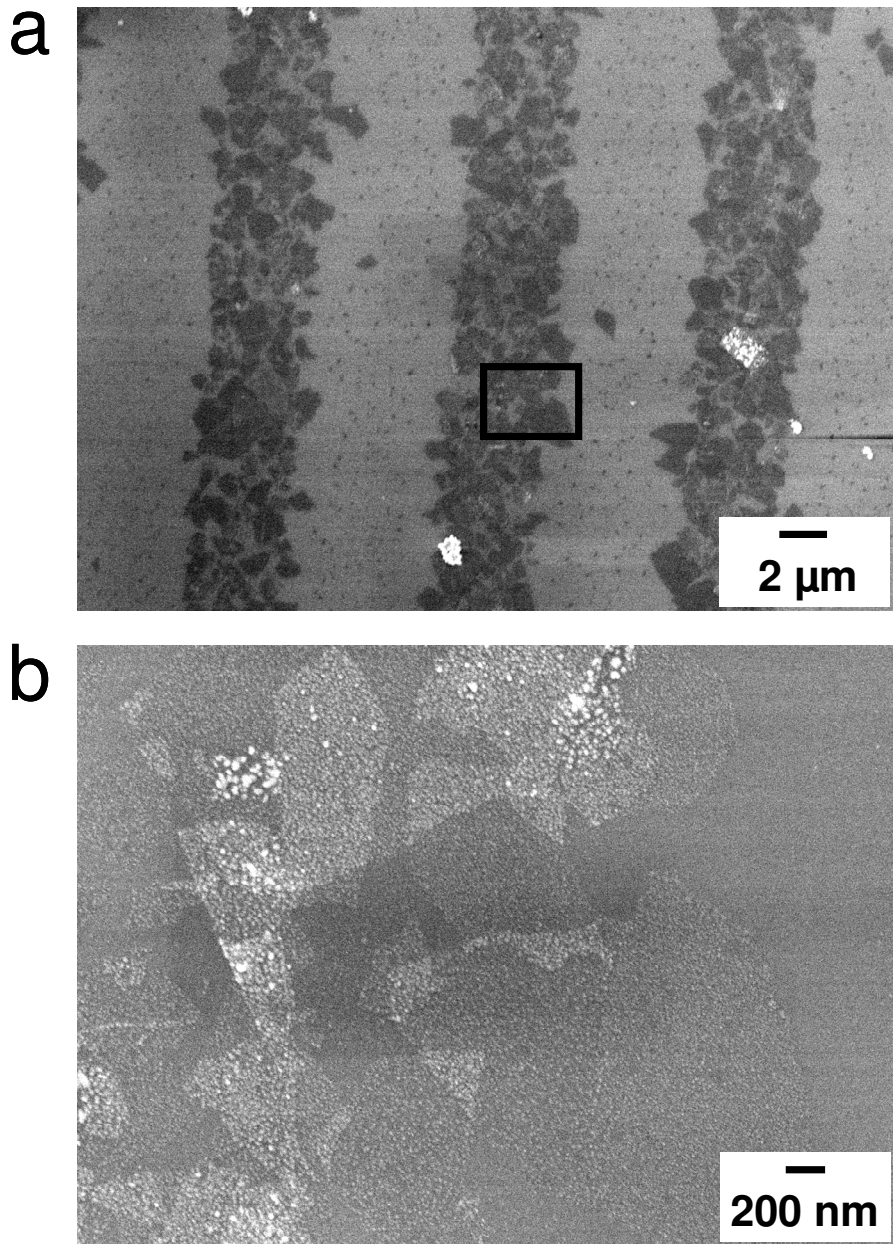

Figure 4-13 (a) SEM image of Ag NPs grown on GO patterns. (b) Zoom-in image from the square in (a).

4.3.3 Surface enhanced Raman spectroscopy

Surface enhanced Raman spectroscopy (SERS) on Ag NPs is well studied [68, 69]. Our experiment proved that the as-synthesized Ag NPs on GO are a suitable substrate for SERS.

The p-aminothiophenol (p-ATP) is used as a probe molecule. By immersing Ag NPs on GO surface in a 10 mM ethanolic p-ATP solution for ~ 12 h, SAMs of p-ATP were formed on the surface of Ag NPs. Since the incubation time of Ag NPs on GO in a very dilute MHA solution is only 1 ~ 2 min[b], only loose disordered and low density MHA SAMs formed on Ag NP surface[67]. Therefore, after the overnight incubation of Ag NPs on GO in a high concentration of p-ATP (10 mM), the p-ATP can form SAMs in the vacant surface area on Ag NPs unoccupied by MHA. Figure 4-14 shows the Raman spectrum of the solid p-ATP on SiO_2 and the SERS spectrum of p-ATP SAMs on Ag NPs on GO surface. The normal Raman spectrum of solid p-ATP, Figure 4-14a, is in accordance with the previous report[69]. By comparing Figure 4-14a and b, it is easily found that the b_2 modes at 1432, 1389, and 1140 cm^{-1}, and the a_1 mode at 1075 cm^{-1} are greatly enhanced. We attribute this enhancement to the electromagnetic effect and charge transfer, which have been suggested elsewhere[69, 70].

[b] A 50 µL of 2 mM MHA ethanolic solution was injected into a 5 mL silver nitrate solution and incubated for 1 ~ 2 min. Therefore, the concentration of MHA in solution was diluted to ~ 20 µM. In this experimental condition, the loose and disordered MHA SAMs are formed on the surface of Ag NPs.

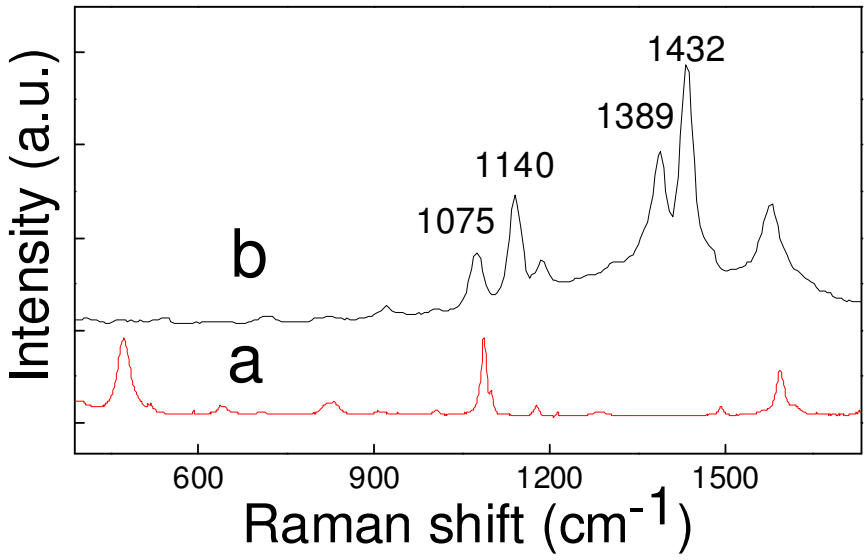

Figure 4-14 (a) Raman spectrum of solid p-ATP and (b) SERS spectrum of p-ATP on Ag NPs on GO surface. 488 nm as excitation source was used.

4.3.4 Growth of Au nanoparticles on GO

In addition to the successful synthesis of Ag NPs-GO composites, the effort for synthesis of Au NP-GO composites was carried out as well.

After the freshly prepared Ag NPs on GO substrate (Figure 4-8 and 4-11b) was immersed in a 2 mM aqueous $HAuCl_4$ solution overnight, Au NPs were formed on GO surface due to the redox reaction between Ag and Au^{3+}. Figure 4-15 shows the Au particles formed on GO surface. Compared to Ag NPs on GO (Figure 4-8 and 4-11b), the number of Au NPs is fewer. This is reasonable because 3 Ag atoms are

needed to provide electrons to reduce 1 Au^{3+} ion. In addition, the Au NPs are less uniform than Ag NPs. It can be explained by the fact that Au NPs formed during the redox process might not firmly attach to GO surface, which are relatively easy to be removed or washed away. This also explains why there are a few Au NPs adsorbed on the bare APTES-modified SiO_2 uncovered by GO sheets. The formed Au NPs was confirmed by EDX and XRD (insets in Figure 4-15).

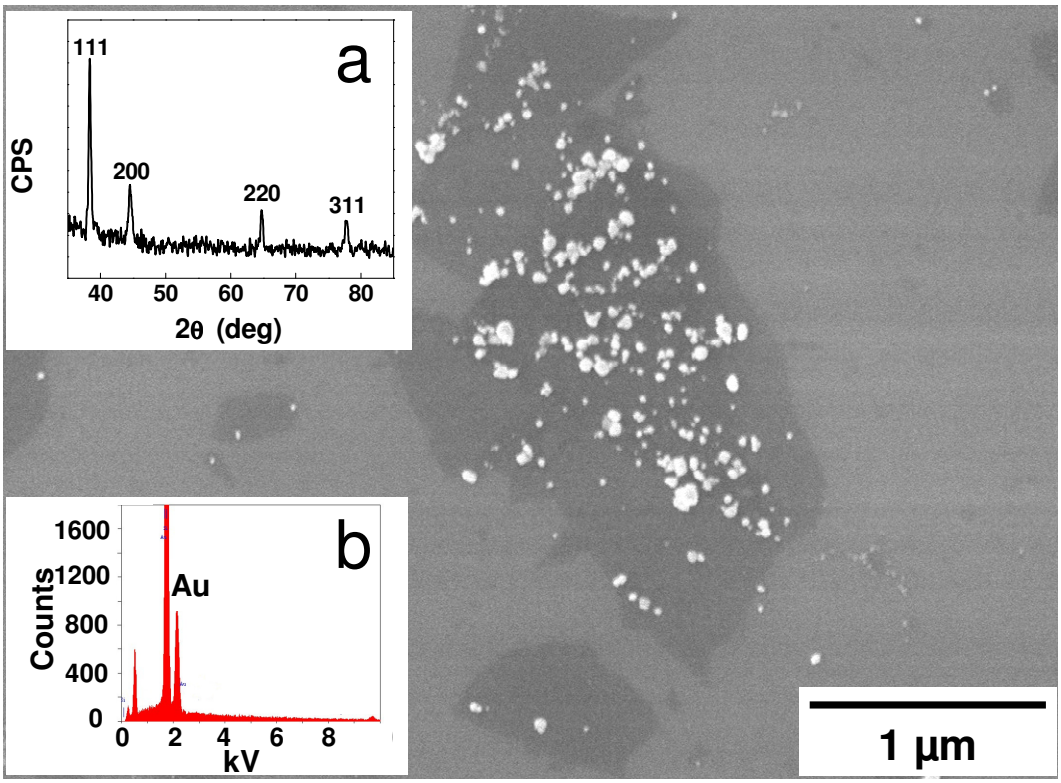

Figure 4-15 SEM image of Au NPs on GO surface. Insets: (a) XRD pattern of Au NPs, and (b) EDX confirmation of Au element.

4.3.5 Short summary

In summary, we have demonstrated that the Ag NPs can be directly reduced on GO and rGO surface without adding any reducing agent. This approach is of considerable interest and importance as it offers a facile way to synthesize Ag NPs with controllable size, which only involves heating aqueous solution of silver nitrate.

4.4 Fabrication of graphene oxide nanoribbons

4.4.1 Introduction

Graphene, made by the mechanical cleavage method[9], or grown epitaxially from surfaces[18] or by CVD method[15, 16], has a zero-bandgap without semi-conducting properties, hindering its application in nanoelectronics. Therefore, it is necessary to open the bandgap in graphene. One typical approach is to make graphene nanoribbons (GNRs), which has been theoretically predicted to be semi-conducting with the width reduced down to sub-10 nm[71, 72]. Thus-resulting semi-conducting characteristics arises from the quantum confinement effect and edge effect from the small width[71-73]. Recent experimental progress has revealed such properties with a great promise for real applications, such as in p-type and n-type graphene field effect transistors (FETs)[3, 74, 75]. The all-semiconducting properties offered by GNRs might rival or even replace CNTs as the extreme chirality is required for CNTs to be metals or semiconductors[76, 77]. Reliable production of such nanoribbons is also needed for various investigations[78]. Therefore, how to make GNRs is key in their applications. A few methods have been reported to make GNRs recently[2, 3, 74, 79-81]. Among them, both of the chemically sonicating expandable graphite[3] and the physically and chemically unzipping CNTs[74, 79] show great promises. GNRs with a width down to 5 nm have been achieved and show outstanding electrical performance. However, new simple methods used to produce GNRs are still required in order to

investigate the potential applications of this material, such as in biology, electronics, magnetism, and catalysis[78].

After the synthesized GO was adsorbed onto APTES-modified SiO_2 substrates (Section 3.2.3), the graphene oxide wrinkles (GOWs) frequently formed when the GO sheets are large (e.g. > several μm). GOWs contain three overlapped layers of GO and are responsible for producing the GO nanoribbons (GONRs) as discussed below. The GOWs are difficult to avoid, which presumably originates from the oxidation process[82, 83]. Inspired by the recent GNR fabrication with plasma etching[80], in which Si nanowires were used as etch masks, we tried to use the top layers (first or second layer, indicated in the Figure 3-3) of the GOWs as sacrificial layers to make double- or even single-layer GONRs by using plasma etching.

It should be clarified that the obtained ribbons in our experiment are actually graphene oxide nanoribbons (GONRs). However, after the hydrazine reduction or heat treatment[22], the GONRs can be reduced to reduced GONRs (rGONRs), which could be used to fabricate the rGONR-based nanodevices.

4.4.2 Fabrication of graphene oxide nanoribbons from graphene oxide wrinkles

Figure 4-16 shows the AFM images of GOWs, and the fabricated double- and single-layer GONRs, which are used to monitor the obtainment of double- and single-layer GONRs during the plasma etching process. A typical GOW with a

height of ~ 3.3 nm as measured by AFM (Figure 4-16a) indicates 3 layer GO sheets overlapped, in accordance with the proposed formation manner of GOWs (Figure 3-3), since the height of single-layer GO is ~ 1 nm. After 20 s plasma etching, the single layer GO sheet surrounding the GOWs is etched away and the GONR with a height of ~ 2.3 nm was obtained (Figure 4-16b), which means that the double-layer GONR was obtained. With continuous plasma etching for another 10 s, the single-layer GONR with a height of ~ 1.2 nm is achieved, Figure 4-16c. These results clearly show that our experiment can achieve the atomic layer control through the plasma etching, and the controlled layer-by-layer etching of the GOWs is obtained by using the first or second layer of GOWs as the sacrificial layer. It is worth noting that during the fabrication of GO sheets in our experiment (section 3.2.1), the mild sonication will yield large pieces of GO sheets with size ranging from several to 10 μm, and the wrinkles can form after adsorption of GO sheets on the APTES-modified SiO_2 substrates. During the strong sonication, only small GO sheets with a size of several hundred nm were obtained, leading to no formation of wrinkles, as the wrinkle lines might be difficult to form in a small GO sheet. Thus, it is reasonable to believe that the longer GONRs could be fabricated if the GO sheets are large enough.

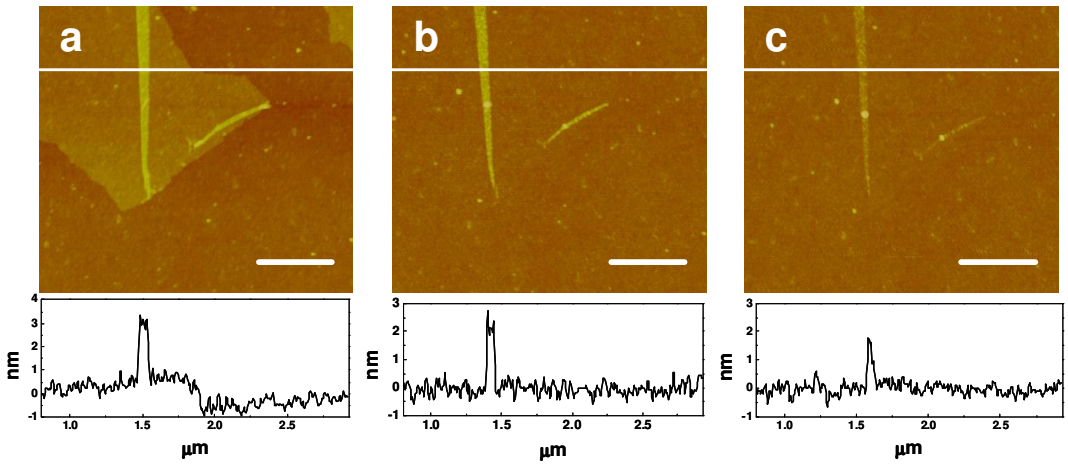

Figure 4-16 AFM images used to monitor the plasma etching process. (a) GOWs form in single GO sheet. The average height is 3.3 nm. (b) After 20 s etching, double-layer GONRs are obtained. The average height is 2.3 nm. (c) After 30 s etching, single-layer GONRs are obtained. The average height is 1 nm. Scale bars = 500 nm. Height scale is 20 nm.

GONRs with different length and width were also achieved by using this method. Figure 4-17 shows AFM images of GONRs. GONRs with a height of ~ 2 nm, corresponding to the double-layer GO, were obtained (Figure 4-17a-c). This can be obtained by selectively etching the top-layer of the GOWs and the other surrounding single layer GO. In order to simplify the experiment and make it easily controllable, we only change the etching time with a fixed etching power and gas pressure (section 3.2.5). The width of the fabricated GONRs varies and depends on the width of GOWs. The double-layer GONRs with an average width of 30, 50, and 90 nm, respectively, were achieved (Figure 4-17a-c). The length of GONRs typically ranges from a few hundred nanometers to a few micrometers. Figure 4-18b shows a ribbon with a length of 2 µm.

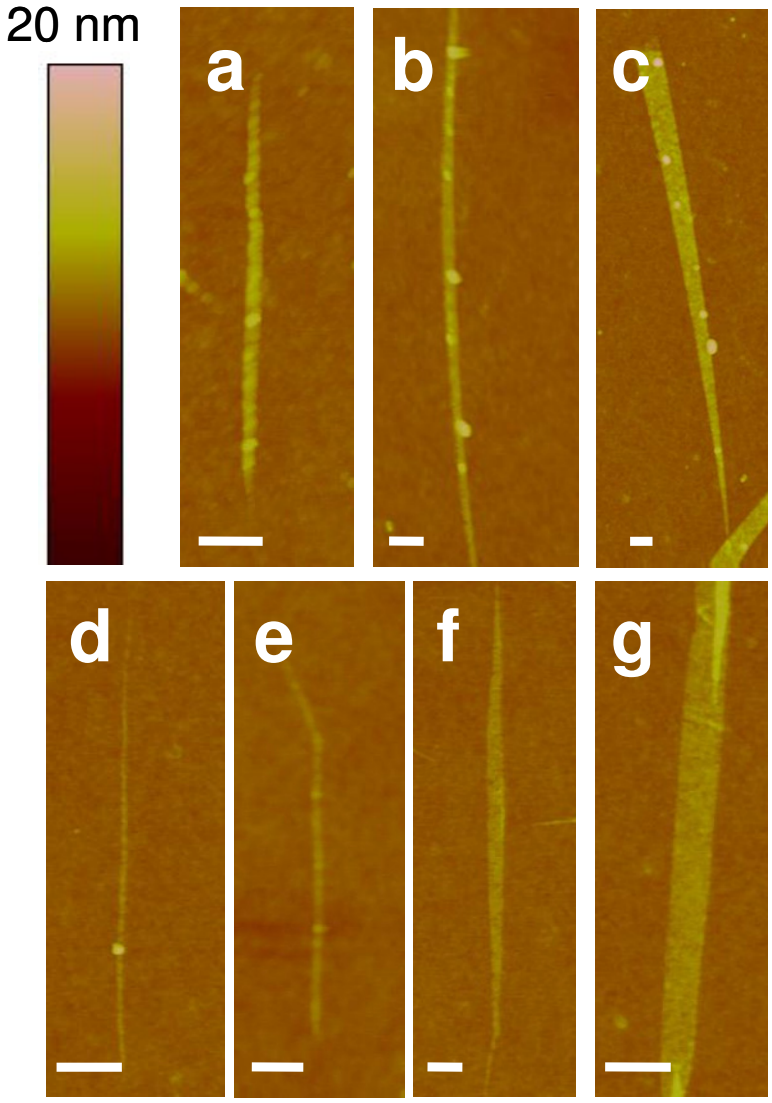

Figure 4-17 AFM images of double- and single-layer GONRs. (a-c) Double-layer GONRs with heights and widths of 2.3 and 30 nm (a), 2.0 and 50 nm (b), and 2.3 and 90 nm (c) measured in the middle of the ribbon, respectively. (d-g) single-layer GONRs with heights and widths of 0.9 and 15 nm (d), 1.1 and 25 nm (e), 1.3 and 40 nm (f), and 1.4 and 100 nm (g), respectively. Scale bars = 100 nm.

If an etching time of 30 s was used, single-layer GONRs can be obtained directly from the GOWs (Figure 4-17d-g), where the height of GONRs is ~ 1 nm, in agreement with the height of single-layer GO. Meanwhile, different widths of GONRs with different lengths were obtained, which depend on those of the GOWs. Until now the smallest width of GONR we obtained is ~ 15 nm (Figure 4-17d). After GONR was reduced by hydrazine or heat treatment, rGONR was obtained. GNR with a width of around this value is interesting as the narrower GNR will give a high I_{on}/I_{off} value, which is needed in the transistor applications[74].

As expected, the plasma condition plays a critical role in the attainment of single- or double-layer GONRs. This is evidenced by the etching process which is monitored by AFM (Figure 4-16). In addition, GONRs obtained from over-etching is shown in Figure 4-18, further evidencing the criticality of etching time. The longer etching time used in Figure 4-18 gives the discontinuity in the remaining ribbons and GO sheets, indicating that an over-etching occurred. Therefore, the etching time should be accurately controlled based on the required layers of GONRs.

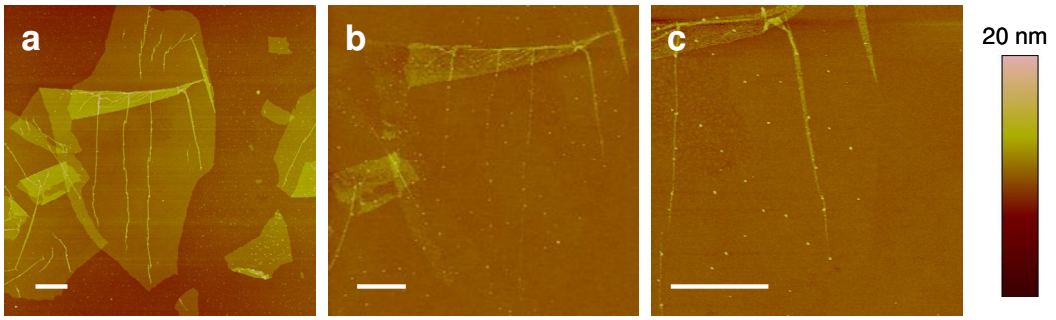

Figure 4-18 Overetching of GOWs. AFM images of (a) GOWs, (b) broken and discontinuous GONRs due to overetching, (c) a magnified image of (b). Scale bars = 1 μm.

After plasma etching, the single layer GO sheet surrounding the GOWs was etched away and GONRs were formed, which was proved by AFM (Figure 4-16). Figure 4-19 shows the SEM, AFM and Raman mapping of the same GONRs. From the Raman mapping and spectra (Figure 4-19c and d), it is further confirmed that GONRs were fabricated because the area surrounding GONRs gives no signal of GO, which means that the surrounding GO was completely etched away after plasma etching. Note that the GONRs will give similar Raman spectra as GO does (Figure 4-19c and d). The positions 1 and 2 show the signal of D and G bands, while the position 3 shows no detectable signal of D and G bands which is the same as that in other empty area without adsorption of GO. This verifies the successful fabrication of GONRs with our method.

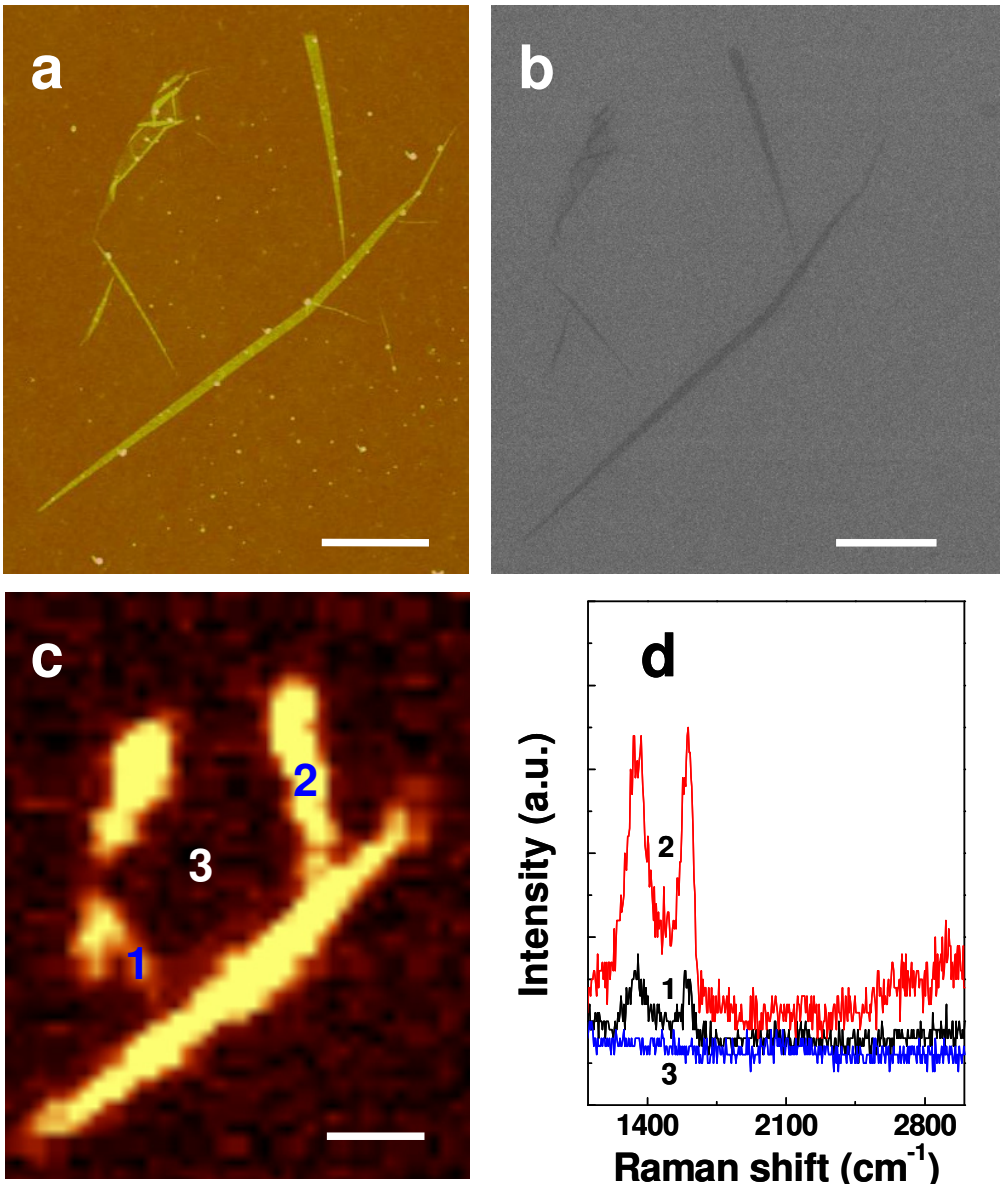

Figure 4-19 (a) AFM, (b) SEM, and (c) Raman mapping of D band (1315 to 1400 cm^{-1}) confirm that GONRs were fabricated. (d) The corresponding spectra of positions at 1, 2 and 3 in (c), respectively. Clearly, outside GONRs, no signal of D and G bands were detected in position 3. Scale bars = 1 µm.

After the GONRs were reduced in a hydrazine vapor environment, the obtained rGONR is further characterized by TEM. Figure 4-20 shows the TEM image of a typical rGONR with a width of ~ 50 nm. Note that the width of the rGONR should be larger if it roll-up behavior is taken into account.

It is worth mentioning that GONRs are frequently observed to be surrounded by some residual GO sheets, Figure 4-18b and c. This could be avoided if GO sheets have no overlapping after they are adsorbed on the APTES-modified SiO_2 substrates. In our experiment, less overlapping is observed when a lower concentration of GO solution is used. However, the amount of the produced GONRs is also decreased. How to optimize experimental conditions to realize the isolated but dense GONRs is currently ongoing in our lab.

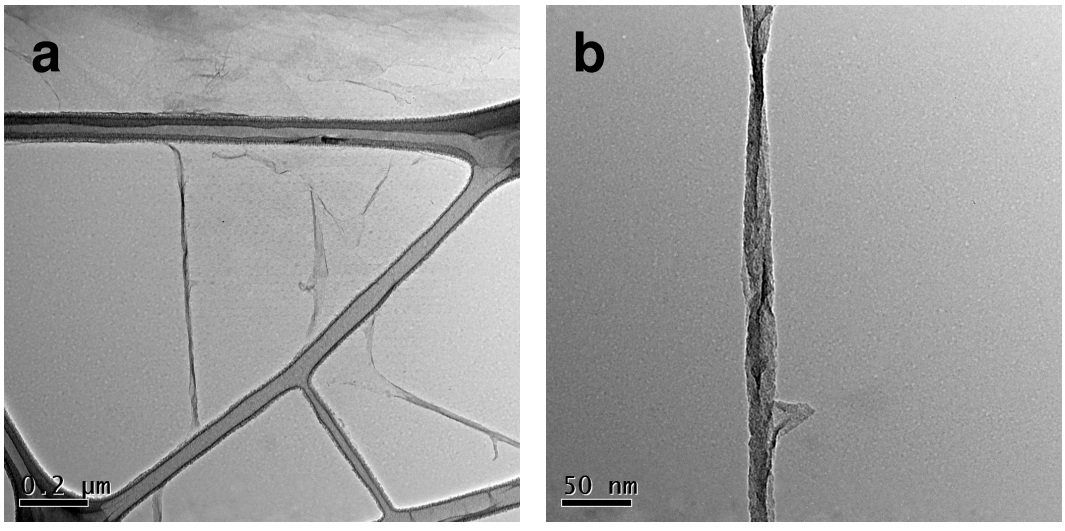

Figure 4-20 TEM images of rGONRs. Roll-up behavior is observed along the rGNORs. (b) The magnified image of (a).

4.4.3 Growth of Ag nanoparticles on GONRs

Thus-fabricated GONRs are subject to decoration with Ag NPs. Figure 4-21 shows the SEM and AFM images of a GONR on which Ag NPs were grown. The size of Ag NPs obtained here is ~ 6 nm measured by AFM, which is similar to that of Ag NPs on GO demonstrated in Section 4.3.2. The obtained Ag NP-GONR composite might have applications in nanoelectronics, optics, etc. The rGONRs were also subjected to decoration with Ag particles, with the finding that larger Ag particles with less density were grown on rGONRs.

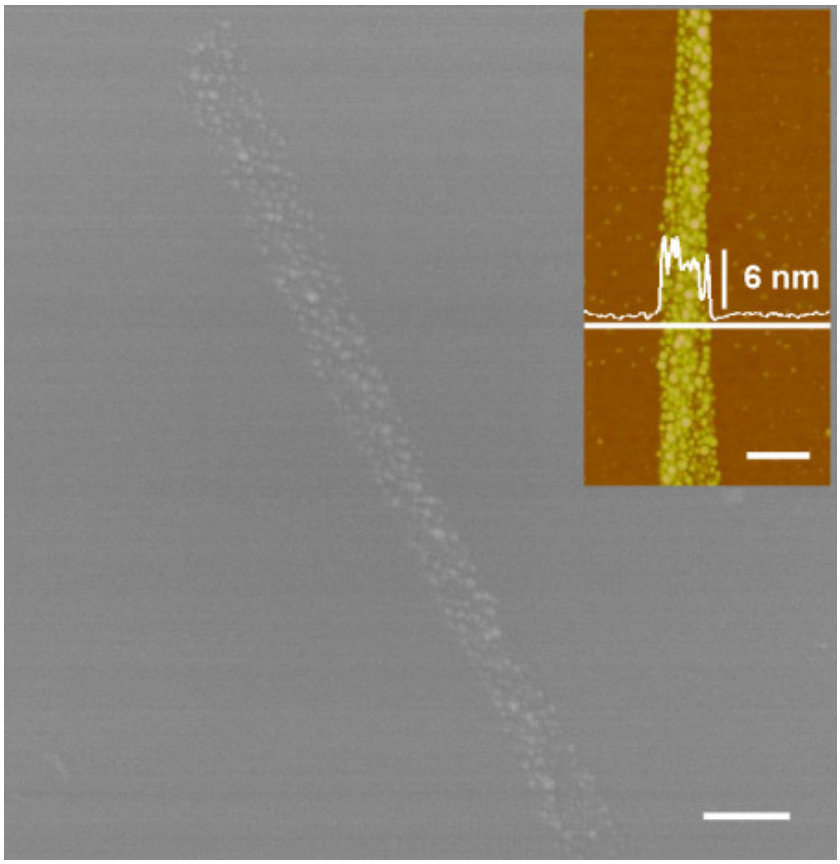

Figure 4-21 SEM image of Ag NPs grown on a fabricated GONR. Inset: AFM image and a height profile of Ag NPs grown on a GONR. Scale bars = 200 nm.

4.4.4 Short summary

With an accurate control of plasma etching conditions, single- or double-layer GONRs were successfully obtained by plasma etching of GOWs, in which the top layers of GOWs act as sacrificial layers. The GONRs as narrow as 15 nm and as long as 2 μm were obtained. GONRs were characterized by AFM, Raman, SEM and TEM, and used as templates to in situ reduce $AgNO_3$ without adding any reducing agent to obtain Ag NP-GONR nanocomposites. Our results clearly show that even the single atomic GO sheet can be used as a sacrifice layer in the plasma etching process for successful fabrication of GONRs with controlled layers.

4.5 Printing graphene oxide

4.5.1 Introduction

Graphene has shown promises in nanoelectronics. Nanodevices require the large-scale assembly and integration of graphene to chips. Much effort has been devoted to the assembly of carbon nanotubes (CNTs), with considerable success[84]. Due to many functional groups on its surface, GO is much easier to process than graphene when assembly is needed. Although Wei et al.[85] recently demonstrated the assembly of GO on Au substrate by using 11-amino-1-undecanethiol (AUT) as molecular templates, other methods are still needed to pattern GO on various substrates. Moreover, Au substrates are not suitable for nanoelectronics. In this thesis, both a direct and an indirect printing process of GO on SiO_2 substrates was investigated, which could be a more suitable substrate for device applications.

4.5.2 Direct printing of graphene oxide

Before the GO film was transferred to the hard-PDMS (h-PDMS) stamp, an attempt was made to transfer it to cleaned SiO_2 substrates based on the Langmuir-Blodgett (LB) film technique. Figure 4-22 shows AFM images of the GO film collected at different surface pressures with a fixed dipping speed of 1.5 mm/min. As expected, at low pressure (~3mN/m), large space-distributed GO sheets were observed (Figure 4-22a), while at higher pressure (~15mN/m) the GO film with

high density was obtained, although slight overlapping was also observed at high pressures (Figure 4-22b).

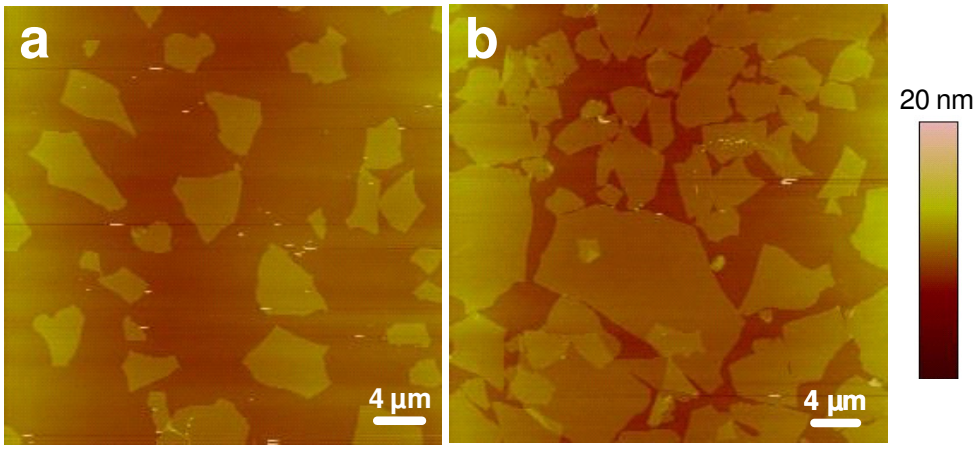

Figure 4-22 AFM topographic images of GO film collected at a pressure of (a) 3 and (b) 15 mN/m, respectively.

Although others had demonstrated that rGO can be transferred under heating[86], in this thesis, an alternative attempt was made to transfer GO to APTES-modified SiO_2 substrates by utilizing electrostatic interaction between negative-charged GO and positive-charged APTES. By using a post-reduction step, the consistent patterns of rGO were obtained. It should be noted that the h-PDMS stamp is crucial for the successful printing. Experimentally, it was found that the soft-PDMS stamps would transfer PDMS precursors to substrates during printing, whereas no precursors were transferred from h-PDMS. This avoids contamination during printing GO.

Figure 4-23 shows the AFM image of GO patterns transferred from the h-PDMS stamp to the APTES-modified SiO_2 substrate. This direct printing method is straightforward and versatile. This method, in principle, is applicable to other substrates, such as glass or even soft substrates (e.g. PET).

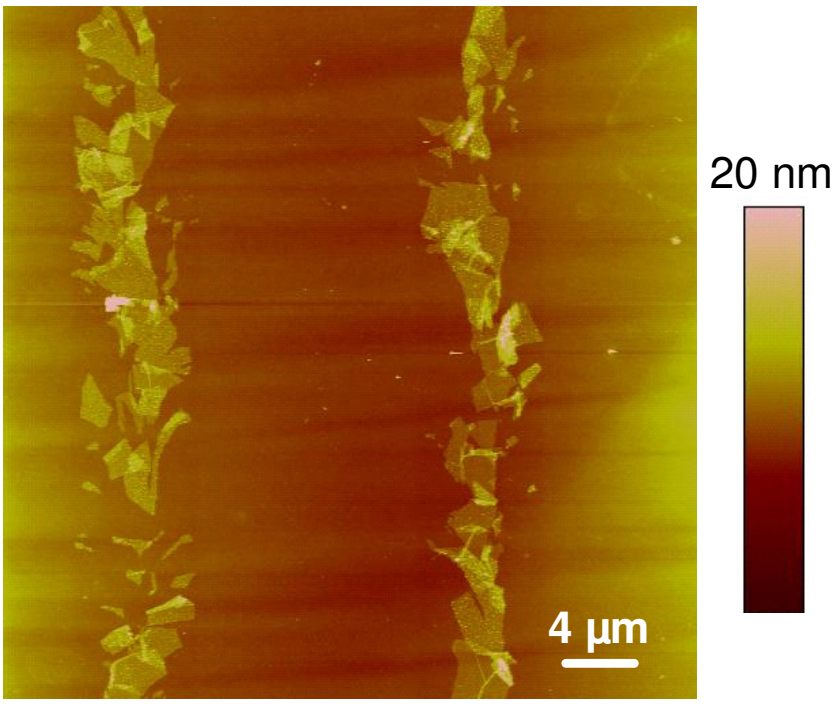

Figure 4-23 AFM topographic image of GO patterns directly transferred from the h-PDMS stamp directly to APTES-modified SiO_2 substrate.

4.5.3 Indirect printing of graphene oxide

In addition to the direct method mentioned above, an indirect printing by using molecular templates to adsorb GO is also carried out.

Figure 4-24 shows the AFM topographical image and the height profile of the APTES patterns on SiO_2 surface generated by micro-contact printing (μCP). The average height of the APTES patterns is 0.5 nm, corresponding to monolayer of APTES. Note that our method of printing APTES is advantageous compared to reported methods in literature because no strict conditions are required, such as the use of glove box and toxic solvent (e.g. toluene).

Figure 4-25 shows the AFM images of the GO patterns by incubating APTES-patterned SiO_2 substrate in GO aqueous solution. By using stamps with different size, GO patterns with different size (0.5 and 8 μm) can be obtained (Figure 4-24 a and b).

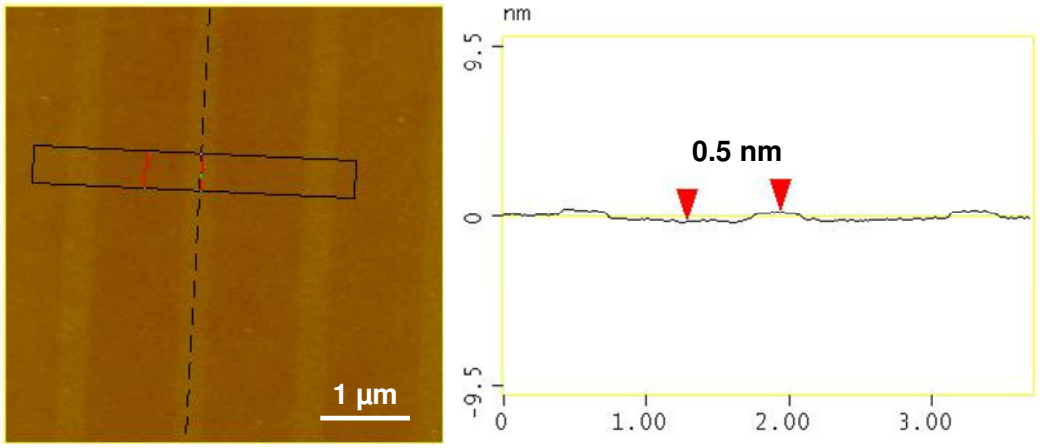

Figure 4-24 AFM topographic image and height profile of APTES patterns. An average height of APTES is 0.5 nm

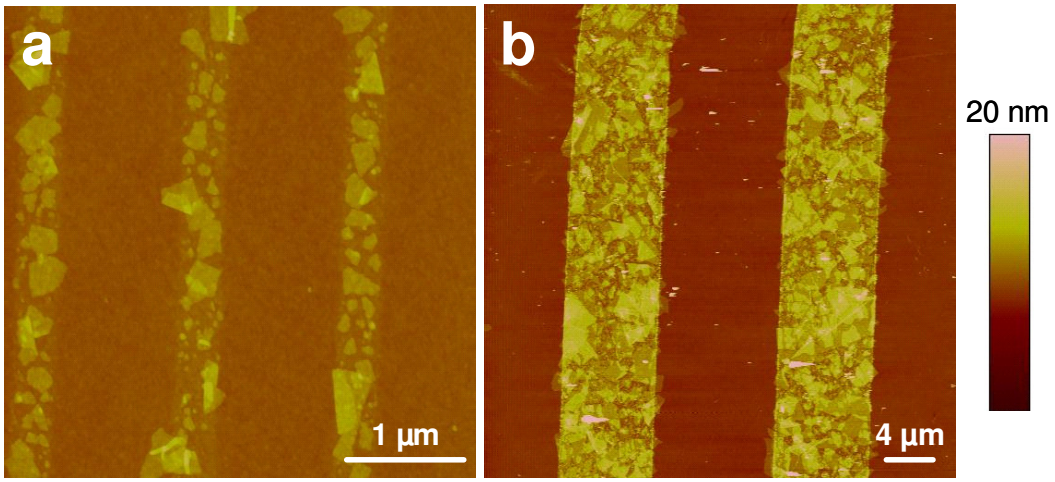

Figure 4-25 AFM topographic image of GO adsorbed on APTES-patterns with size of (a) 0.5 µm and (b) 8 µm, respectively

After GO patterns were formed by this indirect printing method, GO could be reduced to rGO with a hydrazine vapor. Interestingly, the scroll of rGO was observed. Figure 4-26 shows the AFM image of the scrolled rGO. GO did not scroll if GO patterns were heated at 50 or 70 °C without the hydrazine vapor. The reason for rGO to scroll is discussed as follows. After reduction, most of the oxygenated functionalities on GO were removed and rGO lost the negative charges. As such, there is no or little electrostatic interaction between rGO and APTES. Graphene has been observed to scroll under heating, Figure 4-27. Therefore, it is reasonable that rGO will also scroll under reduction and heating. However, due to the attractively electrostatic interaction between GO and APTES film on SiO_2 substrates, GO will not scroll under heating. The scroll of graphene has been studied and interesting properties have been revealed for these carbon nanoscrolls[87, 88]. If GO is decorated with positively charged NPs and reduced in hydrazine, the scroll of rGO will wrap the NPs and make the NPs inside the scrolled rGO. These rGO wrapped NPs may show different electrical and optical properties[89].

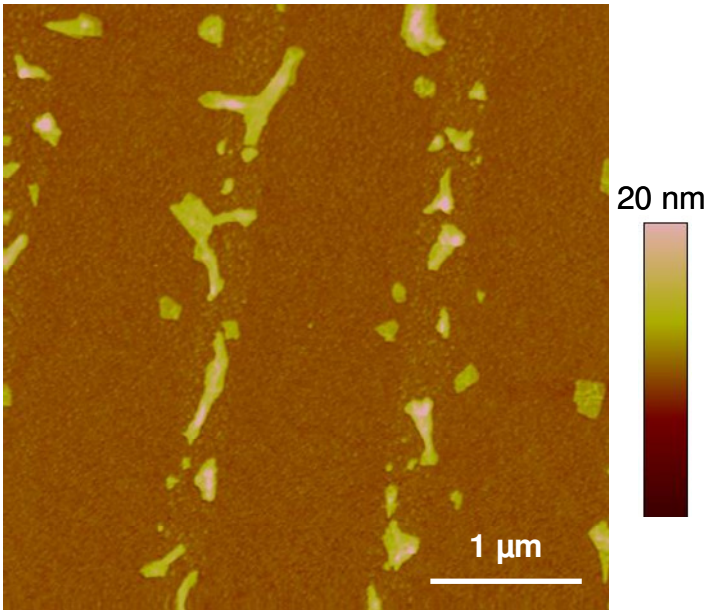

Figure 4-26 AFM topographic image of the scrolled rGO after GO patterns were reduced with a hydrazine vapor at 50 or 70°C.

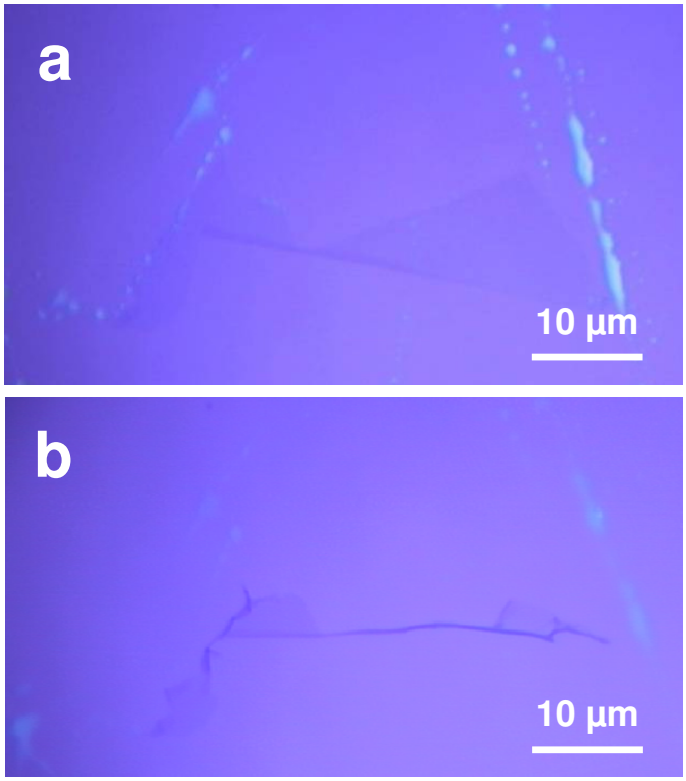

Figure 4-27 OM images of the scrolled graphene (a) before heating and (b) after heating (Courtesy of Ms. Fang Wenjing).

4.5.4 Short summary

In this section, graphene oxide was patterned on the APTES-modified SiO_2 substrates by direct or indirect printing methods. In addition, the scroll of rGO was observed after the reduction of GO patterns with a hydrazine vapor. However, GO did not scroll during heating without hydrazine reduction.

Chapter 5

Properties and Applications of Reduced Graphene Oxide Thin Films

5.1 Overview

The last chapter has focused on the properties and applications of single layer GO and rGO. In this chapter, rGO thin film will be discussed in terms of its biocompatibility with cells and capability as matrix for mass spectroscopic analysis. First, rGO thin film made by spin-coating and the reduction of GO on SiO_2 substrates was used to interface several types of cells to show its good biocompatibility. rGO thin film was shown to be better substrate than single-walled carbon nanotube network (SWCNT-net). Second, rGO thin film was used as matrix for mass spectroscopic analysis of octachlorodibenzo-p-dioxin (OCDD) with high sensitivity and low detection limit. In contrast, other matrices, such as graphite powder and activated carbon, show disadvantages in the analysis of OCDD.

5.2 Interfacing live cells with rGO thin film and SWCNT-net substrates

5.2.1 Introduction

As carbon is the backbone of biomolecules and biological structures, it seems to be a natural attempt to integrate biological systems with nanocarbons. Several lines of evidences have suggested that CNT networks or scaffolds can biocompatibly interface with live cells to support their growth and adhesion[90, 91], whereas some other studies have suggested the cytotoxic effects of CNTs[92]. The difference in cell response to the same material is likely due to the cell-type specific interaction with nanofibrous topographic features of CNT substrates. It has been increasingly recognized that nanotopographic cues introduced by nanostructured materials could have profound influences on cell functions[93, 94]. While CNT is one-dimensional rolled-up carbon sheet, graphene is a flat two-dimensional carbon sheet. As a result of such structural difference, the properties of graphene differ from CNTs. The capability of graphene to biocompatibly interact with biological systems and its potentials in bio-applications is still to be explored. In this study, the interfacial behavior of live cells with chemically reduced graphene oxide (rGO) film and the network of single-walled carbon nanotubes (SWCNT-net) has been studied. This comparative study suggests that cells respond differently to these two types of nanocarbon substrates likely due to their distinct nanotopographic features. The rGO is biocompatible to all tested cells, implying its potential application in biology.

5.2.2 Characterization of the rGO thin film and SWCNT-net

Figure 5-1a shows the SEM and AFM images of SWCNT-net on a glass coverslip. It is evident that SWCNT-net is nanotopographic meshworks formed by nanofibrous SWCNT bundles, giving the substrate roughness of 10.9 nm in 5 × 5 μm^2 (Figure 5-1a, right) and sub-micrometer meshsize. In contrast, rGO film is essentially flat (Figure 5-1b, right) and its roughness is ~1.6 nm in 5 × 5 μm^2 (Figure 5-1b, right), mainly attributable to the wrinkles or foldings of the rGO film obtained by spin-coating, i.e. the lines in the AFM image (Figure 5-1b, right).

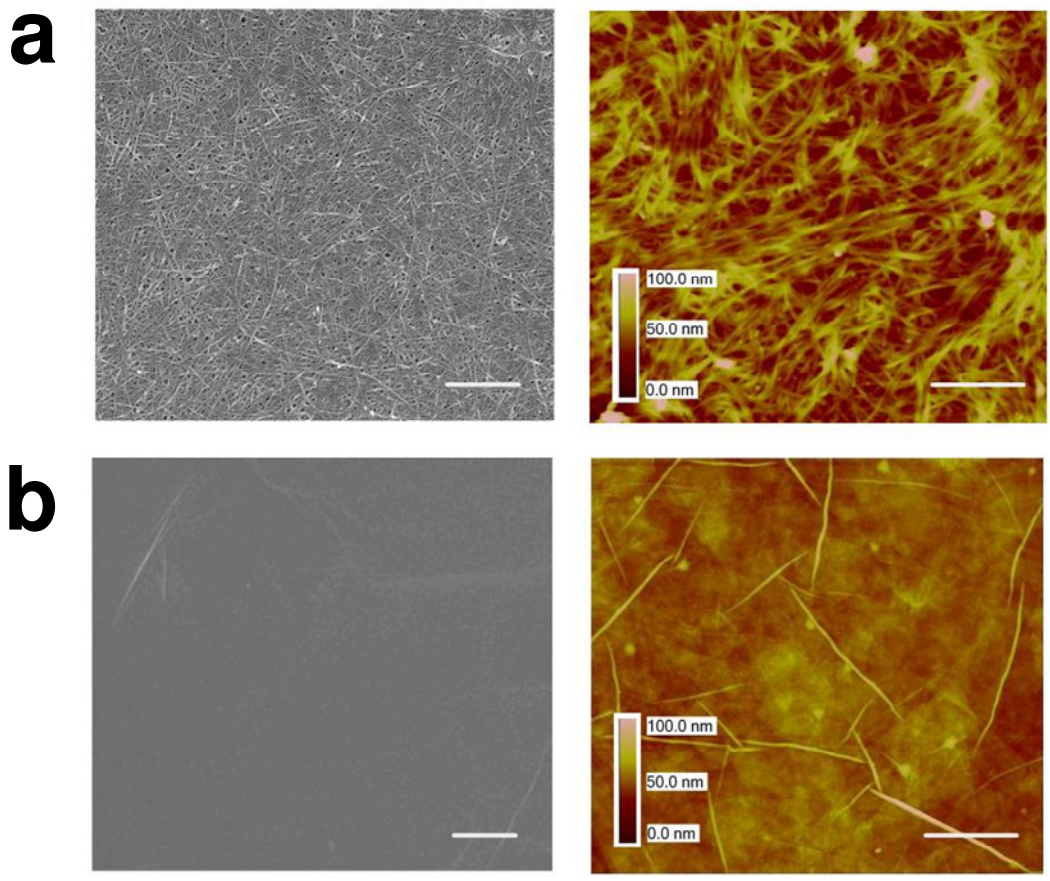

Figure 5-1 SEM (left) and AFM (right) images of (a) SWCNT-net and (b) rGO film. Scale bars = 1 µm.

The chemical characteristics of SWCNT-net and rGO film were analyzed by X-ray photoelectron spectroscopy (XPS). As shown in Figure 5-2, the functional groups (C=O and C-O) on SWCNT-net and on GO film were essentially removed by thermal annealing at 350 °C for 3 h and the chemical reduction with hydrazine vapor, respectively. Although some C-N groups were introduced during the reduction of GO[47], the obtained rGO film is chemically similar to the annealed SWCNT-net, i.e. both of them are essentially π-conjugated networks as evidenced by their dominating C 1s peak in the XPS spectra (Figure 5-2).

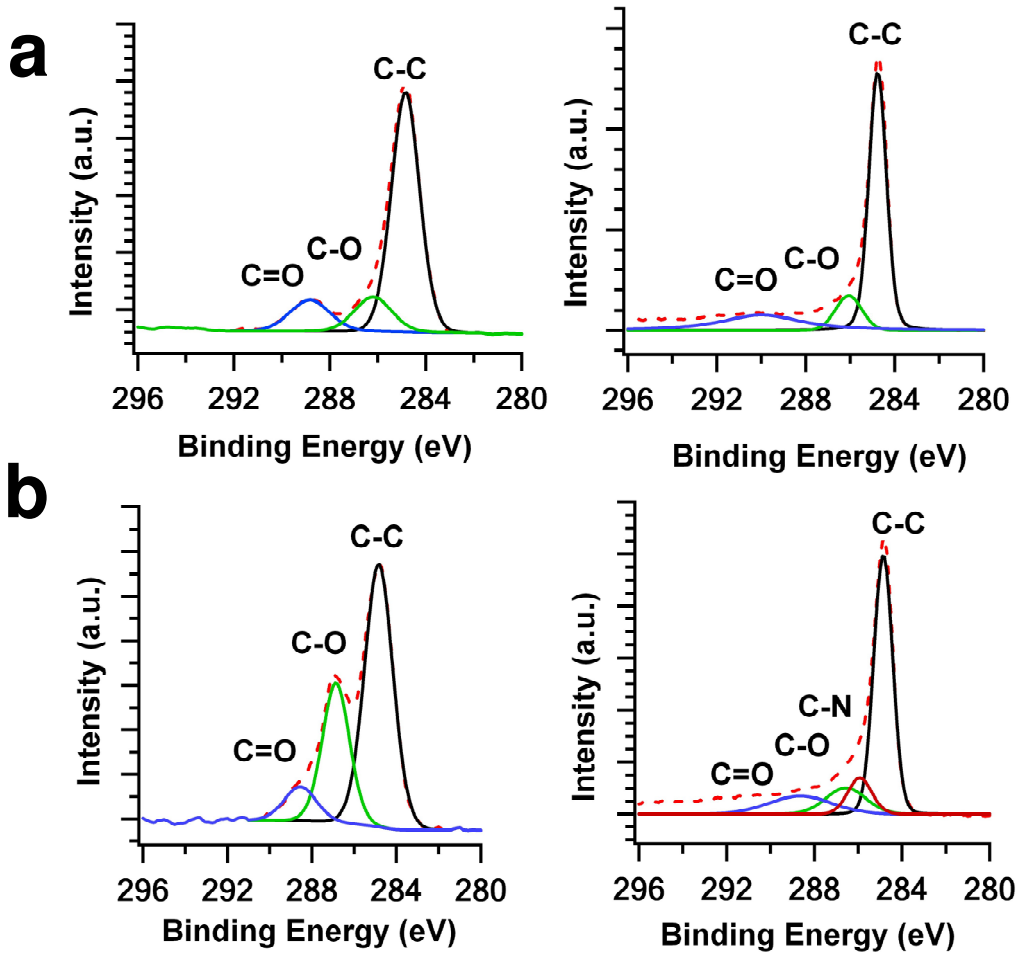

Figure 5-2 XPS spectra of (a) SWCNT-net before (left) and after (right) thermal annealing, and (b) GO film before (left) and after (right) chemical reduction with hydrazine vapor.

5.2.3 Results of cell studies

Rat pheochromocytoma cells (PC12) were cultured in parallel on SWCNT-net and rGO film with the same initial seeding density. Figure 5-3a presents the optical images of PC12 cells grown on SWCNT-net (left) and rGO film (right) for 5 days. PC12 cells grow more confluently on rGO film, while they only sparsely dispersed as clusters and often remained round shape on SWCNT-net, indicating their reluctance in adhesion and spreading. The proliferation of PC12 cells on the two types of substrates was monitored over 5 days after seeding (Figure 5-3b). Obviously, the cells proliferate well on rGO film, whereas their proliferation is largely inhibited on SWCNT-net. MTT assay, which provides a quantitative measurement on alteration of the metabolic status of cells responding to external factors, was used to examine the cell status on the two nanocarbon substrates. As shown in Figure 5-3c, SWCNT-net exhibits cytotoxic effects as compared to rGO film, in agreement with the observation of cell proliferation.

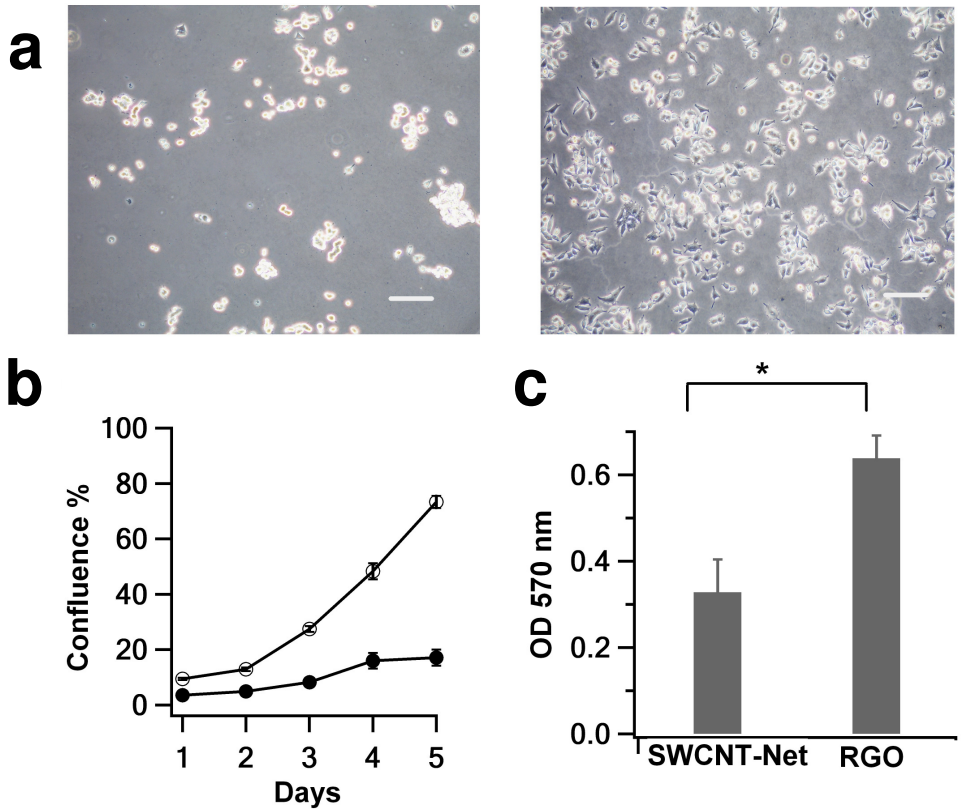

Figure 5-3 (a) Phase-contrast images of PC12 cells grown on SWCNT-net (left) and rGO film (right) for 5 days. Scale bars = 100 µm. (b) Proliferation curves of PC12 cells on SWCNT-net (filled circles) and rGO (open circles). Each data point is the average cell number normalized to the cell number at confluence, from 30 different areas of 1.8 mm^2 (field of view) on 3 samples. The error bars indicate the standard error (SE). (c) MTT assay in which the optical absorbance at 570 nm was measured as the indicator of cell metabolic activities. The data is shown as mean +/- SE from 3 independent experiments.

Because of its exceptional electrical properties, CNTs have been employed to interface with neurons which produce and transmit electrical signals (called action potentials) to communicate with each other and the other cells. It has been demonstrated that the conductive CNT network facilitates propagation of action potentials and consequently boosts neuronal electrical signaling in the neuronal networks[95, 96], suggesting the potential applications of CNTs in neural tissue engineering. In addition, thin-film transistors based on SWCNTs have been used to stimulate neurons grown on SWCNT-net and detect the resulting electrical responses from neurons[97], suggesting the potential applications of CNT devices in neural stimulation and recording. It is conceivable that rGO, which is much more conductive than CNTs and has unique field-effect properties, may serve as a better alternative in neuronal engineering.

Neuroendocrine PC12 cell is a popular model to study neuritegenesis. Nerve growth factor (NGF, 100 ng/ml) induced neurite outgrowth of PC12 cells grown on both substrates was investigated. Figure 5-4a depicts the optical images of neuronal differentiated PC12 cells on SWCNT-net (left) and rGO (right). It is evident that the outgrowth and extension of neurites of PC12 cells on SWCNT-net are significantly suppressed as compared to those grown on rGO. As demonstrated in Figure 5-4b, the percentage of differentiated cells and the average length of the outgrown neurites on SWCNT-net are significantly less than that on the rGO thin film. These observations imply that rGO film may be more desirable in interfacing neurons.

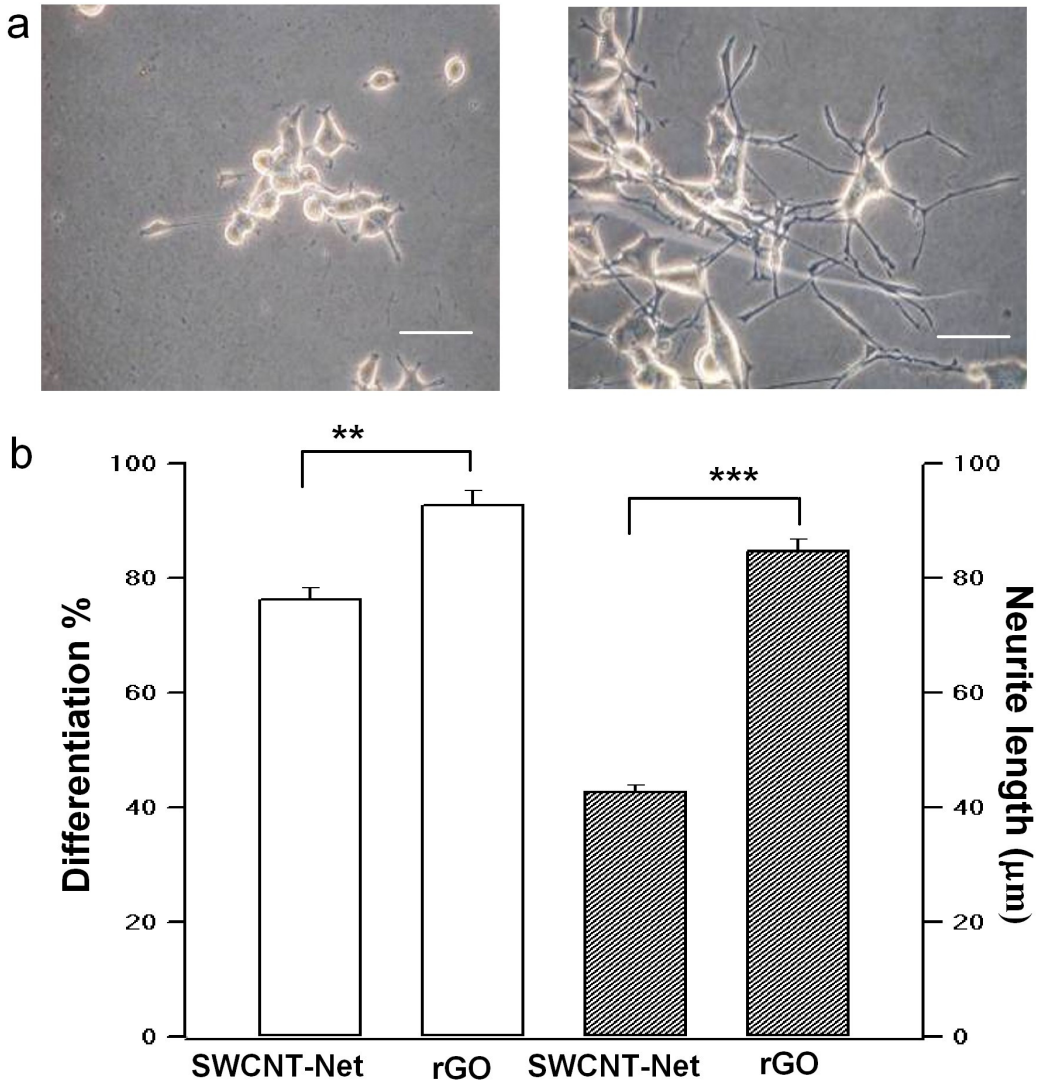

Figure 5-4 (a) Phase-contrast images of neuronal differentiated PC12 cells on SWCNT-net (left) and rGO (right). Scale bars = 50 µm. (b) Left: the percentage of cells differentiated into neuronal phenotype (cells with at least one neurite longer than the length of the cell body). The statistics (mean +/- SE) is from >1000 cells on 3 samples. Right: the average neurite length. The statistics (mean +/- SE) is from 90 cells on 3 samples. Cells were treated with nerve growth factor (100 ng/ml) for 4 days.

Human fetal osteoblasts (hFOB) and human oligodendroglia cells (HOG) were also cultured on both nanocarbon substrates. Similar to PC12 cells, osteoblasts cannot proliferate well on SWCNT-net either (Figure 5-5), suggesting that the pristine SWCNT may not be an ideal construct material for bone formation. On the other hand, oligodendroglia cells, which wrap around and produce myelin sheet on nanosized nerve fiber (axon) in the central nervous system, can reach confluence at 4th day on both types of substrates. Clearly, the different cell types respond to carbonaceous materials differently and have distinct sensitivity to the nanotopographic features.

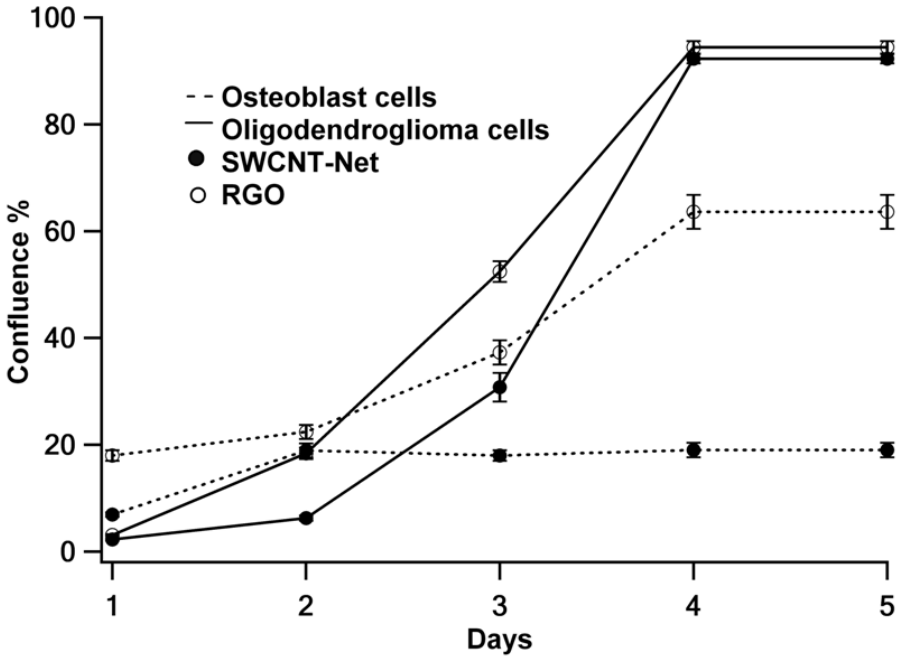

Figure 5-5 Proliferation curves of osteoblast cells (dotted lines) and oligodendroglioma cells (solid lines) on SWCNT-net (filled circles) and rGO (open circles). Each data point is the average from 30 different areas (1.8 mm^2) on 3 samples. The error bars indicate SE.

5.2.4 Short summary

A systematic study has been done the ability of two kinds of nanocarbon substrates to interface with different types of cells. Although SWCNT and rGO are structural forms of the same element (allotropes), they are distinct in their nanotopographic characteristics and their abilities to support cell growth. It has been increasingly recognized that topographic features in nanoscale can have profound influences on cell functionalities[93]. Nanostructures, for example, 10-20 nm SWCNT bundles in our SWCNT-net, may induce deformation of the thin cell membrane (5 nm thick) and affect the fluidity of the lipid membrane, mobility and organizations of membrane proteins (thus their functions)[98]. Comparative studies using SWCNT-net and rGO film may be instrumental in examining how cells respond to nanotopographic cues and revealing the underlying molecular mechanisms. The rGO, a flat 2D nanocarbon structure analogous to 2D cell membrane, has been demonstrated to be more biocompatible to the cells tested, indicating its potential applications in biology.

5.3 rGO thin film as matrix for matrix-assisted laser desorption/ionization time-of-flight mass spectroscopy

5.3.1 Introduction

Matrix-assisted laser desorption/ionization time-of-flight mass spectroscopy (MALDI-TOF-MS)[99-101] has emerged as an important tool for analyzing and characterizing a wide range of molecules (e.g. synthetic polymers and biomolecules)[102-109]. In particular, the mass spectra of biomolecules, including proteins, peptides[103-105] and nucleic acids[106], have been achieved with high accuracy and sensitivity. Structural information can be obtained from the spectra. However, little attention has been paid to the detection of environmentally toxic molecules (e.g. dibenzo-p-dioxins) using MALDI-TOF-MS, which could offer higher accuracy and sensitivity and will help implement measures against the occurrence of these toxic molecules in environment.

One of the environmentally toxic molecules is polychlorinated dibenzodioxins dioxin (simply, dioxin). Dioxins are a family of compounds comprising two benzene rings joined by two oxygen bridges and having zero to eight chlorine atoms around the two rings. Dioxins are highly toxic and the toxicity depends on the number and position of the chlorine atoms. It is well-known human carcinogens, and stable pollutants in air, water, soil and food chains. Therefore, it is of great necessity to detect dioxins with higher accuracy and sensitivity. To date, the MALDI-TOF-MS has not been reported to be used for the analysis and

detection of dioxins. One possible reason is the lack of suitable matrix. The currently used matrix, such as 2, 5-dihydroxybenzoic acid (DHB), does not work well for dioxins.

In this thesis, the rGO thin film, prepared by spin-coating GO and reduction in hydrazine, was used as the matrix of MALDI-TOF-MS for the analysis of octachlorodibenzo-p-dioxin (OCDD), a dioxin with eight chlorine atoms. The rGO thin film, comprising the π-conjugated electron networks, has function to adsorb analytes, absorb energy from laser irradiation, conduct heat, and transfer energy and transfer charges (i.e. electrons) to analytes for desorption/ionization. Highly efficient desorption/ionization was obtained on rGO thin film without the need to locate "sweet spots" which are required for the organic matrix. This simplifies the sample preparation. In comparison, other matrices, including rGO suspension, graphite powder, activated carbon, and silica particles, were also used for the analysis of OCDD.

Preliminary studies found that OCDD can only be detected in the negative ion mode but not in the positive ion mode. As such, unless specifically mentioned, the negative ion mode was used for all experiments.

5.3.2 rGO thin film as matrix

Figure 5-6 shows the spectra of OCDD by using rGO thin film as matrix. 5 ng and 500 pg of OCDD were easily detected (Figure 5-6a, b). Note that no peaks of deprotonated species $[M - H]^-$ were detected. Instead, the dominant peaks for OCDD at m/z 421, 423, 425 and 427, were shown. These peaks are attributed to the de-clorinated species $[M - Cl]^-$, with the isotopic multiplet of Cl well resolved. As such, we propose the ionization of OCDD as: $M + e \rightarrow [M - Cl]^- + Cl\bullet$, where the analyte OCDD captures an electron and releases a chloro-radical.

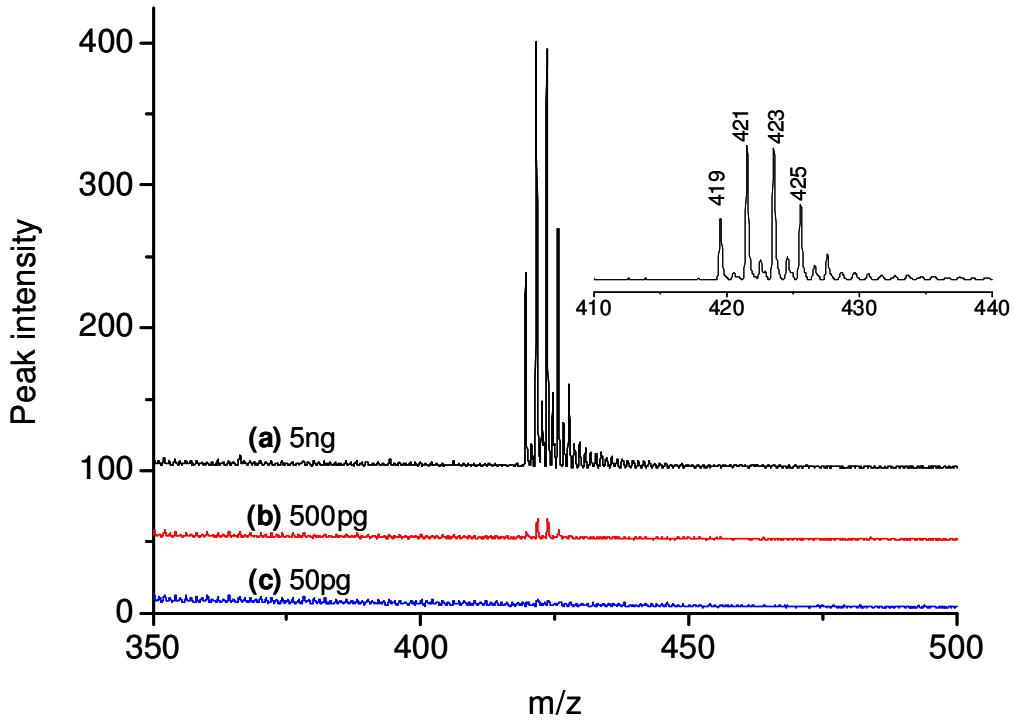

Figure 5-6 Mass spectra of OCDD with a weight of (a) 5 ng, (b) 500 pg, and (c) 50pg adsorbed on the surface of rGO thin film. Inset: the zoom-in of the mass spectrum of (a).

Several organic matrices, such as 2, 5-dihydroxybenzoic acid (DHB), α-cyano-4-hydroxycinnamic acid (CHCA) and sinapic acid (SA), were also tried for the detection of OCDD, but no signals were observed. The rGO thin film is so far the best matrix for the OCDD detection and a great efficiency of desorption/ionization has been achieved. The good desorption/ionization is understandable if the distinct structure of rGO thin film is considered. The rGO thin film is composed of π-conjugated networks which could absorb energy from the UV laser radiation and transfer energy to analytes to assist its desorption/ionization. It is worth mentioning that the residual functional oxygenated groups may play a role in the desorption/ionization process because the pure graphite powder shows lower sensitivity in the detection of OCDD (Section 5.3.4). It is supposed that the released radical Cl• is easily transferred to the residual adjacent hydroxyl or carbonyl or carboxyl groups present in rGO thin films. However, no such oxygenated functional groups exist on graphite to assist such transfer. Besides, the form of rGO as a continuous film is also advantageous since the laser energy is easily absorbed and conducted through the networks[110]. The suspension powder of rGO as matrix shows disadvantages as compared to rGO thin film, as discussed in Section 5.3.3.

After successful detection of 5 ng and 500 pg OCDD, the smaller weight of OCDD was tried. Unfortunately, no observable peaks were shown in the mass spectrum when 50pg OCDD was tested (Figure 5-6c). In order to assist desorption/ionization of OCDD, trifluoroacetic acid (TFA) was added on the rGO film before depositing OCDD solution. Figure 5-7 shows the mass spectra of 50 pg OCDD with and without adding TFA. It clearly shows that 50 pg OCDD was detected when TFA

was added, Figure 5-7a. Significantly stronger signals were observed and signal-to-noise ration increased when TFA was added. However, the mechanism of the role of TFA, which is normally used as a cationizing agent, remains unclear. In our experiment, the detection limit of OCDD is 50 pg by using rGO thin film as matrix with adding TFA.

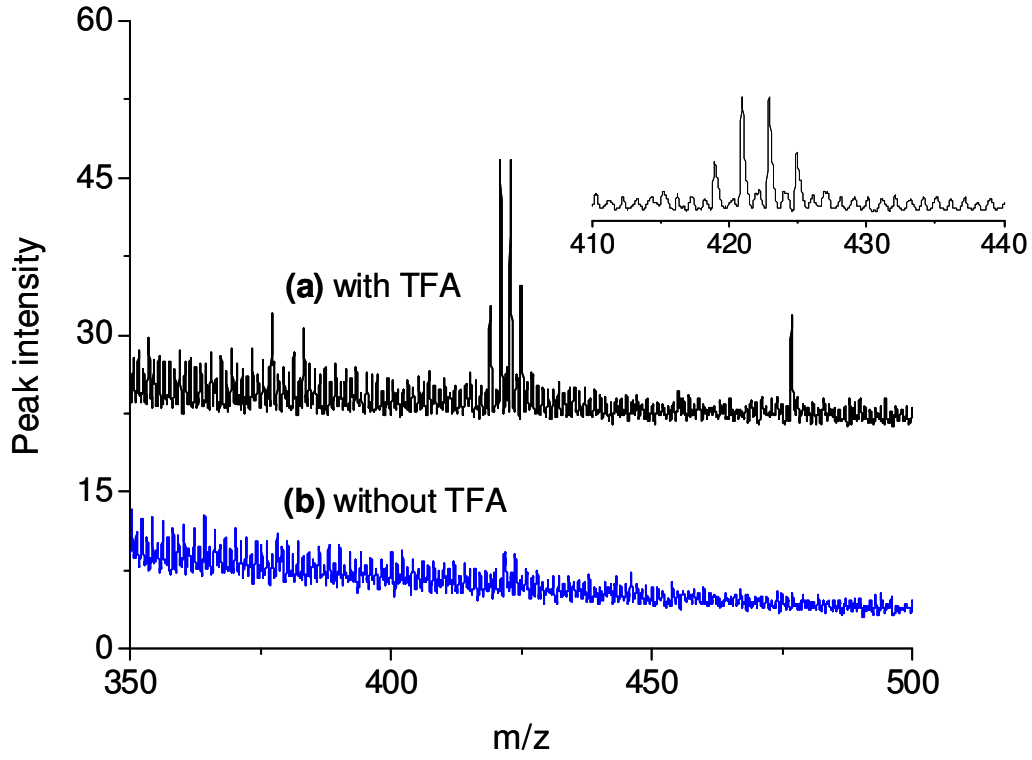

Figure 5-7 Mass spectra of 50 pg OCDD adsorbed on the surface of rGO film with (a) and without (b) adding TFA. Inset: zoom-in of spectrum (a).

5.3.3 rGO suspension powder as matrix

Besides rGO thin film, rGO suspension powder as solid-phase extraction agent and matrix was used for the detection of OCDD. Figure 5-8 shows the mass spectra of different weight of OCDD. 10 ng and 1 ng were easily detected. However, if OCDD is < 500 pg, the signal became weak and the signal-to-noise ratio decreased significantly. Figures 5-9a and b show the spectrum of 500 pg of OCDD by using rGO thin film and rGO suspension powder as matrices, respectively. Comparison of the results in Figure 5-9a and Figure 5-9b shows that the efficiency of desorption/ionization on rGO thin film was much better than that on rGO suspension powder. This is attributed to the fact that the rGO suspension powder was not well connected and thus reduced the ability of the absorbed laser energy to conduct through as it would have for rGO thin film.

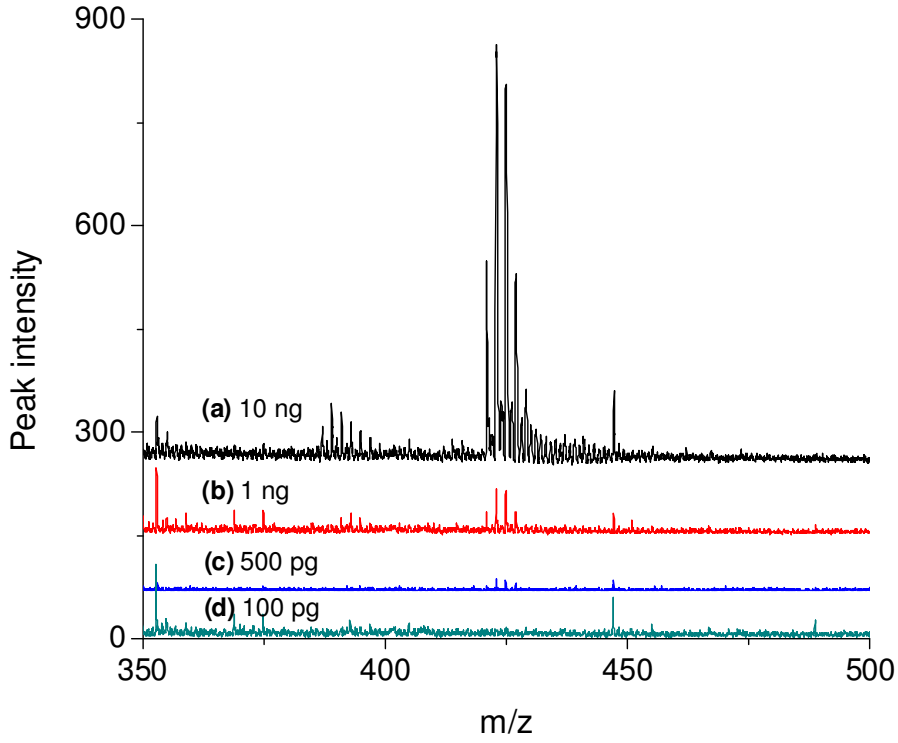

Figure 5-8 Mass spectra of (a) 10 ng (b) 1 ng, (c) 500 pg, and (d) 100 pg OCDD adsorbed on the surface of rGO suspension powder. 24 ng of rGO was used as matrix.

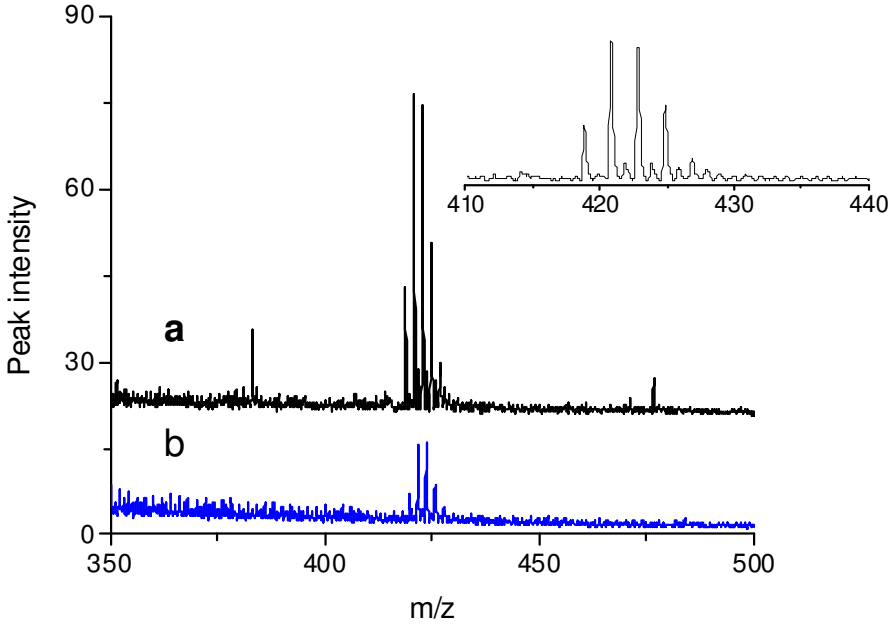

Figure 5-9 Mass spectra of 500 pg OCDD adsorbed on the surface of (a) rGO thin film and (b) rGO suspension powder. Inset: zoom-in view of spectrum (a).

5.3.4 Other materials as matrices

The rGO thin film and rGO powder form have been tried as matrices for the detection of OCDD. A comparison study was also carried out by using other matrices such as natural graphite, activated carbon, SWCNT, and silica particles.

Figure 5-10 shows the mass spectra of OCDD by using graphite as matrix, indicating that 5 ng of OCDD could be detected. However, the peak intensity and signal-to-noise ratio are significantly lower than that obtained with rGO thin film as matrix (Figure 5-6a). The reason is possibly similar to rGO powders. The graphite powder was not continuously connected when it was spread on the plate. Therefore, the energy does not well conduct through the powder and is not easily transferred to the analytes. This needs to be verified by further experiments as graphite powder has been shown as a good matrix for the characterization of proteins and other molecules[111, 112].

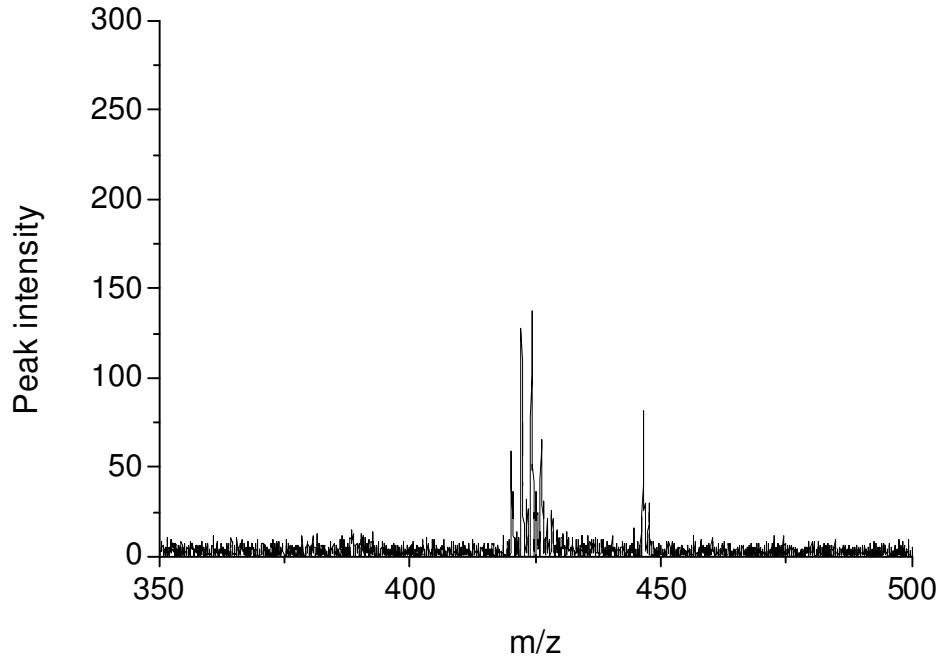

Figure 5-10 Mass spectrum of 5 ng OCDD on graphite powder.

Figure 5-11 shows the mass spectra of OCDD by using activated carbon as matrix. 5 ng of OCDD was tried. Figure 5-11 shows that the peak intensity is very low compared to that in rGO thin film (Figure 5-6a). Therefore, the activated carbon is not a good matrix and cannot give higher efficiency of desorption/ionization for OCDD. Presumably, activated carbon lacks the conjugated electrons which adsorb energy and transfer energy to analytes. Although activated carbon has been successfully used as matrix for other molecules, it is not a suitable matrix for OCDD.

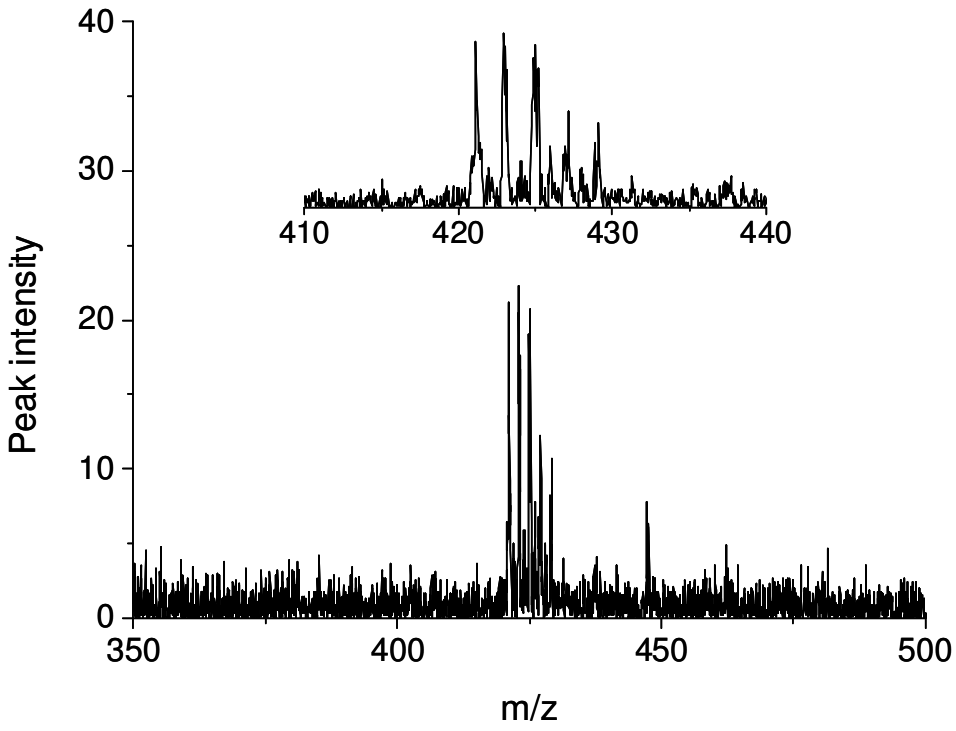

Figure 5-11 Mass spectrum of 5 ng OCDD adsorbed on activated carbon. Inset: zoom-in of the spectrum.

Carbon nanotubes (CNTs) have been recently used as matrix for MALDI-TOF-MS[113, 114]. Figure 5-12 shows the results using SWCNT networks as the matrix to detect OCDD. Very weak signal was observed. As CNTs have been shown as a good matrix for a variety of molecules[114], more work needs to be carried out regarding the lower signal of OCDD in our experiment. The preparation method and source of CNTs may contribute to the low sensitivity.

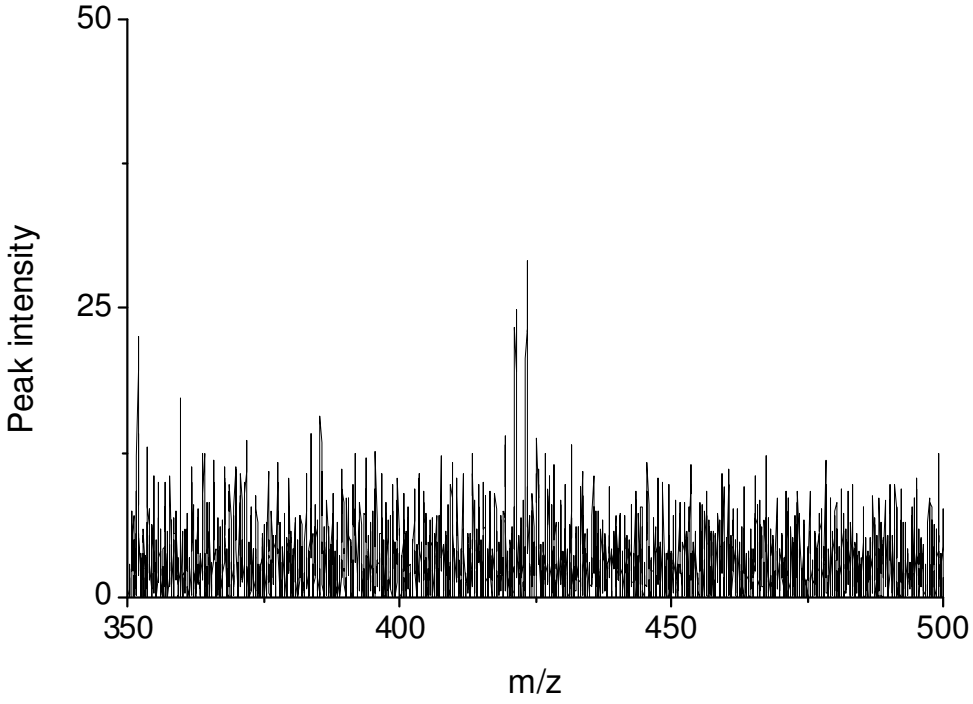

Figure 5-12 Mass spectrum of 5 ng OCDD on SWCNT networks.

Last but not least, in searching for the matrices for OCDD, other materials other than carbon-based have also been tried. For instance, silica particles, with size in tens of μm and surface functionalized with aminophenyl groups, were intensively studied in our group. Figure 5-13 shows the mass spectra of OCDD when silica particles modified with and without carbon blacks were used as matrices. The used carbon black is CABOT 300 and modified with 2-carboxyphenyl groups on its surface. The carbon black was used to improve the conductivity of silica particles to perform MLADI-TOF-MS for OCDD. Although the signals were shown up, the detection limit of OCDD was 1 ng, which is far less than that obtained in rGO thin film (50 pg).

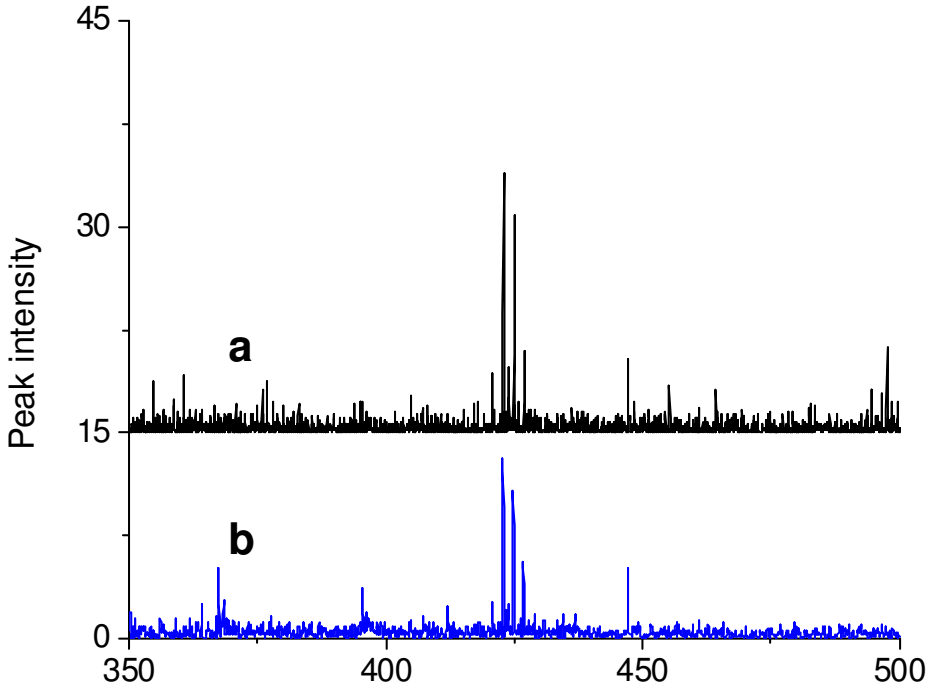

Figure 5-13 Mass spectra of 5 ng OCDD on (a) silica particles and (b) silica particles modified with carbon black.

5.3.5 Short summary

In summary, this section discusses the ability of rGO thin film as matrix in MALDI-TOF-MS for the OCDD detection. High sensitivity with a detection limit of 50 pg was achieved. Although other materials, such as rGO suspension powder, graphite powder, activated carbon, SWCNT, and silica particles, have been used as matrices, the sensitivity is quite low as compared with the results obtained by using rGO thin film as matrix.

Chapter 6

Conclusions and Recommendations

6.1 Conclusions

Based on the results obtained in this thesis, graphene oxide (GO) and reduced graphene oxide (rGO) have been studied in various aspects. The potential of GO to be modified with metal nanoparticles and be fabricated into ribbons have been explored. GO has also been patterned on solid substrates. The rGO thin films have been used to interface cells and as matrix for mass spectroscopy. As such, the structure, properties and application potentials of GO and rGO have been evaluated and summarized as follows.

(i) A simple method for the growth of Ag nanoparticles with different morphology on GO and rGO has been developed. The method involves heating GO and rGO substrates in silver nitrate solution without adding any reducing agent or surfactant. The size of Ag nanoparticles was easily controlled by varying heating time.

(ii) After plasma etching of graphene oxide wrinkles (GOWs), graphene oxide nanoribbons (GONRs) were obtained. This method relies on the fact that the GOWs are composed of three layer GO with a width from tens of nanometers to hundreds of nanometers and a length of several micrometers. By careful control of

plasma etching conditions (e.g. power, pressure and etching time), single- or double-layered GONRs were fabricated. The GONRs were ready to be modified with silver nanoparticles.

(iii) GO has also been successfully patterned on SiO_2 substrates directly by micro-contact printing, or indirectly by adsorption of GO to the patterned molecular templates. The scroll of rGO on patterns was observed.

(iv) The rGO thin films, simply fabricated by spin-coating GO and then reduction of GO on SiO_2 substrates, have found to be biocompatible with several types of cells, including neuroendocrine PC12 cells, oligodendroglia cells, and osteoblasts. However, single-walled carbon nanotubes (SWCNT)-networks showed lower biocompatibility with cells.

(v) The rGO thin film has also been used as matrix for the OCDD detection with MALDI-TOF-MS. High sensitivity with a detection limit of 50 pg OCDD was achieved. Other materials, including rGO suspension powder, graphite powder, activated carbon, SWCNTs, and silica particles were also tried as matrices, but the results showed lower sensitivity for the OCDD detection.

6.2 Recommendations

Although much success has been achieved on the modification of GO and rGO, more work needs to be done to fully evaluate the potential of GO in the

applications mentioned in this thesis, such as growth of nanoparticles on their surface. Specifically, the following studies are recommended.

(i) Growth of semi-conductor and metal oxide nanoparticles: In addition to metal nanoparticles (NPs), other NPs, such as semi-conductor and metal oxide NPs are of great interest if they can grow on GO and rGO. These new nanocomposites may have potential applications. For example, the composite of semi-conductor NPs and graphene will be useful in solar cells. The composite of rare earth metal NPs and graphene will find applications in batteries. The development of a "universal" method to prepare these particles on GO or rGO is significant to extend the potential of these materials.

(ii) Further investigation of the scroll of rGO and its potential application: The scroll of rGO may lend new properties (e.g. electrical properties) to rGO, which deserves more investigations. In addition, it is possible to take advantage of the scroll and wrap other nanomaterials, such as NPs, nanowires and nanorods, during the scroll. These new composites, the scrolled rGO and nanomaterials, will possibly have new properties and may find new applications.

(iii) Field-effect transistors of GONRs or rGONRs: Although the field-effect transistors (FETs) on graphene nanoribbons have been well demonstrated, the FETs on GONRs or rGONRs will be of interest. GONRs (or rGONRs) with different width and length would give different properties, compared to graphene.

(iv) The rGO thin film as matrix for the detection of other molecules: Currently, only OCDD was detected in MALDI-TOF-MS with rGO thin film as matrix. This rGO thin film matrix may be extended to the detection of other molecules, such as proteins, DNAs and polymers. The ability of rGO thin film as matrix will be fully evaluated and established. The mechanism of rGO films as matrix will be fully understood and proposed.

References

[1] Geim, A.K.; Novoselov, K.S.: "The Rise of Graphene". *Nature Materials,* **2007,** *6,* 183-191.

[2] Han, M.Y.; Ozyilmaz, B.; Zhang, Y.; Kim, P.: "Energy Band-Gap Engineering of Graphene Nanoribbons". *Physical Review Letters,* **2007,** *98,* 206805-4.

[3] Li, X.; Wang, X.; Zhang, L.; Lee, S.; Dai, H.: "Chemically Derived, Ultrasmooth Graphene Nanoribbon Semiconductors". *Science,* **2008,** *319,* 1229-1232.

[4] Schedin, F.; Geim, A.K.; Morozov, S.V.; Hill, E.W.; Blake, P.; Katsnelson, M.I.; Novoselov, K.S.: "Detection of Individual Gas Molecules Adsorbed on Graphene". *Nature Materials,* **2007,** *6,* 652-655.

[5] Mohanty, N.; Berry, V.: "Graphene-Based Single-Bacterium Resolution Biodevice and DNA Transistor: Interfacing Graphene Derivatives with Nanoscale and Microscale Biocomponents". *Nano Letters,* **2008,** *8,* 4469-4476.

[6] Stoller, M.D.; Park, S.; Zhu, Y.; An, J.; Ruoff, R.S.: "Graphene-Based Ultracapacitors". *Nano Letters,* **2008,** *8,* 3498-3502.

[7] Novoselov, K.S.; Jiang, D.; Schedin, F.; Booth, T.J.; Khotkevich, V.V.; Morozov, S.V.; Geim, A.K.: "Two-Dimensional Atomic Crystals". *Proceedings of the National Academy of Sciences of the United States of America,* **2005,** *102,* 10451-10453.

[8] Geim, A.K.; Kim, P.: "Carbon Wonderland". *Scientific American,* **2008,** *298,* 90-97.

[9] Novoselov, K.S.; Geim, A.K.; Morozov, S.V.; Jiang, D.; Zhang, Y.; Dubonos, S.V.; Grigorieva, I.V.; Firsov, A.A.: "Electric Field Effect in Atomically Thin Carbon Films". *Science,* **2004,** *306,* 666-669.

[10] Dresselhaus, M.S.; Dresselhaus, G.; Eklund, P.C., *Carbon Materials*, in *Science of Fullerenes and Carbon Nanotubes*. 1996, Academic Press: San Diego. p. 15-59.

[11] Young, A.F.; Kim, P.: "Quantum Interference and Klein Tunnelling in Graphene Heterojunctions". *Nature Physics,* **2009,** *5,* 222-226.

[12] Lee, C.; Wei, X.; Kysar, J.W.; Hone, J.: "Measurement of the Elastic Properties and Intrinsic Strength of Monolayer Graphene". *Science,* **2008,** *321,* 385-388.

[13] Yuanbo, Z.; Joshua, P.S.; William, V.P.; Philip, K.: "Fabrication and Electric-field-dependent Transport Measurements of Mesoscopic Graphite Devices". *Applied Physics Letters,* **2005,** *86,* 073104.

[14] Geim, A.K.: "Graphene: Status and Prospects". *Science,* **2009,** *324,* 1530-1534.

[15] Reina, A.; Jia, X.; Ho, J.; Nezich, D.; Son, H.; Bulovic, V.; Dresselhaus, M.S.; Kong, J.: "Large Area, Few-Layer Graphene Films on Arbitrary Substrates by Chemical Vapor Deposition". *Nano Letters,* **2009,** *9,* 30-35.

[16] Li, X.; Cai, W.; An, J.; Kim, S.; Nah, J.; Yang, D.; Piner, R.; Velamakanni, A.; Jung, I.; Tutuc, E.; Banerjee, S.K.; Colombo, L.; Ruoff, R.S.: "Large-Area Synthesis of High-Quality and Uniform Graphene Films on Copper Foils". *Science,* **2009**, 1171245.

[17] Harrison, B.S.; Atala, A.: "Carbon Nanotube Applications for Tissue Engineering". *Biomaterials,* **2007,** *28,* 344-353.

[18] Berger, C.; Song, Z.; Li, X.; Wu, X.; Brown, N.; Naud, C.; Mayou, D.; Li, T.; Hass, J.; Marchenkov, A.N.; Conrad, E.H.; First, P.N.; de Heer, W.A.: "Electronic Confinement and Coherence in Patterned Epitaxial Graphene". *Science,* **2006,** *312,* 1191-1196.

[19] Hernandez, Y.; Nicolosi, V.; Lotya, M.; Blighe, F.M.; Sun, Z.; De, S.; McGovern, I.T.; Holland, B.; Byrne, M.; Gun'Ko, Y.K.; Boland, J.J.; Niraj, P.; Duesberg, G.; Krishnamurthy, S.; Goodhue, R.; Hutchison, J.; Scardaci, V.; Ferrari, A.C.; Coleman, J.N.: "High-Yield Production of Graphene by Liquid-Phase Exfoliation of Graphite". *Nature Nanotechnology,* **2008,** *3,* 563-568.

[20] Li, D.; Muller, M.B.; Gilje, S.; Kaner, R.B.; Wallace, G.G.: "Processable Aqueous Dispersions of Graphene Nanosheets". *Nature Nanotechnology,* **2008,** *3,* 101-105.

[21] Gomez-Navarro, C.; Weitz, R.T.; Bittner, A.M.; Scolari, M.; Mews, A.; Burghard, M.; Kern, K.: "Electronic Transport Properties of Individual Chemically Reduced Graphene Oxide Sheets". *Nano Letters,* **2007,** *7,* 3499-3503.

[22] Becerril, H.A.; Mao, J.; Liu, Z.; Stoltenberg, R.M.; Bao, Z.; Chen, Y.: "Evaluation of Solution-Processed Reduced Graphene Oxide Films as Transparent Conductors". *ACS Nano,* **2008,** *2,* 463-470.

[23] Zhong-Shuai, W.; Songfeng, P.; Wencai, R.; Daiming, T.; Libo, G.; Bilu, L.; Feng, L.; Chang, L.; Hui-Ming, C.: "Field Emission of Single-Layer Graphene Films Prepared by Electrophoretic Deposition". *Advanced Materials,* **2009,** *21,* 1756-1760.

[24] Zunfeng, L.; Qian, L.; Yi, H.; Yanfeng, M.; Shougen, Y.; Xiaoyan, Z.; Wei, S.; Yongsheng, C.: "Organic Photovoltaic Devices Based on a Novel Acceptor Material: Graphene". *Advanced Materials,* **2008,** *20,* 3924-3930.

[25] Wang, X.; Zhi, L.J.; Mullen, K.: "Transparent, Conductive Graphene Electrodes for Dye-Sensitized Solar Cells". *Nano Letters,* **2008,** *8,* 323-327.

[26] Brodie, B.C.: "On the Atomic Weight of Graphite". *Philosophical Transactions of the Royal Society of London,* **1859,** *149,* 249-259.

[27] Staudenmaier, L.: "Verfahren zur Darstellung der Graphitsäure". *Berichte der Deutschen Chemischen Gesellschaft,* **1898,** *31,* 1481.

[28] Schniepp, H.C.; Li, J.-L.; McAllister, M.J.; Sai, H.; Herrera-Alonso, M.; Adamson, D.H.; Prud'homme, R.K.; Car, R.; Saville, D.A.; Aksay, I.A.: "Functionalized Single Graphene Sheets Derived from Splitting Graphite Oxide". *The Journal of Physical Chemistry B,* **2006,** *110,* 8535-8539.

[29] Hummers, W.S.; Offeman, R.E.: "Preparation of Graphitic Oxide". *Journal of the American Chemical Society,* **1958,** *80,* 1339-1339.

[30] Kovtyukhova, N.I.; Ollivier, P.J.; Martin, B.R.; Mallouk, T.E.; Chizhik, S.A.; Buzaneva, E.V.; Gorchinskiy, A.D.: "Layer-by-Layer Assembly of Ultrathin Composite Films from Micron-Sized Graphite Oxide Sheets and Polycations". *Chemistry of Materials,* **1999,** *11,* 771-778.

[31] Lerf, A.; He, H.; Forster, M.; Klinowski, J.: "Structure of Graphite Oxide Revisited". *The Journal of Physical Chemistry B,* **1998,** *102,* 4477-4482.

[32] Mermoux, M.; Chabre, Y.; Rousseau, A.: "FTIR and 13C NMR Study of Graphite Oxide". *Carbon,* **1991,** *29,* 469-474.

[33] Paredes, J.I.; Villar-Rodil, S.; Sols-Fernndez, P.; Martnez-Alonso, A.; Tascn, J.M.D.: "Atomic Force and Scanning Tunneling Microscopy

Imaging of Graphene Nanosheets Derived from Graphite Oxide". *Langmuir,* **2009,** *25,* 5957-5968.

[34] Gao, W.; Alemany, L.B.; Ci, L.; Ajayan, P.M.: "New Insights into the Structure and Reduction of Graphite Oxide". *Nature Chemistry,* **2009,** *1,* 403-408.

[35] Li, X.; Zhang, G.; Bai, X.; Sun, X.; Wang, X.; Wang, E.; Dai, H.: "Highly Conducting Graphene Sheets and Langmuir-Blodgett Films". *Nature Nanotechnology,* **2008,** *3,* 538-542.

[36] Szabo, T.; Berkesi, O.; Forgo, P.; Josepovits, K.; Sanakis, Y.; Petridis, D.; Dekany, I.: "Evolution of Surface Functional Groups in a Series of Progressively Oxidized Graphite Oxides". *Chemistry of Materials,* **2006,** *18,* 2740-2749.

[37] Cote, L.J.; Kim, F.; Huang, J.: "Langmuir-Blodgett Assembly of Graphite Oxide Single Layers". *Journal of the American Chemical Society,* **2008,** *131,* 1043-1049.

[38] Yin, Z.; Wu, S.; Zhou, X.; Huang, X.; Zhang, Q.; Boey, F.; Zhang, H.: "Electrochemical Deposition of High-Quality ZnO Nanorods on Transparent Conducting Graphene Electrodes Used for Hybrid Solar Cells". *Small,* **2009**. **DOI:** 10.1002/smll.200901968.

[39] Tung, V.C.; Chen, L.-M.; Allen, M.J.; Wassei, J.K.; Nelson, K.; Kaner, R.B.; Yang, Y.: "Low-Temperature Solution Processing of Graphene-Carbon Nanotube Hybrid Materials for High-Performance Transparent Conductors". *Nano Letters,* **2009,** *9,* 1949-1955.

[40] Ramesha, G.K.; Sampath, S.: "Electrochemical Reduction of Oriented Graphene Oxide Films: An in Situ Raman Spectroelectrochemical Study". *The Journal of Physical Chemistry C,* **2009,** *113,* 7985-7989.

[41] Wang, Z.; Zhou, X.; Zhang, J.; Boey, F.; Zhang, H.: "Direct Electrochemical Reduction of Single-Layer Graphene Oxide and Subsequent Functionalization with Glucose Oxidase". *The Journal of Physical Chemistry C,* **2009,** *113,* 14071-14075.

[42] Stankovich, S.; Dikin, D.A.; Dommett, G.H.B.; Kohlhaas, K.M.; Zimney, E.J.; Stach, E.A.; Piner, R.D.; Nguyen, S.T.; Ruoff, R.S.: "Graphene-Based Composite Materials". *Nature,* **2006,** *442,* 282-286.

[43] Park, S.; An, J.; Jung, I.; Piner, R.D.; An, S.J.; Li, X.; Velamakanni, A.; Ruoff, R.S.: "Colloidal Suspensions of Highly Reduced Graphene Oxide in a Wide Variety of Organic Solvents". *Nano Letters,* **2009,** *9,* 1593-1597.

[44] Blake, P.; Hill, E.W.; Neto, A.H.C.; Novoselov, K.S.; Jiang, D.; Yang, R.; Booth, T.J.; Geim, A.K.: "Making Graphene Visible". *Applied Physics Letters,* **2007,** *91,* 063124.

[45] Roddaro, S.; Pingue, P.; Piazza, V.; Pellegrini, V.; Beltram, F.: "The Optical Visibility of Graphene: Interference Colors of Ultrathin Graphite on SiO_2". *Nano Letters,* **2007,** *7,* 2707-2710.

[46] Ferrari, A.C.; Meyer, J.C.; Scardaci, V.; Casiraghi, C.; Lazzeri, M.; Mauri, F.; Piscanec, S.; Jiang, D.; Novoselov, K.S.; Roth, S.; Geim, A.K.: "Raman Spectrum of Graphene and Graphene Layers". *Physical Review Letters,* **2006,** *97,* 187401.

[47] Stankovich, S.; Dikin, D.A.; Piner, R.D.; Kohlhaas, K.A.; Kleinhammes, A.; Jia, Y.; Wu, Y.; Nguyen, S.T.; Ruoff, R.S.: "Synthesis of Graphene-

Based Nanosheets via Chemical Reduction of Exfoliated Graphite Oxide". *Carbon,* **2007,** *45,* 1558-1565.

[48] Stolyarova, E.; Rim, K.T.; Ryu, S.; Maultzsch, J.; Kim, P.; Brus, L.E.; Heinz, T.F.; Hybertsen, M.S.; Flynn, G.W.: "High-Resolution Scanning Tunneling Microscopy Imaging of Mesoscopic Graphene Sheets on an Insulating Surface". *Proceedings of the National Academy of Sciences,* **2007,** *104,* 9209-9212.

[49] Gross, L.; Mohn, F.; Moll, N.; Liljeroth, P.; Meyer, G.: "The Chemical Structure of a Molecule Resolved by Atomic Force Microscopy". *Science,* **2009,** *325,* 1110-1114.

[50] Meyer, J.C.; Geim, A.K.; Katsnelson, M.I.; Novoselov, K.S.; Booth, T.J.; Roth, S.: "The Structure of Suspended Graphene Sheets". *Nature,* **2007,** *446,* 60-63.

[51] Elias, D.C.; Nair, R.R.; Mohiuddin, T.M.G.; Morozov, S.V.; Blake, P.; Halsall, M.P.; Ferrari, A.C.; Boukhvalov, D.W.; Katsnelson, M.I.; Geim, A.K.; Novoselov, K.S.: "Control of Graphene's Properties by Reversible Hydrogenation: Evidence for Graphane". *Science,* **2009,** *323,* 610-613.

[52] Girit, C.O.; Meyer, J.C.; Erni, R.; Rossell, M.D.; Kisielowski, C.; Yang, L.; Park, C.-H.; Crommie, M.F.; Cohen, M.L.; Louie, S.G.; Zettl, A.: "Graphene at the Edge: Stability and Dynamics". *Science,* **2009,** *323,* 1705-1708.

[53] Mkhoyan, K.A.; Contryman, A.W.; Silcox, J.; Stewart, D.A.; Eda, G.; Mattevi, C.; Miller, S.; Chhowalla, M.: "Atomic and Electronic Structure of Graphene-Oxide". *Nano Letters,* **2009,** *9,* 1058-1063.

[54] Park, S.; An, J.; Piner, R.D.; Jung, I.; Yang, D.; Velamakanni, A.; Nguyen, S.T.; Ruoff, R.S.: "Aqueous Suspension and Characterization of Chemically Modified Graphene Sheets". *Chemistry of Materials,* **2008,** *20,* 6592-6594.

[55] Xu, Y.; Bai, H.; Lu, G.; Li, C.; Shi, G.: "Flexible Graphene Films via the Filtration of Water-Soluble Noncovalent Functionalized Graphene Sheets". *Journal of the American Chemical Society,* **2008,** *130,* 5856-5857.

[56] Li, B.; Zhang, Y.; Yan, S.-h.; Lu, J.-h.; Ye, M.; Li, M.-q.; Hu, J.: "Positioning Scission of Single DNA Molecules with Nonspecific Endonuclease Based on Nanomanipulation". *Journal of the American Chemical Society,* **2007,** *129,* 6668-6669.

[57] Robinson, J.T.; Zalalutdinov, M.; Baldwin, J.W.; Snow, E.S.; Wei, Z.Q.; Sheehan, P.; Houston, B.H.: "Wafer-scale Reduced Graphene Oxide Films for Nanomechanical Devices". *Nano Letters,* **2008,** *8,* 3441-3445.

[58] Huang, Y.; Sudibya, H.G.; Fu, D.; Xue, R.; Dong, X.; Li, L.-J.; Chen, P.: "Label-free Detection of ATP Release from Living Astrocytes with High Temporal Resolution using Carbon Nanotube Network". *Biosensors and Bioelectronics,* **2009,** *24,* 2716-2720.

[59] Kuznetsova, A.; Mawhinney, D.B.; Naumenko, V.; Yates, J.T.; Liu, J.; Smalley, R.E.: "Enhancement of Adsorption inside of Single-walled Nanotubes: Opening the Entry Ports". *Chemical Physics Letters,* **2000,** *321,* 292-296.

[60] Xu, C.; Wang, X.; Zhu, J.W.; Yang, X.J.; Lu, L.: "Deposition of Co3O4 Nanoparticles onto Exfoliated Graphite Oxide Sheets". *Journal of Materials Chemistry,* **2008,** *18,* 5625-5629.

[61] Williams, G.; Seger, B.; Kamat, P.V.: "TiO_2-Graphene Nanocomposites. UV-Assisted Photocatalytic Reduction of Graphene Oxide". *ACS Nano,* **2008,** *2,* 1487-1491.

[62] Hodes, G.: "When Small Is Different: Some Recent Advances in Concepts and Applications of Nanoscale Phenomena". *Advanced Materials,* **2007,** *19,* 639-655.

[63] Muszynski, R.; Seger, B.; Kamat, P.V.: "Decorating Graphene Sheets with Gold Nanoparticles". *Journal of Physical Chemistry C,* **2008,** *112,* 5263-5266.

[64] Kong, B.-S.; Geng, J.; Jung, H.-T.: "Layer-by-Layer Assembly of Graphene and Gold Nanoparticles by Vacuum Filtration and Spontaneous Reduction of Gold Ions". *Chemical Communications,* **2009**, 2174-2176.

[65] Choi, H.C.; Shim, M.; Bangsaruntip, S.; Dai, H.J.: "Spontaneous Reduction of Metal Ions on the Sidewalls of Carbon Nanotubes". *Journal of the American Chemical Society,* **2002,** *124,* 9058-9059.

[66] Ou, J.L.; Chang, C.P.; Sung, Y.; Ou, K.L.; Tseng, C.C.; Ling, H.W.; Ger, M.D.: "Uniform Polystyrene Microspheres Decorated with Noble Metal Nanoparticles Formed Without Using Extra Reducing Agent". *Colloids and Surfaces A: Physicochemical and Engineering Aspects,* **2007,** *305,* 36-41.

[67] Sai, T.P.; Raychaudhuri, A.K.: "Adhesion Behaviour of Self-assembled Alkanethiol Monolayers on Silver at Different Stages of Growth". *Journal of Physics D: Applied Physics,* **2007,** *40,* 3182.

[68] Jin, R.; Cao, Y.; Mirkin, C.A.; Kelly, K.L.; Schatz, G.C.; Zheng, J.G.: "Photoinduced Conversion of Silver Nanospheres to Nanoprisms". *Science,* **2001,** *294,* 1901-1903.

[69] Kim, K.; Lee, H.S.: "Effect of Ag and Au Nanoparticles on the SERS of 4-Aminobenzenethiol Assembled on Powdered Copper". *The Journal of Physical Chemistry B,* **2005,** *109,* 18929-18934.

[70] Wang, Y.L.; Chen, H.J.; Dong, S.J.; Wang, E.K.: "Surface Enhanced Raman Scattering of p-aminothiophenol Self-assembled Monolayers in Sandwich Structure Fabricated on Glass". *Journal of Chemical Physics,* **2006,** *124,* 074709.

[71] Son, Y.-W.; Cohen, M.L.; Louie, S.G.: "Energy Gaps in Graphene Nanoribbons". *Physical Review Letters,* **2006,** *97,* 216803-4.

[72] Nakada, K.; Fujita, M.; Dresselhaus, G.; Dresselhaus, M.S.: "Edge State in Graphene Ribbons: Nanometer Size Effect and Edge Shape Dependence". *Physical Review B,* **1996,** *54,* 17954.

[73] Yang, L.; Park, C.-H.; Son, Y.-W.; Cohen, M.L.; Louie, S.G.: "Quasiparticle Energies and Band Gaps in Graphene Nanoribbons". *Physical Review Letters,* **2007,** *99,* 186801-4.

[74] Jiao, L.; Zhang, L.; Wang, X.; Diankov, G.; Dai, H.: "Narrow Graphene Nanoribbons from Carbon Nanotubes". *Nature,* **2009,** *458,* 877-880.

[75] Wang, X.; Li, X.; Zhang, L.; Yoon, Y.; Weber, P.K.; Wang, H.; Guo, J.; Dai, H.: "N-Doping of Graphene Through Electrothermal Reactions with Ammonia". *Science,* **2009,** *324,* 768-771.

[76] Wilder, J.W.G.; Venema, L.C.; Rinzler, A.G.; Smalley, R.E.; Dekker, C.: "Electronic Structure of Atomically Resolved Carbon Nanotubes". *Nature,* **1998,** *391,* 59-62.

[77] Odom, T.W.; Huang, J.-L.; Kim, P.; Lieber, C.M.: "Atomic Structure and Electronic Properties of Single-Walled Carbon Nanotubes". *Nature,* **1998,** *391,* 62-64.

[78] Terrones, M.: "Materials Science: Nanotubes Unzipped". *Nature,* **2009,** *458,* 845-846.

[79] Kosynkin, D.V.; Higginbotham, A.L.; Sinitskii, A.; Lomeda, J.R.; Dimiev, A.; Price, B.K.; Tour, J.M.: "Longitudinal Unzipping of Carbon Nanotubes to form Graphene Nanoribbons". *Nature,* **2009,** *458,* 872-876.

[80] Bai, J.; Duan, X.; Huang, Y.: "Rational Fabrication of Graphene Nanoribbons Using a Nanowire Etch Mask". *Nano Letters,* **2009,** *9,* 2083-2087.

[81] Cano-Mrquez, A.G.; Rodríguez-Macas, F.J.; Campos-Delgado, J.; Espinosa-Gonzlez, C.G.; Tristn-Lpez, F.; Ramírez-Gonzlez, D.; Cullen, D.A.; Smith, D.J.; Terrones, M.; Vega-Cant: "Ex-MWNTs: Graphene Sheets and Ribbons Produced by Lithium Intercalation and Exfoliation of Carbon Nanotubes". *Nano Letters,* **2009,** *9,* 1527-1533.

[82] Schniepp, H.C.; Kudin, K.N.; Li, J.-L.; Prud'homme, R.K.; Car, R.; Saville, D.A.; Aksay, I.A.: "Bending Properties of Single Functionalized Graphene Sheets Probed by Atomic Force Microscopy". *ACS Nano,* **2008,** *2,* 2577-2584.

[83] Li, Z.; Zhang, W.; Luo, Y.; Yang, J.; Hou, J.G.: "How Graphene Is Cut upon Oxidation?" *Journal of the American Chemical Society,* **2009,** *131,* 6320-6321.

[84] Rao, S.G.; Huang, L.; Setyawan, W.; Hong, S.: "Nanotube Electronics: Large-scale Assembly of Carbon Nanotubes". *Nature,* **2003,** *425,* 36-37.

[85] Wei, Z.Q.; Barlow, D.E.; Sheehan, P.E.: "The Assembly of Single-Layer Graphene Oxide and Graphene Using Molecular Templates". *Nano Letters,* **2008,** *8,* 3141-3145.

[86] Matthew, J.A.; Vincent, C.T.; Lewis, G.; Zheng, X.; Li-Min, C.; Kurt, S.N.; Chongwu, Z.; Richard, B.K.; Yang, Y.: "Soft Transfer Printing of Chemically Converted Graphene". *Advanced Materials,* **2009,** *21,* 2098-2102.

[87] Xie, X.; Ju, L.; Feng, X.; Sun, Y.; Zhou, R.; Liu, K.; Fan, S.; Li, Q.; Jiang, K.: "Controlled Fabrication of High-Quality Carbon Nanoscrolls from Monolayer Graphene". *Nano Letters,* **2009,** *9,* 2565-2570.

[88] Li, Q.; Li, Z.; Chen, M.; Fang, Y.: "Real-Time Study of Graphene's Phase Transition in Polymer Matrices". *Nano Letters,* **2009,** *9,* 2129-2132.

[89] Cassagneau, T.; Fendler, J.H.: "Preparation and Layer-by-Layer Self-assembly of Silver Nanoparticles Capped by Graphite Oxide Nanosheets". *Journal of Physical Chemistry B,* **1999,** *103,* 1789-1793.

[90] Garibaldi, S.; Brunelli, C.; Bavastrello, V.; Ghigliotti, G.; Nicolini, C.: "Carbon Nanotube Biocompatibility with Cardiac Muscle Cells". *Nanotechnology,* **2006,** *17,* 391-397.

[91] Meng, J.; Song, L.; Meng, J.; Kong, H.; Zhu, G.J.; Wang, C.Y.; Xu, L.H.; Xie, S.S.; Xu, H.Y.: "Using Single-Walled Carbon Nanotubes Nonwoven Films as Scaffolds to Enhance Long-term Cell Proliferation In Vitro". *Journal of Biomedical Materials Research Part A,* **2006,** *79A,* 298-306.

[92] Abarrategi, A.; Gutierrez, M.C.; Moreno-Vicente, C.; Hortiguela, M.J.; Ramos, V.; Lopez-Lacomba, J.L.; Ferrer, M.L.; del Monte, F.: "Multiwall

Carbon Nanotube Scaffolds for Tissue Engineering Purposes". *Biomaterials,* **2008,** *29,* 94-102.

[93] Oh, S.; Brammer, K.S.; Li, Y.S.J.; Teng, D.; Engler, A.J.; Chien, S.; Jin, S.: "Stem Cell Fate Dictated Solely by Altered Nanotube Dimension". *Proceedings of the National Academy of Sciences,* **2009,** *106,* 2130-2135.

[94] Bettinger, C.J.; Langer, R.; Borenstein, J.T.: "Engineering Substrate Topography at the Micro- and Nanoscale to Control Cell Function". *Angewandte Chemie-International Edition,* **2009,** *48,* 5406-5415.

[95] Lovat, V.; Pantarotto, D.; Lagostena, L.; Cacciari, B.; Grandolfo, M.; Righi, M.; Spalluto, G.; Prato, M.; Ballerini, L.: "Carbon Nanotube Substrates Boost Neuronal Electrical Signaling". *Nano Letters,* **2005,** *5,* 1107-1110.

[96] Cellot, G.; Cilia, E.; Cipollone, S.; Rancic, V.; Sucapane, A.; Giordani, S.; Gambazzi, L.; Markram, H.; Grandolfo, M.; Scaini, D.; Gelain, F.; Casalis, L.; Prato, M.; Giugliano, M.; Ballerini, L.: "Carbon Nanotubes Might Improve Neuronal Performance by Favouring Electrical Shortcuts". *Nature Nanotechnology,* **2009,** *4,* 126-133.

[97] Gheith, M.K.; Pappas, T.C.; Liopo, A.V.; Sinani, V.A.; Shim, B.S.; Motamedi, M.; Wicksted, J.R.; Kotov, N.A.: "Stimulation of Neural Cells by Lateral Currents in Conductive Layer-by-Layer Films of Single-Walled Carbon Nanotubes". *Advanced Materials,* **2006,** *18,* 2975-2979.

[98] Zhang, J.; Fu, D.L.; Chan-Park, M.B.; Li, L.J.; Chen, P.: "Nanotopographic Carbon Nanotube Thin-Film Substrate Freezes Lateral Motion of Secretory Vesicles". *Advanced Materials,* **2009,** *21,* 790-793.

[99] Karas, M.; Bachmann, D.; Bahr, U.; Hillenkamp, F.: "Matrix-assisted Ultraviolet Laser Desorption of Non-volatile Compounds". *International Journal of Mass Spectrometry and Ion Processes,* **1987,** *78,* 53-68.

[100] Koichi, T.; Hiroaki, W.; Yutaka, I.; Satoshi, A.; Yoshikazu, Y.; Tamio, Y.; Matsuo, T.: "Protein and Polymer Analyses up to m/z 100 000 by Laser Ionization Time-Of-Flight Mass Spectrometry". *Rapid Communications in Mass Spectrometry,* **1988,** *2,* 151-153.

[101] Karas, M.; Hillenkamp, F.: "Laser Desorption Ionization of Proteins with Molecular Masses Exceeding 10,000 daltons". *Analytical Chemistry,* **1988,** *60,* 2299-2301.

[102] Nielen, M.W.F.: "Maldi Time-Of-Flight Mass Spectrometry of Synthetic Polymers". *Mass Spectrometry Reviews,* **1999,** *18,* 309-344.

[103] Karas, M.; Hillenkamp, F.: "Laser desorption ionization of proteins with molecular masses exceeding 10,000 daltons". *Analytical Chemistry,* **2002,** *60,* 2299-2301.

[104] Chaurand, P.; Luetzenkirchen, F.; Spengler, B.: "Peptide and Protein Identification by Matrix-assisted Laser Desorption Ionization (MALDI) and MALDI-Post-source Decay Time-Of-Flight Mass Spectrometry". *Journal of the American Society for Mass Spectrometry,* **1999,** *10,* 91-103.

[105] Egelhofer, V.; Gobom, J.; Seitz, H.; Giavalisco, P.; Lehrach, H.; Nordhoff, E.: "Protein Identification by MALDI-TOF-MS Peptide Mapping: A New Strategy". *Analytical Chemistry,* **2002,** *74,* 1760-1771.

[106] Thomas, A.S.; Christopher, H.B.; Yuping, T.; Juanita, N.W.; Kuang Jen, W.: "Analysis of Enzymatic DNA Sequencing Reactions by Matrix-

assisted Laser Desorption/Ionization Time-Of-Flight Mass Spectrometry". *Rapid Communications in Mass Spectrometry,* **1995,** *9,* 942-947.

[107] Schiller, J.; Arnhold, J.; Benard, S.; Muller, M.; Reichl, S.; Arnold, K.: "Lipid Analysis by Matrix-assisted Laser Desorption and Ionization Mass Spectrometry: A Methodological Approach". *Analytical Biochemistry,* **1999,** *267,* 46-56.

[108] Pan, C.S.; Xu, S.Y.; Hu, L.G.; Su, X.Y.; Ou, J.J.; Zou, H.F.; Guo, Z.; Zhang, Y.; Guo, B.C.: "Using Oxidized Carbon Nanotubes as Matrix for Analysis of Small Molecules by MALDI-TOF MS". *Journal of the American Society for Mass Spectrometry,* **2005,** *16,* 883-892.

[109] Harvey, D.J.: "Quantitative Aspects of the Matrix-assisted Laser Desorption Mass Spectrometry of Complex Oligosaccharides". *Rapid Communications in Mass Spectrometry,* **1993,** *7,* 614-619.

[110] Balandin, A.A.; Ghosh, S.; Bao, W.; Calizo, I.; Teweldebrhan, D.; Miao, F.; Lau, C.N.: "Superior Thermal Conductivity of Single-Layer Graphene". *Nano Letters,* **2008,** *8,* 902-907.

[111] Sunner, J.; Dratz, E.; Chen, Y.-C.: "Graphite Surface-assisted Laser Desorption/Ionization Time-of-Flight Mass Spectrometry of Peptides and Proteins from Liquid Solutions". *Analytical Chemistry,* **2002,** *67,* 4335-4342.

[112] Dale, M.J.; Knochenmuss, R.; Zenobi, R.: "Graphite/Liquid Mixed Matrices for Laser Desorption/Ionization Mass Spectrometry". *Analytical Chemistry,* **1996,** *68,* 3321-3329.

[113] Xu, S.; Li, Y.; Zou, H.; Qiu, J.; Guo, Z.; Guo, B.: "Carbon Nanotubes as Assisted Matrix for Laser Desorption/Ionization Time-of-Flight Mass Spectrometry". *Analytical Chemistry,* **2003,** *75,* 6191-6195.

[114] Pan, C.; Xu, S.; Zou, H.; Guo, Z.; Zhang, Y.; Guo, B.: "Carbon Nanotubes as Adsorbent of Solid-phase Extraction and Matrix for Laser Desorption/Ionization Mass Spectrometry". *Journal of the American Society for Mass Spectrometry,* **2005,** *16,* 263-270.

List of Publications

(i) Peer-reviewed journal papers

[1] Agarwal, S.†; **Zhou, X.**†; Ye, F.; He, Q.; Chen, G.C.K.; Boey, F.; Zhang, H.*; Chen, P.*: "Interfacing Live Cells with Nanocarbon Substrates". **2009**, submitted. († These authors contribute equally)

[2] **Zhou, X.**; Lu, G.; Qi, X.; Wu, S.; Li, H.; Boey, F.; Zhang, H.*: "A Method for Fabrication of Graphene Oxide Nanoribbons from Graphene Oxide Wrinkles". *The Journal of Physical Chemistry C,* **2009,** *113,* 19119-19122.

[3] **Zhou, X.**; Huang, X.; Qi, X.; Wu, S.; Xue, C.; Boey, F.Y.C.; Yan, Q.; Chen, P.; Zhang, H.*: "In Situ Synthesis of Metal Nanoparticles on Single-Layer Graphene Oxide and Reduced Graphene Oxide Surfaces". *The Journal of Physical Chemistry C,* **2009,** *113,* 10842-10846.

[4] Wang, Z.; **Zhou, X.**; Zhang, J.; Boey, F.; Zhang, H.*: "Direct Electrochemical Reduction of Single-Layer Graphene Oxide and Subsequent Functionalization with Glucose Oxidase". *The Journal of Physical Chemistry C,* **2009,** *113,* 14071-14075.

[5] Yin, Z.; Wu, S.; **Zhou, X.**; Huang, X.; Zhang, Q.; Boey, F.; Zhang, H.*: "Electrochemical Deposition of ZnO Nanorods on Transparent Reduced Graphene Oxide Electrodes for Hybrid Solar Cells". *Small,* **2009**. **DOI:** 10.1002/smll.200901968.

[6] **Zhou, X.**; Chen, Y.; Li, B.; Lu, G.; Boey, F.Y.C.; Ma, J.; Zhang, H.*: "Controlled Growth of Peptide Nanoarrays on Si/SiOx Substrates". *Small,* **2008,** *4,* 1324-1328.

[7] Li, B.; Lu, G.; **Zhou, X.**; Cao, X.; Boey, F.; Zhang, H.*: "Controlled Assembly of Gold Nanoparticles and Graphene Oxide Sheets on Dip Pen Nanolithography-Generated Templates". *Langmuir,* **2009,** *25,* 10455-10458.

[8] Li, B.; Goh, C.F.; **Zhou, X.**; Lu, G.; Tantang, H.; Chen, Y.; Xue, C.; Boey, F.Y.C.; Zhang, H.*: "Patterning Colloidal Metal Nanoparticles for Controlled Growth of Carbon Nanotubes". *Advanced Materials,* **2008,** *20,* 4873-4878.

[9] Lu, G.; Chen, Y.; Li, B.; **Zhou, X.**; Xue, C.; Ma, J.; Boey, F.Y.C.; Zhang, H.*: "Dip-Pen Nanolithography-Generated Patterns Used as Gold Etch Resists: A Comparison Study of 16-Mercaptohexadecanioc Acid and 1-Octadecanethiol". *The Journal of Physical Chemistry C,* **2009,** *113,* 4184-4187.

[10] Qi, X.; C., X.; Huang, X.; Huang, Y.; **Zhou, X.**; Li, H.; Liu, D.; Boey, F.; Yan, Q.; Huang, W.; De Feyter, S.; Müllen, K.; Zhang, H.*: "Polyphenylene Dendrimer-Templated In-Situ Construction of Inorganic-Organic Hybrid Rice-Shaped Architectures". *Advanced Functional Materials,* **2009**. **DOI:** 10.1002/adfm.200900982.

(ii) Book chapters

[1] **Zhou, X.**; Liu, X.*; Boey, F.Y.C.; Zhang, H.*: "Integrated Nanostructures and Nanodevices Fabricated by Dip-Pen Nanolithography". *Topics in Multifunctional Biomaterials & Devices,* N. Ashammakhi (Ed.), **2008**, *Chapter 13*, Pages 1-18.

[2] He, Q.; **Zhou, X.**; Boey, F.Y.C.; Zhang, H.*: "Fabrication of Bio- and Nano-patterns by Dip-Pen Nanolithography". *Scanning Probe Microscopy:*

Techniques, Applications and Future Directions, N. Tomczak and E. Cox (Ed.), World Scientific, Singapore, **2010**, in press.

(iii) Presentations

[1] **Zhou, X.**; Li, B.; Lu, G.; Cao, X.; Boey, F.; Ma, J.; Zhang, H.: "Controlled Growth of Peptide and Carbon Nanotube Arrays on Dip-Pen Nanolithography Generated Templates". in *International Conference on Materials for Advanced Technologies 2009 (ICMAT2009)*. 28 June-3 July **2009**. Singapore. **Oral presentation.**

[2] **Zhou, X.**; Chen, Y.; Li, B.; Lu, G.; Boey, F.; Ma, J.; Zhang, H.: "*Controlled Growth of Peptide Nanoarrays on Si/SiOx substrates*". in *AsiaNano Conference 2008 (AsiaNano2008)*. 3-6 November **2008**. Singapore. **Oral presentation.**